SYSTEM AND THERMAL MODELING OF HYDRAULIC HYBRIDS: THERMAL CHARACTERISTICS ANALYSIS

by

Hyukjoon Kwon

A Dissertation

Submitted to the Faculty of Purdue University

In Partial Fulfillment of the Requirements for the degree of

Doctor of Philosophy

School of Mechanical Engineering

West Lafayette, Indiana

May 2018

THE PURDUE UNIVERSITY GRADUATE SCHOOL
STATEMENT OF COMMITTEE APPROVAL

Dr. Monika Ivantysynova, Chair
School of Mechanical Engineering
Dr. Andrea Vacca
School of Mechanical Engineering
Dr. Sadegh Dabiri
School of Mechanical Engineering
Dr. Dennis Buckmaster
School of Agriculture and Biological Engineering

Approved by:
Dr. Jay P. Gore
Head of the Graduate Program

ACKNOWLEDGMENTS

I am forever indebted to my research advisor, Prof. Monika Ivantysynova, for her belief, guidance, and support to finish my Ph.D. study. I would also like to acknowledge to my Ph.D. committee members, Prof. Dennis Buckmaster, Prof. Andrea Vacca, Prof. Sadegh Dabiri, and Prof. John Starkey, for their kind advice and feedback. I appreciate it to the systems group members, who helped and worked together on several projects and I will not forget the moments. Also, I am grateful to all other Maha group members for making the wonderful and comfortable place to study. Personally, I would like to thank my family for supporting me with love during my long Ph.D. journey. Thanks to the rest of my friends I didn't acknowledge by name. I appreciate your support and consideration.

TABLE OF CONTENTS

LIST OF TABLES

LIST OF FIGURES

LIST OF SYMBOLS

A	Area, m^2
a	Acceleration of the vehicle, m s^{-2}
C_{check}	Coefficient of the check valve, m^4 s^{-1} $N^{-0.5}$
C_d	Drag coefficient
C_h	Hydraulic capacitance, m^5 N^{-1}
C_r	Rolling resistance coefficient
C_{relief}	Coefficient for the pressure relief valve, m^4 s^{-1} $N^{-0.5}$
c_p	Isobaric specific heat, J kg^{-1} $^oC^{-1}$
d	Diameter of the pipe, m
F_D	Aerodynamic drag, N
F_g	Gravitational force, N
F_r	Rolling resistance, N
F_t	Traction force, N
F_{tot}	Net force, N
Gr	Grashof number
g	Gravitational acceleration, m s^{-2}
H	Enthalpy, J
h	Specific enthalpy, J kg^{-1}
h_{conv}	Convection coefficient, W m^{-2} $^oC^{-1}$
h_{rad}	Radiation coefficient, W m^{-2} $^oC^{-1}$
J_e	Engine rotational inertia, kg m^2
K	Bulk modulus, N m^{-2}
k	Thermal conductivity, W m^{-1} $^oC^{-1}$
k_{cooler}	Heat transfer coefficient of the cooler, W m^{-1} $^oC^{-1}$
l_{pipe}	Length of the pipe, m
M	Torque, Nm
M_e	Effective torque, Nm
M_f	Torque loss due to the friction, Nm

M_i	Theoretical torque, Nm
M_s	Torque loss, Nm
M_{WOT}	Wide open throttle torque, Nm
M_w	Torque loaded on the wheel, Nm
m	Mass, kg
Nu	Nusselt number
n	Polytropic coefficient
n_1	Angular speed of Unit-1, rpm
n_2	Angular speed of Unit-2, rpm
Pr	Prandtl number
p	Pressure, N m^{-2}
p_0	Precharge pressure, N m^{-2}
p_4	Pressure in CV-4, N m^{-2}
p_5	Pressure in CV-5, N m^{-2}
p_{check}	Pressure of the check valve, N m^{-2}
p_{cooler}	Pressure of the hydraulic oil in the cooler, N m^{-2}
p_{relief}	Pressure of the pressure relief valve, N m^{-2}
Q_1	Flow rate of Unit-1, m^3 s^{-1}
Q_2	Flow rate of Unit-2, m^3 s^{-1}
Q_4	Flow rate through CV-4, m^3 s^{-1}
Q_{check}	Flow rate through the check valve, m^3 s^{-1}
Q_{cooler}	Flow rate through the cooler, m^3 s^{-1}
Q_e	Effective flow rate of the hydraulic unit, m^3 s^{-1}
Q_i	Theoretical flow rate of the hydraulic unit, m^3 s^{-1}
Q_{in}	Flow rate at the inlet of the hydraulic unit, m^3 s^{-1}
Q_{out}	Flow rate at the outlet of the hydraulic unit, m^3 s^{-1}
Q_{relief}	Flow rate through the pressure relief valve, m^3 s^{-1}
Q_s	Volumetric loss of the hydraulic unit, m^3 s^{-1}
Q_{se}	Volumetric loss of the hydraulic unit, m^3 s^{-1}
R	Thermal resistance, ºC W^{-1}
Re	Reynolds number
R_{eq}	Total equivalent thermal resistance, ºC W^{-1}

r	Wheel dynamic radius, m
s	Specific entropy, J kg^{-1} $^oC^{-1}$
T	Temperature, ^oC
T_1	Temperature in CV-1, ^oC
T_4	Temperature in CV-4, ^oC
T_5	Temperature in CV-5, ^oC
T_{air}	Temperature in the ambient air, ^oC
T_d	Temperature in the drain pipe, ^oC
T_r	Temperature in the reservoir, ^oC
t	Time, s
U	Internal energy, J
u_{CE}	Normalized throttle input
V	Volume, m^3
V_0	Initial gas volume, m^3
V_{eng}	Displacement volume of the engine, m^3
v	Velocity, m/s
W	Work, J
W_{CV}	Work done by the control volume, J

Greeks

β_1	Displacement of Unit-1, %
β_2	Displacement of Unit-2, %
β_T	Volumetric thermal expansion coefficient, $^oC^{-1}$
η	Efficiency
θ	Angle of the slope, ^{o}
ρ	Density, kg m^{-3}
φ	Heat, J
φ_{in}	Energy transferred into the system, J

Abbreviations

EHA	Electro-hydrostatic actuator
FTP	Federal test procedure
HEV	Hybrid electric vehicle
HHT	Hydraulic hybrid transmission
HHV	Hydraulic hybrid vehicle
HIL	Hardware-in-the-loop
HP	High pressure
HPA	High pressure accumulator
LP	Low pressure
SUV	Sport utility vehicle
UDDS	Urban dynamometer driving schedule

ABSTRACT

Author: Kwon, Hyukjoon. PhD
Institution: Purdue University
Degree Received: May 2018
Title: System and Thermal Modeling of Hydraulic Hybrids: Thermal Characteristics Analysis.
Committee Chair: Monika Ivantysynova

Hybrid vehicles have become a popular alternative to conventional powertrain architectures by offering improved fuel efficiency along with various other environmental benefits. Among them, hydraulic hybrid vehicles (HHVs) have several benefits, which make it the superior technology for certain applications over other types of hybrid vehicles, such as lower component costs, more environmentally friendly construction materials, higher power densities, and more regenerative energy available from braking. There have been various studies on HHVs, such as energy management optimization, control strategies for various system configurations, the effect of system parameters on the hybrid system, and proposals for novel hybrid architectures. One area not been thoroughly covered in the past is a detailed modeling and examination of the thermal characteristics for HHVs due to a difficulty of describing the rapid thermal transients in the unsteady state systems.

In this dissertation, a comprehensive system and thermal modeling has been studied for hydraulic hybrid transmissions (HHTs). The main motivation behind developing a thermal model of HHTs is to gain a deeper understanding of the system's thermal performance, and key influencing factors, without relying on experimental data. This will enable HHVs to be designed more efficiently by identifying and addressing potential issues with transmission's thermal performance prior to hardware testing. Since there exists no thermal study on HHVs in the past, a thermal modeling method has been introduced, which can be applicable to hydraulic hybrid

architectures. A thermal modeling methodology based on a novel numerical scheme and accurate theoretical description has been developed in order to capture the rapid thermal transient in the hydraulic system under unsteady state conditions.

The model has been applied to a series HHT and validated with measured data from the hardware-in-the-loop (HIL) test rig with a standard driving cycle, FTP-72. In addition, the proposed thermal modeling methodology has been used to analyze and optimize the cooling system of a novel HHV architecture, which is implemented in a sport utility vehicle (SUV) in Maha Fluid Power Research Center. The modeling results have been compared with the measured data while driving the vehicle. In both studies, the simulation results have shown a good correlation with the experimental data in terms of the overall trends and variation ranges.

The goal of the developed model is the application to the system and thermal issues in HHVs, such as thermal stability analysis, management of the cooling system, packaging and hydraulic component optimization, and evaluation of thermal characteristics of different architectures. As an advanced topic of this research, thermal management of an open and a closed circuit hydraulic hybrid systems has been studied by simulation. The comparison results show a potential to a better thermal management for the open circuit systems with smaller heat exchangers, as well as less power consumption with incorporation of smaller charge pumps compared to the closed circuit systems.

In the future, the developed comprehensive system and thermal modeling method can be applied to different advanced topics, such as analysis of performance and thermal characteristics, systems and components optimization, and systems evaluation with different external conditions, for different hydraulic hybrid systems.

CHAPTER 1. INTRODUCTION

1.1 Motivation

The unstable price of petroleum in recent years together with new gas emission regulations have pushed automotive companies to develop new vehicle architectures with high fuel efficiency. Figure 1 shows the US petroleum production and consumption from 1973 to 2050 (Davis, Williams, and Boundy 2017). 70.0% of the total consumption of petroleum is used for the transportation in 2015. Thus, fossil fuel consumption can significantly be reduced by using fuel efficient systems in the on-road vehicles.

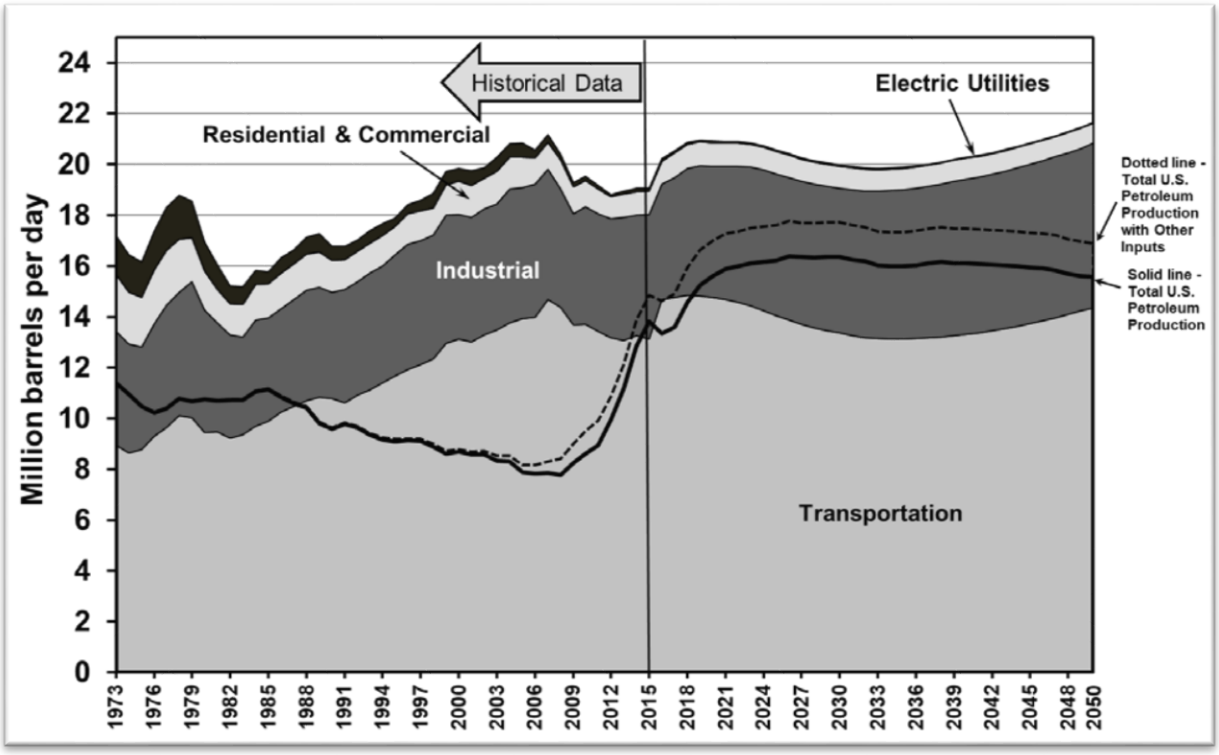

Figure 1. US petroleum production and consumption, 1973–2050 (Davis, Williams, and Boundy 2017).

Among several technologies for energy efficient vehicles, hybrid vehicles have become a popular alternative to conventional power train architectures by offering improved fuel efficiency along with various other environmental benefits. Even though hybrid electric vehicles (HEVs) are dominating the current on-road vehicle market, hydraulic hybrid vehicles (HHVs) have been studied by several research groups. Hydraulic hybrids have several important advantages compared to electric hybrids (Baseley et al. 2007; J.-S. Chen 2015). The lower cost of the system and lower weight of components including the energy storage device are one of the advantages of HHVs. Figure 2 shows the Ragone diagram for different energy storage devices (Lu et al. 2014; Wachsman, Marlowe, and Lee 2012; Werkstetter 2015). In the figure, we see that the hydraulic accumulators have the highest specific power among the storage devices. Also, HHVs can capture more regenerative power from braking with the high power density of the energy storage (Chicurel 1999; Midgley and Cebon 2012). The advantages of HHVs make them utilized in appropriate purposes like refuge trucks (Bender, Bosse, and Sawodny 2014; Soriano et al. 2016), and buses (Heskitt, Smith, and Hopkins 2012; Ramdan and Stelson 2016).

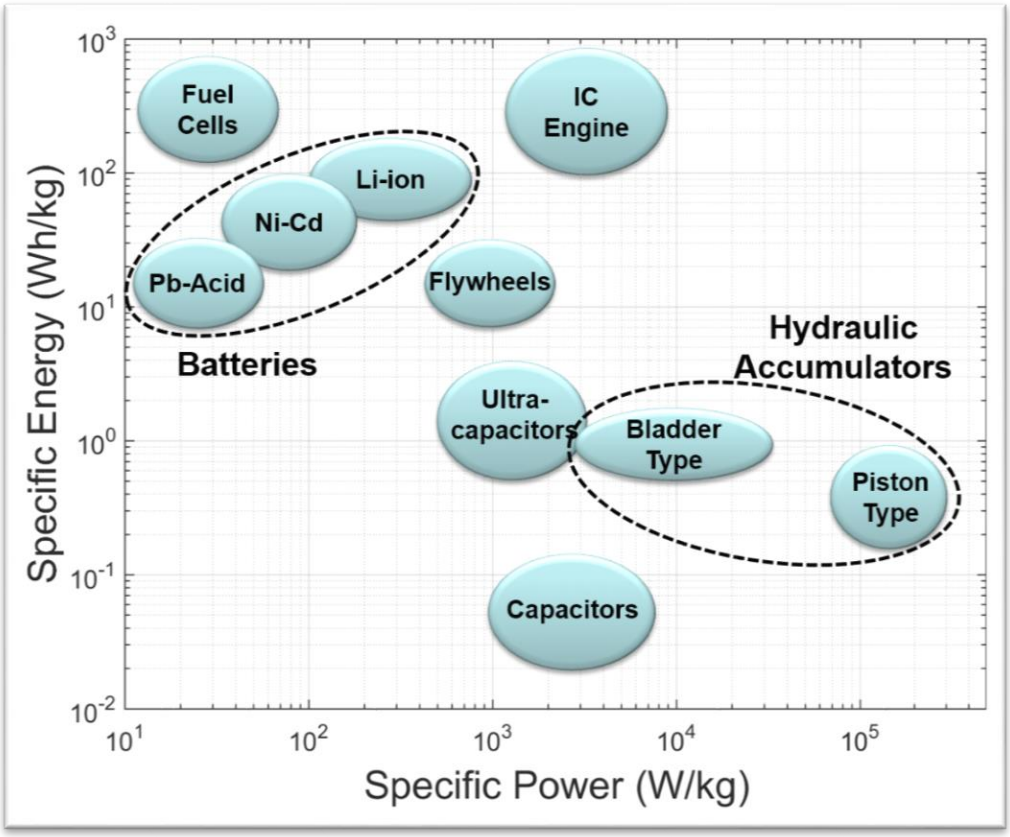

Figure 2. Ragone diagram for different energy sources (Lu et al. 2014; Wachsman, Marlowe, and Lee 2012; Werkstetter 2015).

Hydraulic hybrid transmissions (HHTs) have been investigated by numerous researchers and institutions since the 1970's. The areas of the research for HHVs include parameter design and the propulsion characteristics (W. Wu et al. 2014), energy management optimizations (Deppen et al. 2012; B. Wu et al. 2004), control strategies for various system configurations (Filipi and Kim 2010), the effect of system parameters on series hybrids (Ramakrishnan, Hiremath, and Singaperumal 2012), and proposals for novel hybrid architectures (Haria and Ivantysynova 2016; Sprengel et al. 2015) among many others. One area which has thoroughly not been covered in the past is a detailed examination of the thermal characteristics of such a system, while, for HEVs, there have been several studies related to thermal characteristics such as thermal analysis of the

transmission and weather impact on the vehicle efficiency (N. Kim and Rousseau 2015; Pesaran 2002). Thermal analysis of the system is vital for hybrid vehicles since it cannot only be utilized for observing the thermal stability of the system, but thermal characteristics of the system are also related to the system performance.

The main motivation behind developing a comprehensive system and thermal model for HHTs is to gain a deeper understanding of the system's thermal performance, and key influencing factors, without relying on experimental data. This will enable HHVs to be designed more efficiently by identifying and addressing potential issues with transmission's thermal performance prior to hardware testing. While sometimes overlooked, maintaining system temperature within an acceptable range is essential for maximizing the performance and longevity of HHVs. Specifically, temperature has a direct impact on oil viscosity which in turn strongly influences efficiency. If excessively high oil temperatures are present, the viscosity of oil may drop too low as to impair the load carrying ability of lubricating interfaces within the positive displacement machines resulting in excessive wear and in extreme cases catastrophic failure. Excessive oil temperature may also harm other system components such as seals and elastomeric accumulator bladders while also causing oil degradation. The thermal model can be utilized for analyzing and optimizing the thermal management system while designing the hydraulic system. The optimization of the cooler will not only reduce the cost, weight and space of the cooler, but the consumed energy for the cooler can also be reduced. In addition, the thermal model can be utilized for several purposes such as a thermal stability analysis of the HHV system, optimization of the packaging of hydraulic components, and evaluation of the thermal characteristics of different hybrid architectures, without iterative and time-consuming experimental measurements.

1.2 Organization

This dissertation includes following chapters. First, backgrounds of the HHTs are handled in Chapter 2 including the types of the HHTs and the state of the art for HHVs and thermal studies on hydraulic systems. The theoretical study on modeling is described for the hydraulic system model and thermal model in Chapter 3. In Chapter 4, thermal modeling for a series HHT is covered with simulation study and measurement in the test rig. In Chapter 5, thermal modeling of a novel HHT, which has recently been suggested by Maha Fluid Power Research Center, is studied with the data measured in vehicle. As an advanced topic of the model, thermal management of open and closed circuit series hydraulic systems have been compared by simulation in Chapter 6. Finally, Chapter 7 concludes this research and possible future work.

CHAPTER 2. BACKGROUND

In this chapter, background provides a brief discussion of the HHTs. First, this chapter begins with a classification of the various types of the HHTs. Then, the state of the art is described including overall studies on HHTs and thermal studies on hydraulic systems.

2.1 Types of Hydraulic Hybrid Transmissions

Hydraulic transmissions can be classified into hybrid and non-hybrid transmissions. Hydraulic accumulators are utilized in hydraulic hybrid systems as energy storage devices. The types of hydraulic hybrids can generally be divided into three architectures, series hydraulic hybrid, parallel hydraulic hybrid, and power split hydraulic hybrids.

- *Series Hydraulic Hybrid Transmission*

In a series HHT, the hydraulic units working as a pump or a motor are connected in series. One unit is connected to the engine and the other unit is connected to the wheel. As an energy storage device, a high pressure accumulator and a low pressure accumulator are implemented in the hydraulic line. Figure 3 shows an example circuit of the series HHT.

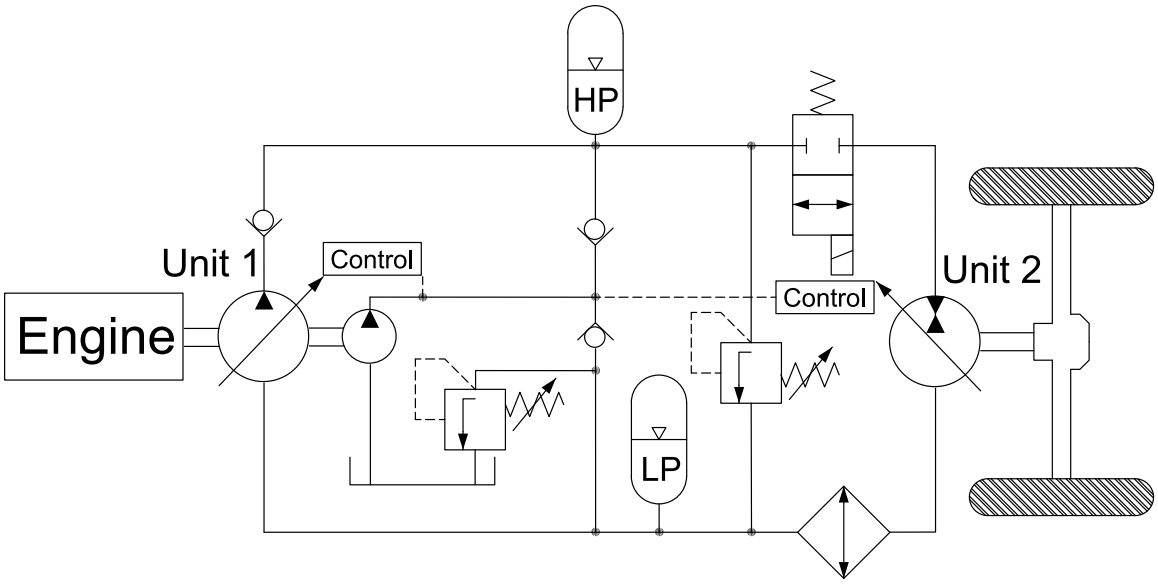

Figure 3. An example circuit of the series HHT.

In the series hybrid HHT, Unit 1 controls the state of charge of the high pressure accumulator through controlling the system pressure, and Unit 2 controls the vehicle speed. The design of the series HHT can be divided into open and closed circuits. The open circuit design does not include a low pressure accumulator, instead uses an open reservoir. On the other hand, series hybrids with closed circuit utilize the state of charge of the low pressure accumulator determining the low pressure of the system.

- *Parallel Hydraulic Hybrid Transmission*

In the parallel HHT, the hydraulic unit is connected in parallel to the main transmission. The accumulator is used to store energy from vehicle braking and to run it for propulsion. Figure 4 shows an example circuit of a parallel hydraulic hybrid. The hydraulic unit works as a pump during braking and as a motor while using the stored energy and propelling the vehicle. Since the architecture of the parallel HHT is much simpler than other types of HHTs, it is generally easier to install. Mostly parallel hybrid configurations are used for retrofitting existing drive trains.

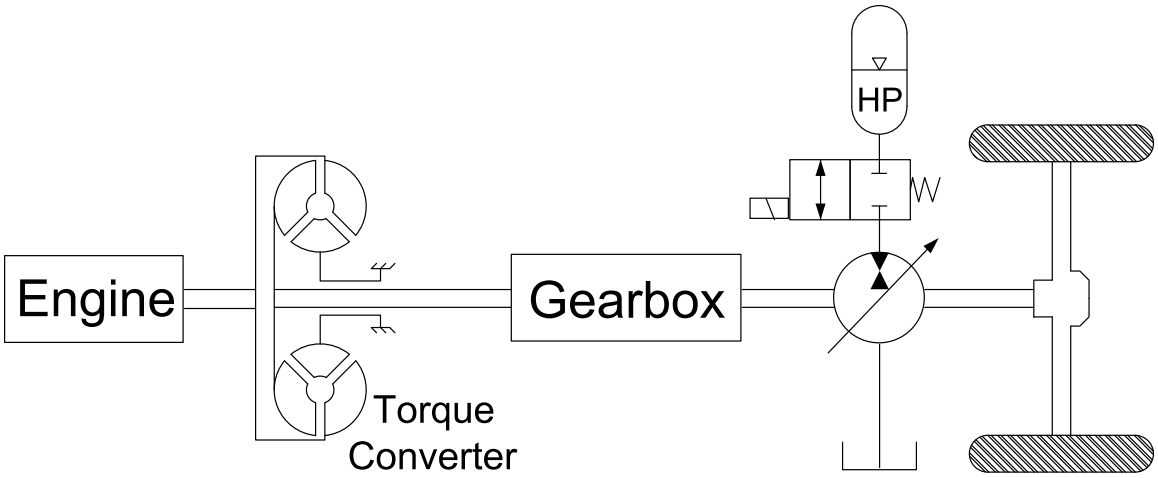

Figure 4. An example circuit of the parallel HHT.

- *Power Split Hydraulic Hybrid Transmission*

The power split HHT utilizes a planetary gear together with a hydraulic hybrid system and there exist more than a thousand possible configurations. Figure 5 shows an example circuit of output coupled power split hydraulic hybrid systems. A planetary gear is used to split power from the engine between a mechanical path and a hydraulic path. Power split HHTs utilize different operating modes, such as power additive mode, full mechanical mode, and power recirculation mode. In the power additive mode, when the speed of the vehicle is increasing, the power through the hydraulic path is decreasing and the power through the mechanical path is increasing. Once the power through the hydrostatic power path reaches zero, the transmission is under the full mechanical mode. After the full mechanical mode, the power through the hydraulic path becomes minus, and the vehicle drives with the power recirculation mode. Figure 6 shows the schematic of the main operational modes of an output coupled power split transmission, where ω_A is the angular speed of the sun gear, ω_B is the angular speed of the gear carrier, and ω_C is the angular speed of the ring gear.

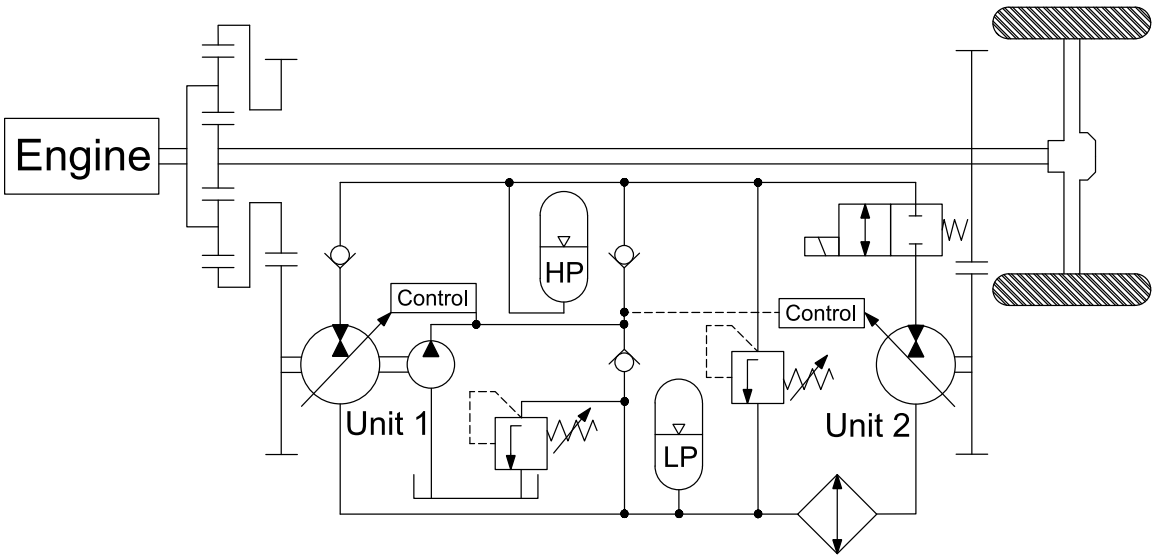

Figure 5. An example circuit of output coupled power split hydraulic hybrid systems.

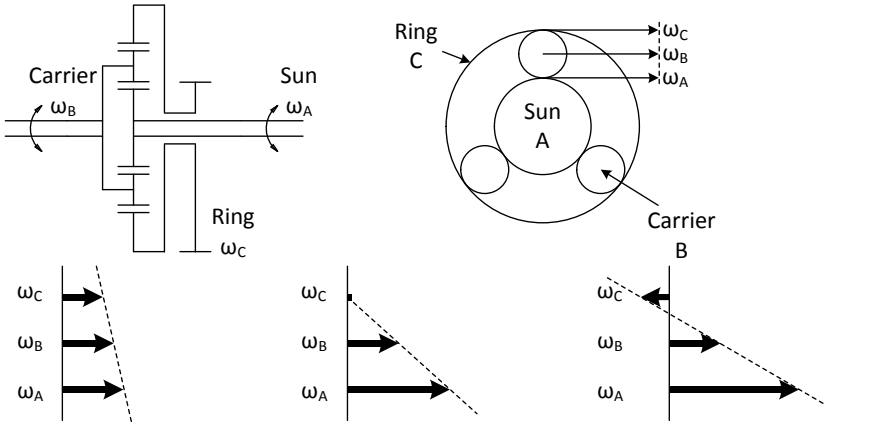

Figure 6. Schematic of the main operating modes of an output coupled power split transmission.

2.2 State of the Art

2.2.1 Studies on Hydraulic Hybrid Transmissions

- *Series Hydraulic Hybrid Systems*

Series HHTs have been studied for several decades from the 1970s. In the earliest studies, the main focus of the research on the series HHT was the development of a prototype. A series HHV for passenger cars has been studied by simulation, which showed substantial fuel savings and a possibility to be applicable to the real architecture (Elder and Otis 1973). A mechanical bypass in parallel with a series hybrid has been studied, which indicated fuel savings between 17% and 22% compared to the conventional series hydraulic hybrid (Heggie and Sandri 1980). In the early 1990s, Volvo introduced the prototype work on series hydraulic hybrids with Cumulo Hydrostatic Drive. A bus was used for dynamometer testing with a trapezoidal drive cycle, which indicated potential fuel savings of 48% (Hugosson 1993). UPS delivery truck with series HHT has been equipped in 2006 by EPA, Eaton, and UPS with other industrial partners and fuel savings of 60% to 70% has been achieved during the field testing (Wendel et al. 2007). In recent studies, FTA, Altair, and Parker partnered each other to develop a series HHT for city buses with a more efficient engine and reduced vehicle mass. The hybrid bus showed fuel improvement of 29% over the most efficient electric hybrids, 47% over the identical nonhybrid bus, and 109% over the conventional city bus (Heskitt, Smith, and Hopkins 2012).

There have been diverse simulation studies on the series HHT in a purpose of evaluation of the performance and fuel savings. A series hybrid in a passenger car has been simulated and a fuel economy of 60 mpg has been achieved with Federal Urban Driving Schedule (FUDS) cycle

in the simulation (P. Wu, Fronczak, and Beachley 1985). Power bond graph approach has been applied to predicting the dynamic response characteristics of a series HHT (Ramachandran, Hiremath, and Singaperumal 2010). Fuel economy of the medium truck with a series HHT showed improvement of the fuel economy by 72% and reduction of the particulate emission by 74% compared to the conventional baseline, which was studied by simulation and the engine-in-the-loop (EIL) techniques (Filipi and Kim 2010). The dynamic simulation for the series HHT has been studied to improve the system output for different system parameters (Ramakrishnan, Hiremath, and Singaperumal 2012). A model predictive control approach has been studied for fuel economy improvement of a series HHT (Vu, Chen, and Hung 2014). Also, the analysis of the performance of a rule-based, SDP, and MPC energy management strategy has been studied according to varying drive cycles and model parameters for a series HHT (Deppen et al. 2015). A topological analysis of a series hydraulic hybrid refuse-collecting vehicle was studied based on the simulation and it shows fuel savings of up to 14% (Soriano et al. 2016).

For the control of the series HHT, the engine power management based on the state of the charge control, which of the series hydraulic hybrid for a light truck, has been studied by simulation work and fuel economy predictions for the optimized system indicated fuel savings of over 50% under urban driving conditions (Y. J. Kim and Filipi 2007). Johri and Filipi proposed an optimized supervisory control for a series HHT and fuel economy for FUDS driving cycle was shown 93 mpg with engine idling and 110 mpg with engine shut-downs (Johri and Filipi 2010). The procedure for the design and implementation of a control strategy has been studied to optimize energy of a light duty series HHT (Deppen et al. 2012). A model predictive controller was studied for a series HHV to improve a fuel economy (Vu, Chen, and Hung 2014). A neural network power management was studied for series HHTs to decrease average fuel consumption and it shows

around 26% decrease compared to a baseline constant control strategy (Sprengel and Ivantysynova 2017).

In addition, An open circuit series HHT has been used for the study on minimizing the size of the energy storage (Beachley, Anscomb, and Burrows 1983). The pros and cons of open and closed circuits of series HHTs have been studied in terms of the weight of hydraulic components (Cross and Ivantysynova 2011). Energy management strategies for series HHTs has been study with an open circuit system (Deppen et al. 2015).

- *Parallel Hydraulic Hybrid Systems*

Parallel HHTs have been studied for several decades with series HHTs due to relative ease of implementation. The previous studies include a variety of areas, such as development of a prototype, control of the system, performance prediction and fuel efficiency optimization.

For the development of the prototype, the earliest studies for parallel HHTs, the round trip energy storage efficiency of a parallel HHT has been studied by using experimental setup, which showed the round trip efficiency of over 50% (Dunn and Wojcienchowski 1972) and after the study, they achieved the round trip efficiency of 66% in the improved test rig (Dunn and Wojcienchowski 1974, 1975). Also, in a subsequent study, the round trip efficiency of 75% was achieved with the account of the aerodynamic drag of the flywheel (Dewey, Elder, and Otis 1974). In the early 1980s, a prototype of parallel HHT has been developed by MAN and demonstrated fuel savings of 25% compared to the conventional bus (Martini 1984). A fuel savings of 30% was achieved with the braking storage system and downsized engine by Mitsubishi Motors (Nakazawa et al. 1987). A parallel HHT for a bus was also developed by the Canadian National Research Council, which indicated a reduction in fuel consumption of 17% in comparison with the

conventional bus (Davies 1987, 1989). In 2000s, Ford, Eaton, and EPA developed a parallel HHT for SUV, which showed fuel savings of 24% (Kepner 2002). A refuge truck with a parallel HHT has been developed by Eaton with fuel savings of 30% in 2008. A hydraulic power system, which can be easily installed in conventional buses, has been studied by experiment and simulation, and it shows fuel savings of 28% in the real road tests (Liu et al. 2009; Yan, Liu, and Chen 2010).

In early simulation studies, the accuracy of the results is limited due to the lack of computational ability. In a simulation study, a parallel HHT for a bus has been studied and validated with a small delivery van, which indicated possible fuel savings of 25 to 30% (Buchwald et al. 1979). A parallel HHT for a passenger car has been simulated with three different driving cycles, and fuel economy up to 64 mpg is possible for urban driving cycles, while few fuel economy improvement was achieved for a highway cycle due to the less regenerative braking compared to urban driving (Tollefson, Beachley, and Fronczak 1985). A simulation of HHTs with bond graph has been developed as a design tool to optimize the performance and efficiency of the system (Pease and Henderson 1988). After 2000, a regenerative energy system with a parallel HHT has been studied in simulation for use on heavy commercial vehicles (Matheson and Stecki 2003). A systematic analysis of a different proposed parallel hydraulic hybrid powertrain has been conducted for the Family of Medium Tactical Vehicles (FMTV) by Filipi and et al. (Filipi et al. 2004). Toulson studied a parallel HHT for small road vehicles in urban driving conditions through modeling and simulation (Toulson 2008). Stochastic dynamic programming (DP) has been studied for a parallel hybrid for maximizing the performance of the system (Johri, Baseley, and Filipi 2011). Several author used simulation to study the energy management of parallel HHTs for fuel savings, fuel savings of around 20% has been achieved for refuge vehicles compared to the conventional vehicle (Bender, Bosse, and Sawodny 2014; Bender, Kaszynski, and Sawodny 2013).

For the control of the system, Wu and coworkers proposed a power management strategy through a dynamic programming for a parallel HHT for a medium-size delivery truck, which yielded the potential fuel savings of 47% (B. Wu et al. 2002, 2004). The optimal energy distribution with a fuzzy torque control strategy has been studied for a parallel HHT with an urban driving cycle (Hui, Ji-hai, and Xin 2009; Hui and Junqing 2010). A control strategy of optimal brake energy recovery has been proposed in simulation for a parallel HHT, and the results yielded recapturing of 42.7% of the brake energy (Z. Zhang, Chen, and Wu 2012). The front-mounted parallel HHT has been analyzed for control strategies and system optimization (Y. Chen et al. 2017).

- *Power Split Hydraulic Hybrid Systems*

For the power split HHTs, the first prototype has been developed and patented in 1980 for a passenger car, which indicated fuel savings of 100% (Shiber 1979, 1980). Various transmissions of power split HHTs have been studied for city buses by simulation work and they achieved fuel economy improvement of 5% for a hydrostatic power split transmission, 14% for a compound hydrostatic power split transmission, and 28% for a power split HHT using a compound planetary gear train compared to the baseline bus (Bowns, Vaughan, and Dorey 1981; Dorey and Vaughan 1984).

After 2000, the dynamic analysis and controller of a power split HHT were studied for a passenger vehicle (Cheong et al. 2014; Cheong, Li, and Chase 2011; P. Y. Li 2010; Sim and Li 2009; H. Zhang, Wang, and Stelson 2017). All possible configurations of a power split HHT with two planetary gears were explored with the three-step design methodology (C.-T. Li and Peng 2010). Kumar and Ivantysynova proposed an output coupled power split HHT for a passenger car

application (Kumar and Ivantysynova 2009, 2010). The power split drive transmissions with energy recovery have been invented for automotive applications (Ivantysynova, Carl, and Williams 2008). Peugeot and Bosch Rexroth developed an output coupled power split HHT for a passenger car and demonstrated fuel savings up to 45% in 2013 (Hybrid Air, an innovative full hybrid gasoline system n.d.). A power split HHT for medium duty vehicles has been tested on a dynamometer test rig showing a fuel economy improvement of 19% for the Baltimore driving cycle and 52% for the New York City Composite cycle (Lammert et al. 2014). An optimal power split HHT has been studied for a city bus (Ramdan and Stelson 2016). A power split HHT has been studied for system optimization and compared with a power split hydrostatic transmission by simulation (Macor et al. 2017; Rossetti and Macor 2013).

- *Other studies on Hydraulic Hybrid Systems*

There have been studies on comparison among different hybrid architectures. The HHV and HEV transmissions have been studied by comparison in terms of the fuel efficiency and performance (J.-S. Chen 2015; N. Kim and Rousseau 2013; Soriano et al. 2016; Yang, Luo, and Li 2017; Zhao and Tatari 2017). Dynamic programming for the series hybrid transmission and the power split HHT has been studied by comparison with the manual transmission and automatic transmissions (Sprengel and Ivantysynova 2013, 2014a, 2014b). The fuel economy of the series HHV, parallel HHV, and power split HHV are studied and the power split HHT showed the best fuel economy for various hydraulic efficiencies (Du et al. 2013).

In addition to the series HHT, parallel HHT, and power split HHT, there have been several studies on transmission architectures for other types of HHVs. Other several unique architectures have been studied in recent studies, such as hybrid transmission with a series of check valves for

various modes of operation (Gray 2004), the hydro-mechanical drive train with independent wheel torque control (Van de Ven, Olson, and Li 2008), hydraulic hybrid drive with a series hybrid and a hydrostatic transmission (Schneider and Krautler 2009), a new hydraulic closed-loop energy saving transmission based on a hydrostatic transmission (Ho and Ahn 2010, 2012), and a new energy efficient hydraulic hybrid propulsion system (W. Wu et al. 2014, 2016). In Maha Fluid Power Research Center, there have recently been studies on novel hydraulic hybrid architectures for the blended HHT (Sprengel et al. 2015) and the mode switching HHT (Haria and Ivantysynova 2016).

There have been several studies related to the hydraulic energy storages for HHVs, such as regenerative brake of hydraulic system (Pourmovahed, Beachley, and Fronczak 1992a, 1992b; Scott and Yamaguchi 1984), comparison of different types of energy storage units (Baseley et al. 2007; Chicurel 1999; Clegg 1996; Midgley and Cebon 2012; Xu et al. 2017), energy recovery of the hydraulic system, and a novel hydraulic accumulators (P. Y. Li, Van de Ven, and Sancken 2007; Strohmaier, Cronk, and Van de Ven 2015; Van de Ven 2013). There have been several studies on hydraulic-electric synergy systems, which use advantages from both types of hybrid vehicles (Hui et al. 2011; Hui, Lifu, and Junqing 2010; Ramakrishnan, Hiremath, and Singaperumal 2014). Also, a hydraulic-pneumatic synergy system was studied recently for a mining truck (Yi et al. 2018).

2.2.2 Thermal Studies on Hydraulic Systems

Thermal studies on hydraulic operating systems can largely be divided into two areas, studies at the component level and studies at the system level. There have been fewer studies on

the thermal characteristics of the hydraulic systems compared to other research topics mentioned previously. There was no thermal study on HHTs in the past.

Different studies on the thermal behavior of the hydraulic components have been studied for several decades. In the early studies, the losses of the hydraulic pumps and motors have been studied by thermodynamic methods to monitor the efficiency of the system (Kjolle 1978; Norgard 1973; Witt 1974; Witt and Schlosser 1977). In addition, several studies for hydraulic pumps and motors have been studied based on thermal approaches until recently (Bae, Vuong, and Park 2012; C. Li and Jiao 2006; Y. Li et al. 2008; Manco and Nervegna 1989; Nykanen 2003; Shang and Ivantysynova 2015). For the hydraulic accumulator, which is one of the main components of HHV, several thermal works have been studied for accumulators, such as thermal damping and thermal constants, and thermal enhancement of the compressed air in the accumulator (Frank Wicks et al. 2002; J. Li et al. 2011; Pourmovahed and Otis 1984, 1990; Puddu and Paderi 2013).

For the thermal studies on hydraulic systems, the efficiency of a hydraulic transmission has been calculated by hydraulic and thermodynamic methods (Kjolle 1989, 1993). Also, the thermal and hydraulic performance of the open circuit hydraulic transmission has been simulated by a lumped parameter model based on mass and energy conservation equations (Sidders, Tilley, and Chapple 1996). Hydraulic systems for the electro-hydrostatic actuator (EHA), which have widely been used for commercial aircrafts, have been studied for several research topics in different research groups, such as losses and temperature calculations, heat generation and thermal-hydraulic modeling on EHA systems (Andersson et al. 1999; K. Li et al. 2014; Svensson, Andersson, and Rydberg 1999). Condition monitoring of the system based on thermodynamic analysis has been studied to observe the efficiency of the propel drive of a combine harvester in the unsteady state (Pomierski 1999, 2001). A thermal model based on a lumped parameter model

has been developed with an integration method to solve coupled equations of the hydraulic system model and thermal model (Chenggong and Zongxia 2008). A thermal model to predict the temperature of the hydraulic system has been studied based on thermodynamic approaches for the displacement controlled system with multiple actuators (Busquets and Ivantysynova 2013). A thermodynamic analysis of the hydraulic system has been studied based on the pseudo-bond graph (Hu and Li 2015). The cavitation in the hydraulic system was predicted by a thermal-hydraulic modeling concept with calculated oil temperature (Zhou, Wei, and Hu 2015). Thermodynamic analysis of a hydraulic braking energy recovery system has been studied to observe the charging and discharging efficiencies of the braking system (Panchal, Dincer, and Agelin-Chaab 2016).

In summary, the temperature of the hydraulic system predicted from the previous studies generally showed accuracy around 5 to 10ºC, which is possible to predict the temperature trend and some absolute temperature degrees of the system. In system scales, there exists no thermal study on HHTs, and only a few of thermal studies focused the modeling of the hydraulic system under unsteady state conditions.

2.3 Research Objectives

In this dissertation, a comprehensive system and thermal model for HHTs is proposed and verified with measurement data. The model was comprised of both a hydraulic system model and a thermal model, using a lumped parameter modeling approach. The model was used to analyze different types of HHTs, such as open and closed circuit series hydraulic hybrids and a novel hybrid architecture. The simulation results were validated through different measured data collected from the HIL test rig and the Maha hybrid vehicle, recently proposed by researchers at the Maha lab (Sprengel et al. 2015). The model contains a novel simulation scheme for capturing

rapid thermal transients within the hydraulic system under unsteady state conditions. The proposed model allows conducting thermal stability analysis of the hybrid system, analysis and optimization of the cooling system, packaging analysis and optimization of the system. To this end, the following detailed objectives were pursued:

- Develop a comprehensive thermal system model for HHTs of various architectures considering unsteady state conditions.
- Suggest a novel simulation scheme to describe the rapid thermal transients of the hydraulic systems under unsteady state conditions with a better theoretical description of the system.
- Validate the simulation results with experimental data measured in the test rig and in the vehicle.
- Analyze the thermal management system of hydraulic hybrid power trains based on the thermal model.
- Compare the thermal stability of the open and closed circuits of series hydraulic hybrids.

Based on the state of the art of the research on HHTs, the original contributions of this research can be described as follows:

- First study on thermal modeling of HHTs
- Development of a combined system and thermal modeling methodology based on a novel simulation scheme and physics-based models for capturing the rapid thermal transient of the hydraulic system under unsteady state conditions
- First thermal management analysis of open and closed circuit hybrid systems by simulation

CHAPTER 3. MODELING APPROACH

There are mainly two types of models based on physical laws. The first one is the lumped parameter model approach leading to ordinary differential equations, which can be solved analytically or numerically. One of the advantages of the lumped parameter approach is quick simulation time over relatively large domains. The other modeling approach uses distributed parameters, which leads to partial differential equations. The modeling with distributed parameters is solved using numerical methods such as FEM (finite element method), FVM (finite volume method), and FDM (finite difference method). An advantage of the distributed parameter approach is that those models are generally more accurate than the lumped parameter models, even though they require expensive computation time for large areas. Thus, the lumped parameter model is suitable for the system analysis with relatively large areas, while the distributed parameter models are proper for the component analysis with more exact prediction and expensive computation time. In this research, a lumped parameter model approach is used for the system level analysis.

The main difference of the hydraulic hybrid transmission from the nonhybrid hydraulic transmission is the existence of the accumulator. The energy variation stored in the hydraulic accumulator needs to be modeled. The polytropic process with a quasi-adiabatic condition can be assumed for the accumulator, which is generally charged by nitrogen gas. In the HHT, most of the heat is generated in the hydraulic units due to the power loss while transferring energy. In this study, the heat generated in hydraulic lines is neglected since the amount is minor for the overall system. The nitrogen gas inside the accumulator is considered as adiabatically insulated from hydraulic oil. The heat generated outside of the hydraulic system such as the engine and

mechanical shaft is not considered in the modeling and the measured ambient air temperature is used as a boundary condition.

3.1 Methodology

The main purpose of the modeling in this thesis proposed for thermal analysis is to predict the system temperature distribution and the required cooling power for the given driving cycle of HHVs. Figure 7 shows the structure of the tool proposed for thermal analysis of any kind of HHTs. The tool requires the input of the system structure together with all parameters of the system components. In a next step, the hydraulic system is modeled with the system controller and vehicle dynamics as described in Chapter 3.2 in more detail. The modeling results from the hydraulic system model are used as input parameters for the thermal model. The modeling results from the hydraulic system model are used as input parameters for the thermal model. The theoretical descriptions for each control volume are determined based on the operating conditions and assumptions. In the thermal model, a novel modeling approach is utilized for describing the rapid thermal transient in the hydraulic hybrid systems under the unsteady state conditions. In addition, compressible flow is considered in the modeling for an accurate theoretical description of the highly compressed fluid up to 450 bars, while the fluid is assumed as incompressible in most previous studies. The results from the hydraulic system model and thermal model are validated with the measured data by different sources such as data from test rigs and vehicles. The validated model is used for the system and thermal analysis, and if necessary, the system design and components are changed for optimization of the systems. The combined system and thermal model can be applied for further advanced topics such as thermal characteristics comparison of different systems, system and thermal prediction of new systems, and thermal management optimization.

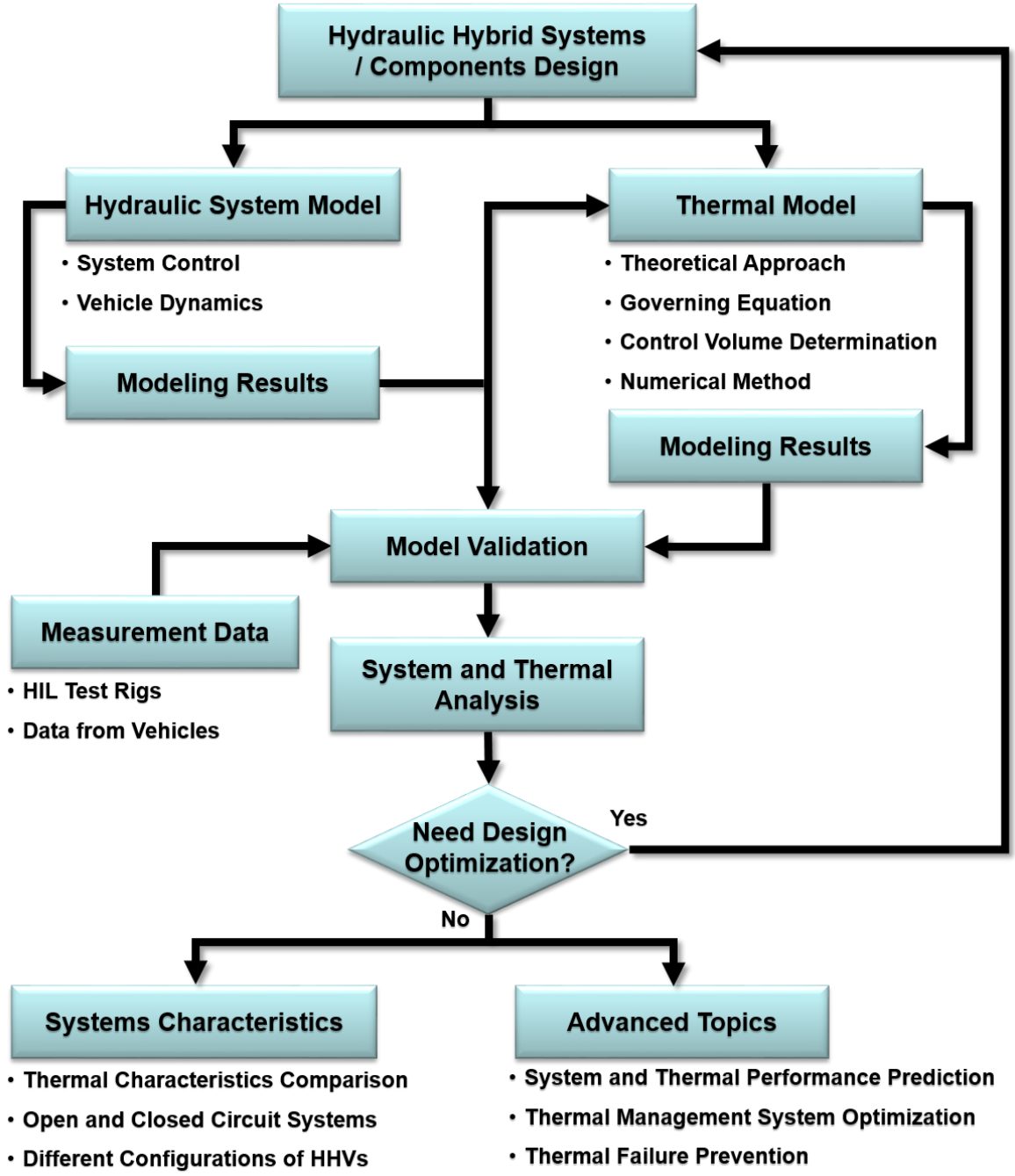

Figure 7. Methodology for the system and thermal modeling study for HHTs.

For calculating the system temperature of the hydraulic system, the flow rate and pressure can be used as input parameters, which can be obtained from the hydraulic system. Figure 8 shows the block diagram of the thermal model used in this study. First, pressure and temperature lookup

tables are utilized to determine oil properties, such as density, viscosity, enthalpy, and specific heat. For the simulation of the HHTs, it is not easy to capture the rapid thermal transient due to the rapid flow variation in the hydraulic system. To handle the issue, a novel numerical scheme for switching parameters in the control volumes is applied based on the direction of the flow in this study, while the other previous studies the parameters are determined according to the control volume location. Second, the input and output energy flows are calculated by the flow rate, density, and enthalpy, which are also determined by the switching parameter scheme in the control volume. Third, the work done in the system is determined differently for different hydraulic components with pressure and flow rate. The work term of the positive displacement machines is described by the work through the mechanical shaft. Then, the heat transfer is calculated with the material properties, system temperature and flow rate. As the last step, the energy flow, heat transfer, and work in the system are utilized in the governing equation for calculating the system temperature, which is derived for the compressible flow to improve the accuracy of the model. The detailed methods used in this study is described in the following sections.

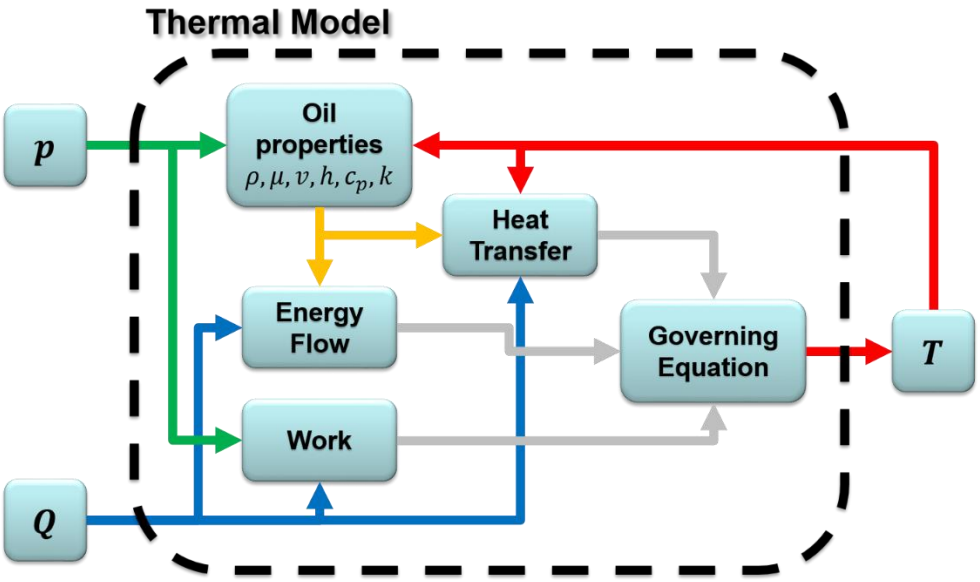

Figure 8. Block diagram of the thermal modeling approach
(p: pressure, Q: flow rate, T: temperature).

In order to obtain the flow rate and pressure for thermal modeling, the hydraulic system needs to be modeled together with vehicle dynamics. Figure 9 shows the block diagram of the overall system model approach proposed and studied in this research for the hydraulic hybrid system. The hydraulic system model calculates the flow rate and pressure of the system based on the duty cycle, vehicle dynamics, and controller of the system. The thermal model utilizes the flow rate and pressure data from the hydraulic system model to calculate the system temperature. The details of each model for the hydraulic system, thermal system, system control, engine dynamics, and vehicle dynamics are described in the following sections.

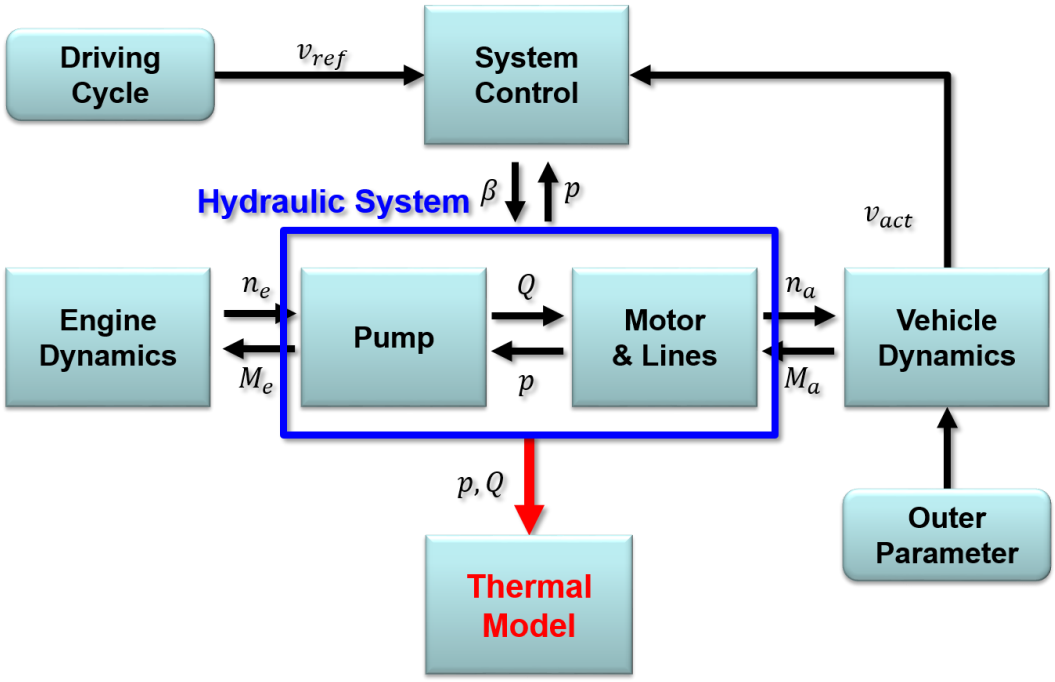

Figure 9. Block diagram of the overall system model approach for the hydraulic hybrid system.

3.2 Hydraulic System Model

We utilize the lumped parameter approach for the hydraulic system model due to its advantages for system scale analysis. Governing equations are included for hydraulic components which could be accurately described analytically, while empirical models, based on steady state measurements, can be used to describe the positive displacement machine's loss characteristics. For calculating the displacement of the pump, the pump dynamics are neglected. The displacement volume is obtained based on the system feedback control signal. The details of the models used in this research study are described for calculating the flow rate through the hydraulic components and pressure of the hydraulic line. The hydraulic system model can be used for calculating the flow rate and pressure of the overall system and those data can be used as input parameters for the thermal model.

3.2.1 Model for the Positive Displacement Machines

The effective flow rates delivered by the positive displacement pump or required at the inlet of a positive displacement motor can be modeled through an empirical loss model, which is based on the measured data utilizing steady state measurement according to ISO standard. Figure 10 shows the schematics of the loss behavior of the positive displacement machines. When the positive displacement machine works as pump, the effective flow rate Q_e can be calculated through the theoretical flow rate Q_i minus volumetric loss Q_s. The effective torque M_e of the pump is given by the sum of theoretical torque M_i and torque loss of the pump M_s. In case of the positive displacement machine working as motor, the effective flow Q_e of the motor equals the theoretical flow Q_i plus volumetric losses Q_s. The effective torque M_e of the motor is given by the theoretical torque M_i minus the torque losses M_s.

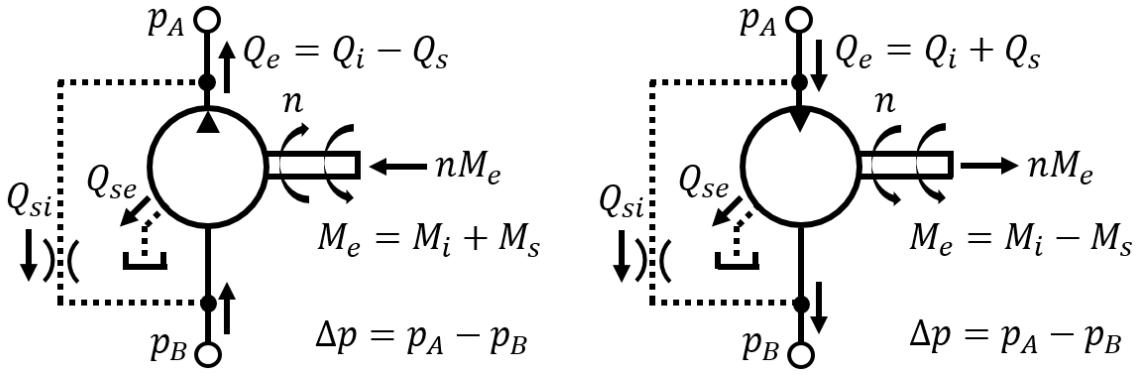

(a) (b)

Figure 10. Schematics of the loss behavior of the positive displacement machines, (a) pump and (b) motor)

According to DIN ISO 4391, the volumetric losses include external volumetric losses Q_{se}, internal volumetric losses Q_{si}, filling losses Q_{sf}, and volumetric losses due to the compressibility of the fluid Q_{sk} (Ivantysyn and Ivantysynova 2001). The internal and external volumetric losses

happen due to the internal and external leakage flow. The filling losses occur because of the incomplete filling of the displacement chamber. The volumetric losses due to the compressibility of the fluid are proportional to the differential pressure between the inlet and outlet of the hydraulic unit. The summation of these four volumetric losses determines the volumetric losses of the positive displacement machines.

The torque losses include mainly four types of losses. First, the torque losses due to the turbulent flow $M_{s\rho}$ include the friction loss in the turbulent flow region like churning losses and the torque loss due to the impulse change. The torque loss dependent on unit speed $M_{s\mu}$ is proportional to the unit speed and it occurs due to the viscous friction between the sliding surfaces of the unit. The torque loss dependent on pressure M_{sp} occur due to the normal force, which is proportional to the operating pressure. The last one is the torque loss independent on operating parameters M_{sc} and it is affected by manufacturing tolerances, initial stresses on seals, preloaded springs and other preloaded parts, which is generally constant for a given hydraulic unit.

In this research study, an empirical loss model is used for describing the volumetric losses and torque losses. Figure 11 shows an example of the loss model for an axial piston pump. Due to these power losses, energy is dissipated and the temperatures of the fluid and the pump ports increase. The energy dissipation and heat generation is considered in the chapter for the thermal model with the energy balance equation.

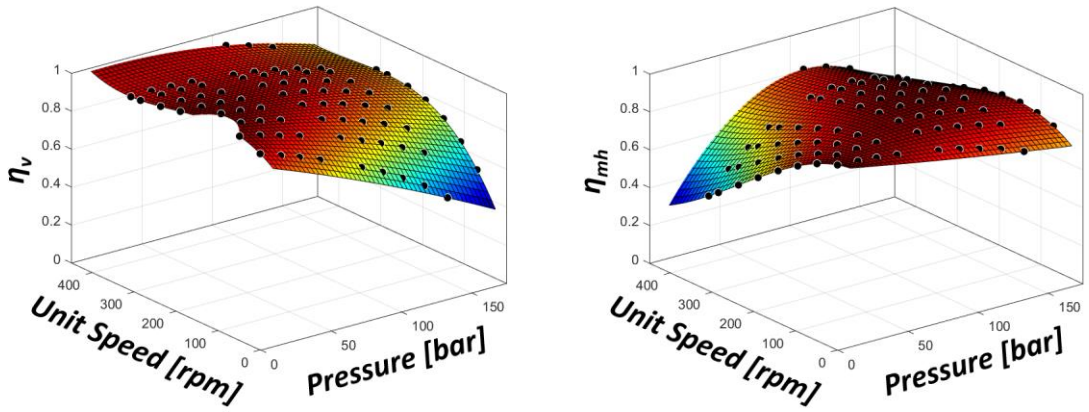

(a) (b)

Figure 11. Example of the loss model for a hydraulic unit, (a) volumetric efficiency and (b) torque efficiency.

The theoretical flow can be calculated with the unit speed and derived displacement as follows:

$$Q_i = n\beta V_i \tag{1}$$

where Q_i is the theoretical flow rate, n is the speed of the unit, β is the adjusted displacement of the unit normalized to the maximum displacement, and V_i is the derived displacement volume. Theoretical torque M_i can be obtained from the following equation:

$$M_i = \frac{\beta V_i \Delta p}{2\pi} \tag{2}$$

where Δp is the differential pressure between the inlet and outlet ports. Theoretical flow rate and theoretical torque are used for calculating the effective flow rate and effective torque as described in the previous pages.

3.2.2 Hydraulic Line Model

The pressure in the hydraulic line is built up based on the summation of the inlet and outlet flows of the hydraulic line. The derivative of pressure with respect to time of each control volume can be obtained from the pressure build-up equation (Klop and Ivantysynova 2011):

$$\dot{p} = \frac{1}{C_h}\left(\sum Q_{in} - Q_{out} + \frac{dV}{dt}\right) \tag{3}$$

where $\dot{p}$ is the pressure variation rate, C_h is the hydraulic capacitance, and Q_{in} and Q_{out} are the flow rates in and out of the control volume, respectively.

Pressure build-up in a rigidly constrained volume can be expressed by the following hydraulic capacitance term:

$$C_{h,line} = \frac{V}{K} \tag{4}$$

where $C_{h,line}$ is the hydraulic capacitance for the hydraulic line, V is the control volume, and K is the bulk modulus of the hydraulic oil.

The hydraulic capacitance of the accumulator can be derived based on a polytropic process assumption. Figure 12 shows the pressure and volume diagram of the accumulator based on the polytropic process. From the polytropic process equation, the hydraulic capacitance in the accumulator is obtained as follows:

$$C_{h,acc} = \frac{V_0}{n}\left(\frac{p_0}{p^{n+1}}\right)^{\frac{1}{n}} \tag{5}$$

where $C_{h,acc}$ is the hydraulic capacitance for the accumulator, V_0 is the initial gas volume, n is the polytropic coefficient, p_0 is the precharge pressure, and p is the current system pressure.

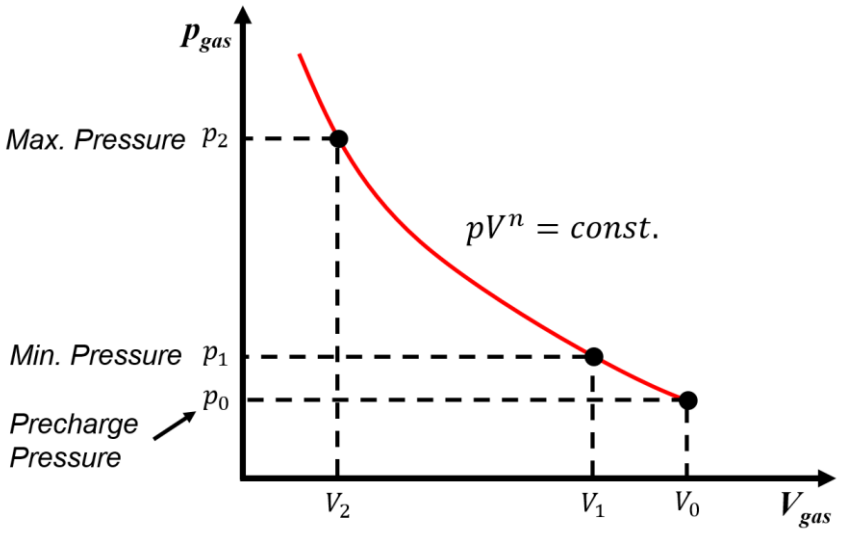

Figure 12. Pressure and volume diagram of the accumulator based on the polytropic process.

For the pressure build-up of the hydraulic line, the flow rates through the valves in the system also need to be modeled. The valves in the system can be modeled by using the orifice equation. Figure 13 shows the hydraulic circuit symbols of the check valve and pressure relief valve with parameter notations.

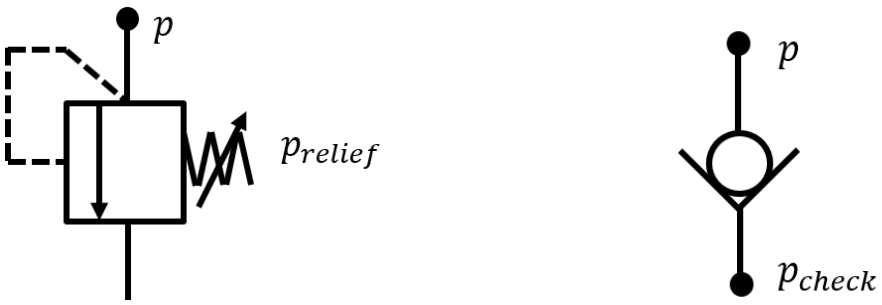

(a) (b)

Figure 13. Hydraulic circuit symbols of valves, (a) pressure relief valve and (b) check valve.

For pressure relief valves, when the inlet pressure exceeds the valve's set pressure, the valve opens allowing flow thereby limiting pressure. Flow through a relief valve can be described as follows:

$$Q_{relief} = \begin{cases} C_{relief}\sqrt{p - p_{relief}} & for\ p - p_{relief} > 0 \\ 0 & for\ otherwise \end{cases} \quad (6)$$

where Q_{relief} is the flow rate through the pressure relief valve, C_{relief} is the coefficient for the pressure relief valve, p is the pressure before the pressure relief valve, and p_{relief} is the pressure after the pressure relief valve.

Similarly, check valves can be modeled as follows:

$$Q_{check} = \begin{cases} C_{check}\sqrt{p_{check} - p} & for\ p_{check} - p > 0 \\ 0 & for\ otherwise \end{cases} \quad (7)$$

where Q_{check} is the flow rate through the check valve, C_{check} is the coefficient for the check valve, p_{check} is the pressure before the check valve, and p is the pressure after the check valve.

3.3 Thermal Model

The system temperature can be calculated based on the flow rate and pressure data from the hydraulic system model. The energy rate balance of each hydraulic component can be determined based on the first law of thermodynamics. In the modeling, we separated the overall hydraulic system into several control volumes and energy rate balance in each control volume is calculated during thermal modeling. Compressible flow is considered for the governing equation to improve the accuracy of the model, while most previous studies consider the fluid as incompressible.

Figure 14 shows the block diagram of the energy rate balance in a control volume used in this study. For the unsteady open system, the total energy variation can be expressed by three physical terms. The first term is determined by the mass flow rate and enthalpy. The second term is the work done by the system such as shaft work and volumetric work. The last term is the heat term, which includes convection, conduction, and radiation in the system. The energy rate balance in the control volume is utilized to determine the temperature rate of the control volume.

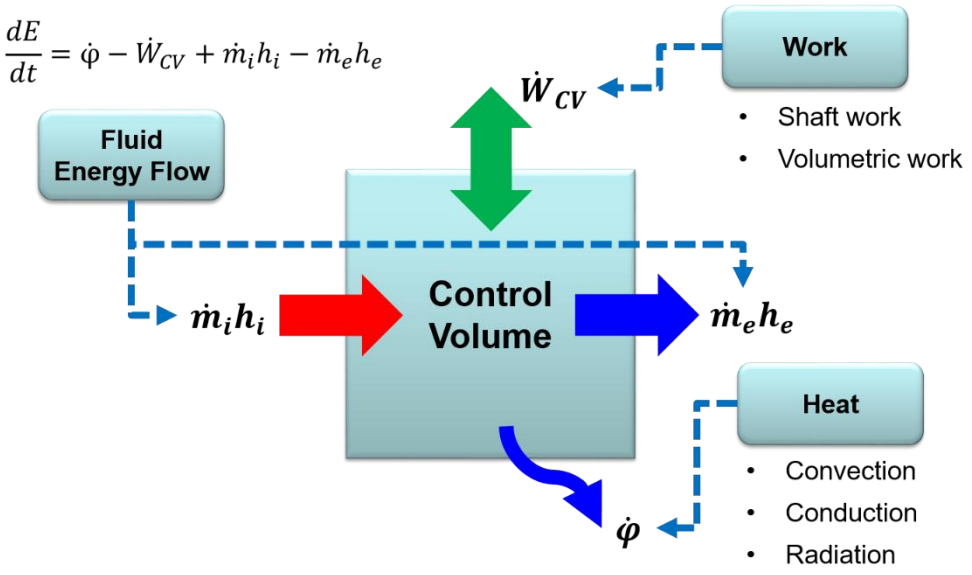

Figure 14. Block diagram of the energy rate balance in a control volume.

3.3.1 Governing Equations

The governing equation can be derived from the first law of thermodynamics for an open system in the unsteady state, with the assumption that there is no variation in the kinetic and potential energy, which can be written as follows (Moran et al. 2010):

$$\frac{dU}{dt} = \dot{\varphi} - \dot{W}_{CV} + \dot{m}_i h_i - \dot{m}_e h_e \tag{8}$$

where U is the internal energy, t is the time, φ is the heat, W_{CV} is the work done by control volume, m is the mass, h is the specific enthalpy, and the dot on the parameter means the derivatives of the variable with respect to time.

The governing equation of the thermal model is derived from the first law of thermodynamics. The internal energy can be expressed by enthalpy as:

$$U = H - pV \tag{9}$$

where H is the enthalpy, p is the pressure, and V is the volume size of the control volume.

Equation (8) can be organized by replacing internal energy with Equation (9) as:

$$\frac{dh}{dt} = \frac{1}{\rho V}\left[\dot{\varphi} - \dot{W}_{CV} + \dot{m}_i h_i - \dot{m}_e h_e - Vh\frac{d\rho}{dt} - (\rho h - p)\frac{dV}{dt} + V\frac{dp}{dt}\right] \tag{10}$$

where ρ is the density.

The derivative of enthalpy with respect to time can be written as a partial differential equation of density and temperature as follows:

$$\frac{dh}{dt} = \left.\frac{\partial h}{\partial p}\right|_T \frac{dp}{dt} + \left.\frac{\partial h}{\partial T}\right|_p \frac{dT}{dt} \tag{11}$$

The terms in Equation (11) can be expressed as:

$$\left.\frac{\partial h}{\partial p}\right|_T = \frac{1}{\rho} - \beta_T T v \tag{12}$$

$$\left.\frac{\partial h}{\partial T}\right|_p = c_p \tag{13}$$

where v is the specific volume, and c_p is the isobaric specific heat capacity.

Finally, the derivative of temperature with respect to time can be formulated using Equation (10) with constitute equations as follows:

$$\frac{dT}{dt} = \frac{1}{c_p \rho V}\left[\dot{\varphi} - \dot{W}_{CV} + \dot{m}_i h_i - \dot{m}_e h_e - h(\dot{m}_i - \dot{m}_e) + p\frac{dV}{dt} + \beta_T TV\frac{dp}{dt}\right] \tag{14}$$

The derivative of pressure with respect to time yields a partial differential equation of density and temperature as:

$$\frac{dp}{dt} = \left.\frac{\partial p}{\partial \rho}\right|_T \frac{\partial \rho}{dt} + \left.\frac{\partial p}{\partial T}\right|_\rho \frac{\partial T}{dt} \tag{15}$$

where T is the temperature.

The derivative of density with respect to time can be derived from the mass conservation equation. The mass conservation equation is written as follows:

$$\frac{dm}{dt} = \dot{m}_i - \dot{m}_e = V\frac{d\rho}{dt} + \rho\frac{dV}{dt} \tag{16}$$

$$\frac{d\rho}{dt} = \frac{1}{V}\left(\dot{m}_i - \dot{m}_e - \rho\frac{dV}{dt}\right) \tag{17}$$

From the definition of the bulk modulus and thermal expansion coefficient, pressure derivative terms in Equation (15) can be replaced with the following equations as:

$$K = \rho \frac{\partial p}{\partial \rho}\Big|_T \tag{18}$$

$$\beta_T = \frac{1}{V}\frac{\partial V}{\partial T}\Big|_p \tag{19}$$

$$\frac{\partial p}{\partial \rho}\Big|_T = \frac{K}{\rho} \tag{20}$$

$$\frac{\partial p}{\partial T}\Big|_\rho = \beta_T K \tag{21}$$

where K is the bulk modulus, and β_T is the volumetric thermal expansion coefficient.

The derivative of pressure with respect to time becomes:

$$\frac{dp}{dt} = \frac{K}{\rho V}\left(\dot{m}_i - \dot{m}_e - \rho\frac{dV}{dt}\right) + \beta_T K \frac{\partial T}{dt} \tag{22}$$

The derivative of pressure with respect to time in Equation (14) can be replaced with Equation (22), and therefore, the derivative of temperature with respect to time yields:

$$\frac{dT}{dt} = \frac{1}{V\left(c_p\rho - \beta_T^2 KT\right)}\Big[\dot{\varphi} - \dot{W}_{CV} + \dot{m}_i h_i - \dot{m}_e h_e + \left(\frac{\beta_T KT}{\rho} - h\right)(\dot{m}_i - \dot{m}_e) + (p - \beta_T KT)\frac{dV}{dt}\Big] \tag{23}$$

The governing equation describing the derivative of temperature with respect to time can be simplified differently for each control volume of the thermal model according to the different assumptions and working conditions.

- *Pump and Motor*

Hydraulic pumps and motors are the main heat source of the hydraulic system. The heat is generated due to the power losses occurring within the real working process of the pump or motor. The internal energy of the hydraulic unit is increased due to the power losses while transferring energy, and finally, increase of the internal energy results in increase of the temperature.

For hydraulic units, the control volume can be assumed as constant. Figure 15 shows the energy flow diagram for hydraulic units. The figure (a) shows the main unit of the system which is generally connected to the engine and works as a pump. The figure (b) is the diagram for the motor, which transfers fluid power to the mechanical work. The derivative of temperature with respect to time becomes:

$$\frac{dT}{dt} = \frac{1}{V\left(c_p\rho - \beta_T^2 KT\right)}\left[\dot{\varphi} - \dot{W}_{CV} + \dot{m}_i h_i - \dot{m}_e h_e + \left(\frac{\beta_T KT}{\rho} - h\right)(\dot{m}_i - \dot{m}_e)\right] \qquad (24)$$

In the hydraulic pumps and motors, the work term expresses the mechanical shaft work and it can be calculated by flow rate and differential flow as follows:

$$\dot{W}_s = Q\Delta p \qquad (25)$$

where W_s is the shaft work in the hydraulic unit.

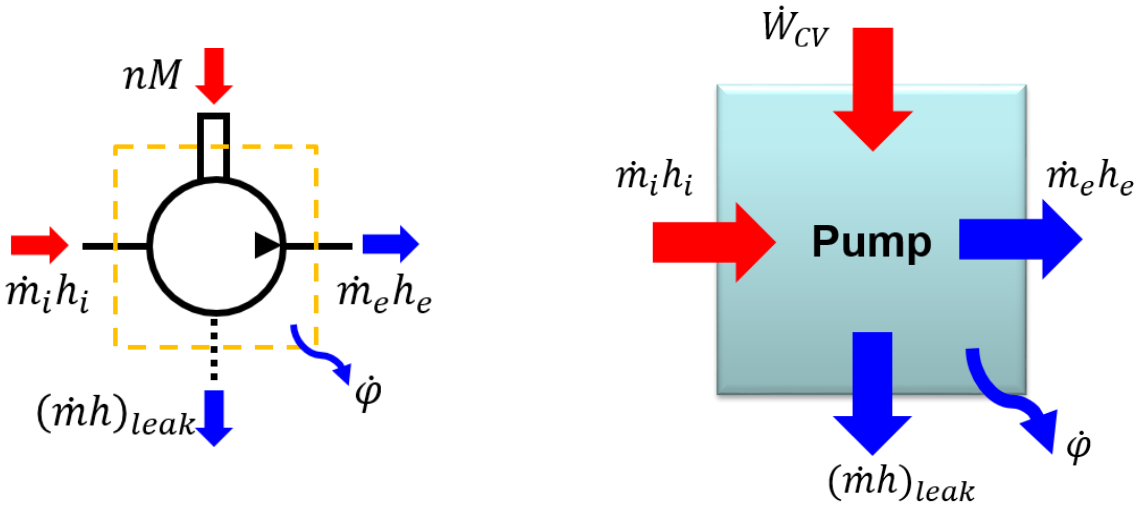

(a)

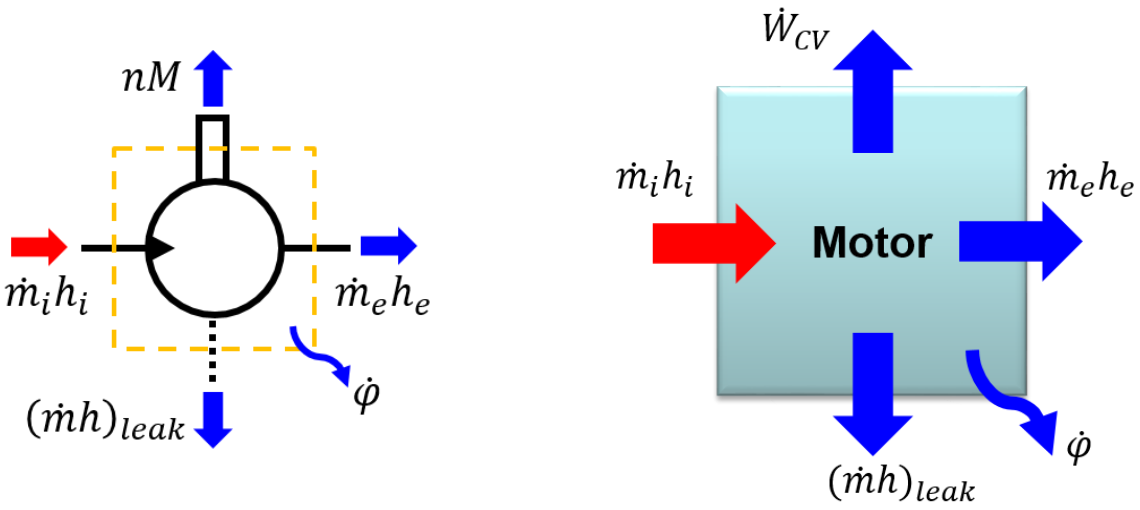

(b)

Figure 15. Energy flow diagram for hydraulic units, (a) pump and (b) motor

- *Accumulator*

For the hydraulic accumulators, the energy is stored in the compressed gas through the volumetric work. Figure 16 shows the energy flow diagram for hydraulic accumulators. The work term in the governing equation expresses volumetric work by the moving boundaries. The volumetric work can be obtained from the pressure and the derivative of the volume with respect to time as follows:

$$\dot{W}_v = p\frac{dV}{dt} \tag{26}$$

where W_v is the volumetric work done by the accumulator. In the governing equation, the term for the volumetric work is compensated with one of the term in Equation (23). The derivative of temperature with respect to time can be obtained as follows:

$$\frac{dT}{dt} = \frac{1}{V\left(c_p\rho - \beta_T^2 KT\right)}\left[\dot{\varphi} + \dot{m}_i h_i - \dot{m}_e h_e - h(\dot{m}_i - \dot{m}_e) + \frac{\beta_T KT}{\rho}V\frac{d\rho}{dt}\right] \tag{27}$$

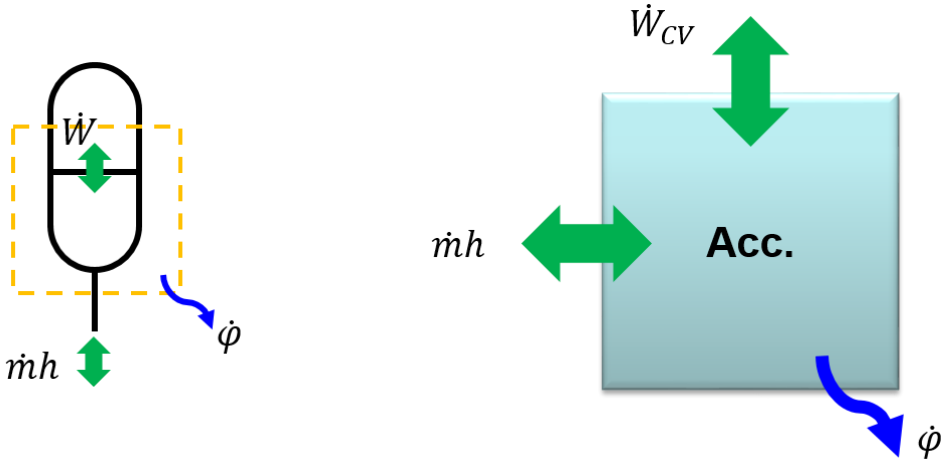

Figure 16. Energy flow diagram for the accumulator.

- *Hydraulic Line*

For the hydraulic pipelines, Figure 17 shows the energy flow diagram. The derivative of temperature with respect to time for the pipeline, assuming that there is no volume change and work done by the control volume, becomes:

$$\frac{dT}{dt} = \frac{1}{V\left(c_p\rho - \beta_T^2 KT\right)}\left[\dot{\varphi} + \dot{m}_i h_i - \dot{m}_e h_e + \left(\frac{\beta_T KT}{\rho} - h\right)(\dot{m}_i - \dot{m}_e)\right] \tag{28}$$

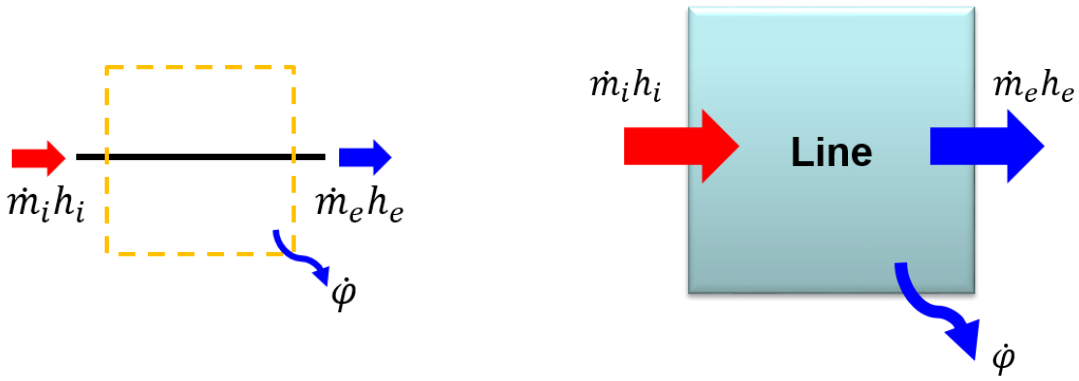

Figure 17. Energy flow diagram for the hydraulic line.

- *Reservoir*

In simulation, the reservoir pressure can be assumed to be constant volume. Figure 18 shows the energy flow diagram for the reservoir. The derivative of reservoir temperature with respect to time becomes then:

$$\frac{dT}{dt} = \frac{1}{c_p\rho V}[\dot{\varphi} + \dot{m}_i h_i - \dot{m}_e h_e - h(\dot{m}_i - \dot{m}_e)] \tag{29}$$

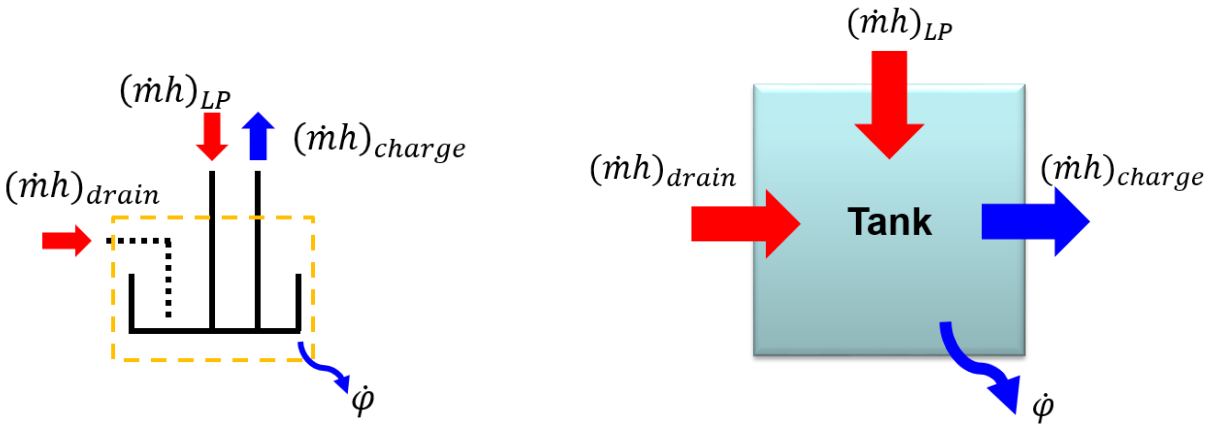

Figure 18. Energy flow diagram for the reservoir.

- *Cooler*

For the cooler, the heat transfer is predicted by a function of the flow rate through the cooler since it is difficult to predict the nonlinear behavior of the heat transfer by using the lumped parameter model due to its complex geometry. Figure 19 shows the energy flow diagram for a cooler. It is assumed that the heat transfer coefficient is a function of the flow rate as follows:

$$k_{cooler} = f(Q_{cooler}) \tag{30}$$

where k_{cooler} is the heat transfer coefficient of the cooler, Q_{cooler} is the flow rate of hydraulic oil through the cooler. The function can be assumed based on the empirical data for the cooling capacitance of the coolers from the manufacturers.

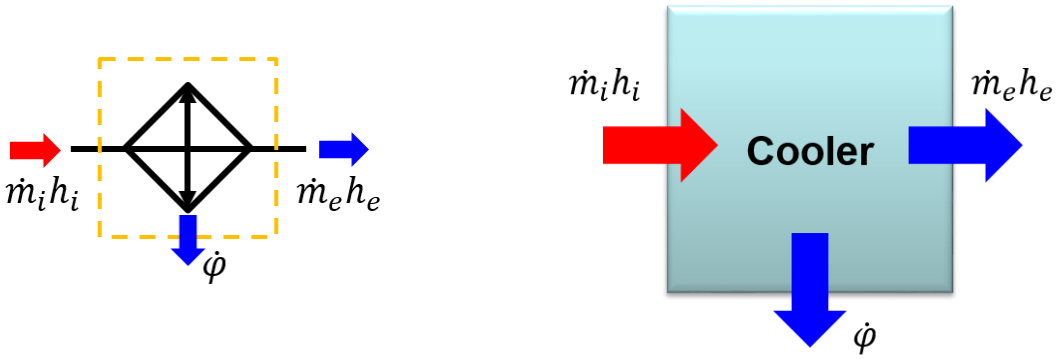

Figure 19. Energy flow diagram for the cooler.

3.3.2 Calculation of Heat Transfer

The heat release term in the governing equation can be calculated from the heat transfer relations. Figure 20 shows the schematic of heat transfer through the pipeline wall. The heat transfer coefficient between hydraulic oil and ambient air can be calculated using a lumped parameter heat transfer model as:

$$\dot{\varphi} = \frac{\Delta T}{R_{eq}} \tag{31}$$

$$R_{eq} = R_1 + R_2 + R_3 \tag{32}$$

$$R_1 = \frac{1}{h_{in} A_{in}} \tag{33}$$

$$R_2 = \frac{\ln\left(\frac{d_0}{d_i}\right)}{2\pi l_{pipe} k} \tag{34}$$

$$R_3 = \left(\frac{1}{h_{out} + h_{rad}}\right)\frac{1}{A_{out}} \tag{35}$$

where R_{eq} is the total equivalent thermal resistance between the hydraulic oil and ambient air, R_1 is the thermal resistance between the hydraulic oil and the inside of the wall, R_2 is the thermal resistance between the inside and outside of the wall, R_3 is the thermal resistance between the outside wall and ambient air, h_{in} is the convection coefficient of the inside wall, A_{in} is the area of the inside wall, d_0 is the diameter to the outside wall, d_i is the diameter to the inside wall, l_{pipe} is the length of the pipe, k is the thermal conductivity of the wall, h_{out} is the convection coefficient of the outside wall, h_{rad} is the radiation coefficient of the outside wall, and A_{out} is the area of the outside wall. The radiation effect is neglected in the thermal model since its contribution is very minor within the temperature range of the system. The thermal conductivity of steel is used for the wall conductivity.

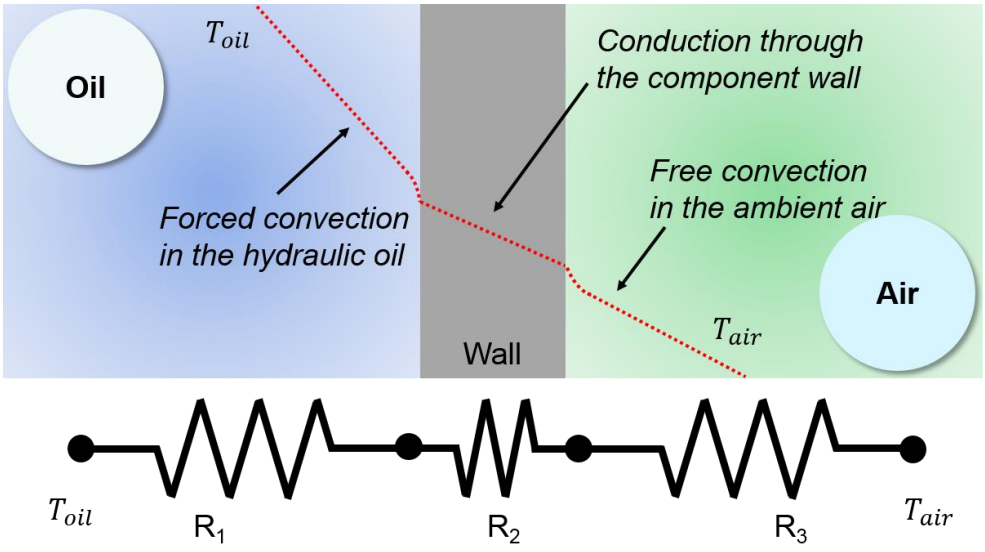

Figure 20. Schematic of heat transfer through the pipeline wall.

The convection coefficient can be calculated from Nusselt number. Table 1 shows the equations for the Nusselt number, which is used for calculating the convection coefficient (Boetcher 2014; Churchill and Chu 1975; Sparrow and Stretton 1985; Stephan et al. 2014). The dimensionless numbers can be defined as follows:

$$Nu = \frac{hL}{k} \tag{36}$$

$$Re = \frac{\rho u L}{\mu} \tag{37}$$

$$Pr = \frac{c_p \mu}{k} \tag{38}$$

$$Gr = \frac{g\beta(T_s - T_\infty)L^3}{\nu^2} \tag{39}$$

where Nu is the Nusselt number, Re is the Reynolds number, Pr is the Prandtl number, and Gr is the Grashof number. For the inside wall, the convection process is assumed as a forced convection, and the flow is considered transiting to the turbulent flow when the Reynolds number is 2300. For the outside wall, the convection is considered as a free convection process and the shapes of components are assumed as simple geometries such as cylinder and cubic. Heat transfer for each control volume of the hydraulic components is calculated using the thermal resistance with the heat transfer coefficients as described in the previous pages.

Table 1. Equations for Nusselt number used for the calculation of the convection coefficient (Boetcher 2014; Churchill and Chu 1975; Sparrow and Stretton 1985; Stephan et al. 2014).

Forced convection

Laminar flow: ($Re < 2300$)

$$Nu = \left(3.66^3 + 0.7^3 + \left[1.615\sqrt[3]{Re \cdot Pr \cdot d_i/L} - 0.7\right]^3\right)^{\frac{1}{3}} \left(\frac{Pr}{Pr_w}\right)^{0.11}$$

Turbulent flow: ($Re > 2300$)

$$Nu = \frac{\frac{(Re - 1000)Pr}{8(1.82\log(Re) - 1.64)^2}\left[1 + \left(\frac{d_i}{L}\right)^{\frac{2}{3}}\right]}{1 + 12.7\left(Pr^{\frac{2}{3}} - 1\right)\sqrt{0.125(1.82\log(Re) - 1.64)^{-2}}} \left(\frac{Pr}{Pr_w}\right)^{0.11}$$

Free Convection

Cylinder shape:

$$Nu = \left(0.6 + 0.387\left[Gr \cdot Pr\left(1 + \left(\frac{0.559}{Pr}\right)^{\frac{9}{16}}\right)^{-\frac{16}{9}}\right]^{\frac{1}{6}}\right)^2$$

Cube shape:

$$Nu = 5.748 + 0.752\left(\frac{Pr \cdot Gr}{\left[1 - \left(\frac{0.492}{Pr}\right)^{\frac{9}{16}}\right]^{\frac{16}{9}}}\right)^{0.252}$$

3.3.3 Thermal Properties of Materials

Thermal properties of materials like steel and air used in this research can be taken from reference (Incropera and DeWitt 2001). Properties of the HLP32 hydraulic oil, such as specific heat, thermal conductivity, kinematic viscosity can be obtained from reference (Oppermann 2007).

Table 2. Constants for the hydraulic oil (Oppermann 2007).

Description	Parameter	Value
Specific heat	c_0	1807 [J kg^{-1} K^{-1}]
	c_1	4.21 [J Kg^{-1} K^{-2}]
Thermal conductivity	k_0	0.135 [W K^{-1} m^{-1}]
	k_1	7.35E-05 [W K^{-2} m^{-1}]
Bulk modulus	a	0.0733
	b	999.93 [bar]
Thermal expansion coefficient	β_T	7.00E-04 [K^{-1}]

Temperature dependent coefficients can be calculated with temperature dependent equations as follows:

$$c_p = c_0 + c_1 T \tag{40}$$

$$k = k_0 + k_1 T \tag{41}$$

where c_p is the isobaric specific heat, k is the thermal conductivity, and subtitles 0 and 1 mean the constants for the constant part and temperature-dependent part, respectively. Also, bulk modulus of the HLP32 hydraulic oil can be obtained as (Sprengel 2015):

$$K = (p + b)\left[\frac{1}{a} - \ln\left(1 + \frac{p}{b}\right)\right] \quad (42)$$

where K is the bulk modulus and a and b are the constants based on empirical data. Table 2 shows the temperature-dependent coefficients of the hydraulic oil used in the modeling.

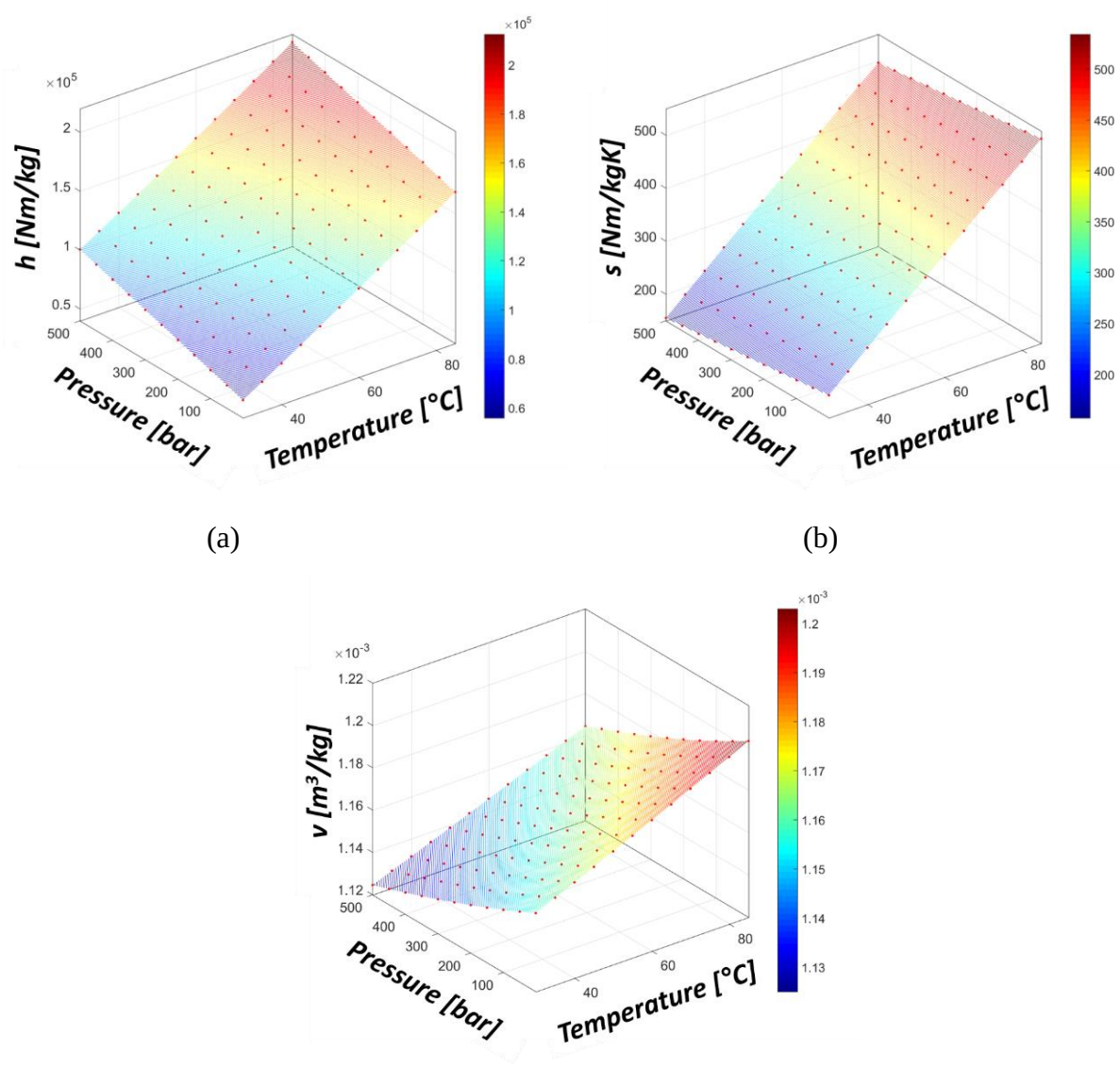

(a) (b)

(c)

Figure 21. Graphs of oil properties in terms of temperature and pressure, (a) specific enthalpy, (b) specific entropy, and (c) specific volume

The enthalpy and entropy of the hydraulic oil can be calculated as a function of temperature and pressure as follows (Oppermann 2007):

$$h = h_0(T_0) + \int_{T_0}^{T} c_p(T)dT + \int_{p_0}^{p} \left[v - T\left(\frac{\partial v}{\partial T}\right)_p \right] dp \tag{43}$$

$$s = s_0(T_0) + \int_{T_0}^{T} \frac{c_p(T)}{T} dT - \int_{p_0}^{p} \left(\frac{\partial v}{\partial T}\right)_p dp \tag{44}$$

where s is the specific entropy. Figure 21 shows the graphs oil properties in terms of the temperature and pressure. Properties of the hydraulic oil like enthalpy and density are stored in the program by lookup tables as a function of temperature and pressure.

3.3.4 Parameter Switching Scheme

A novel method, the parameter switching scheme, is suggested for the thermal model in order to capture the rapid temperature variation of each control volume with the open system under unsteady state conditions. The parameter switching scheme is motivated from the upwind scheme, which is a numerical discretization method considering the flow direction. In previous thermal studies on hydraulic systems by a thermodynamic approach, the input and output parameters of each control volume are determined by the location of each control volume, not by varying flow direction. In the parameter switching scheme, the direction of flow is utilized for determining the inlet and outlet parameters during the calculation of the system temperature of each control volume.

Figure 22 shows the parameter switching scheme for the control volumes considering varying flow directions. In the figure, u_{CV} is the parameter of the control volume, u_1 is the

parameter of the left side source of the control volume, u_2 is the parameter of the right side source of the control volume, $u_{CV,1}$ is the parameter of the left port of the control volume, $u_{CV,2}$ is the parameter of the right port of the control volume and v is the velocity of the flow. The parameters of the hydraulic oil and materials are determined based on the lookup tables from the reference. When the flow direction is from left to right, the parameters of each control volume are determined by the properties from the left side. On the other hand, the parameters are decided by the properties from the right side with the flow direction from right to left. Thus, the parameters for the numerical simulation in the control volumes are changed according to the direction of the flow, even though the location is still same. This novel scheme makes the model possible to describe successfully the rapid thermal transient in the hydraulic system, which could not be described by the previous studies. The results from the novel scheme are applied to the governing equation, which is derived for the compressible flow, to calculate the system temperature.

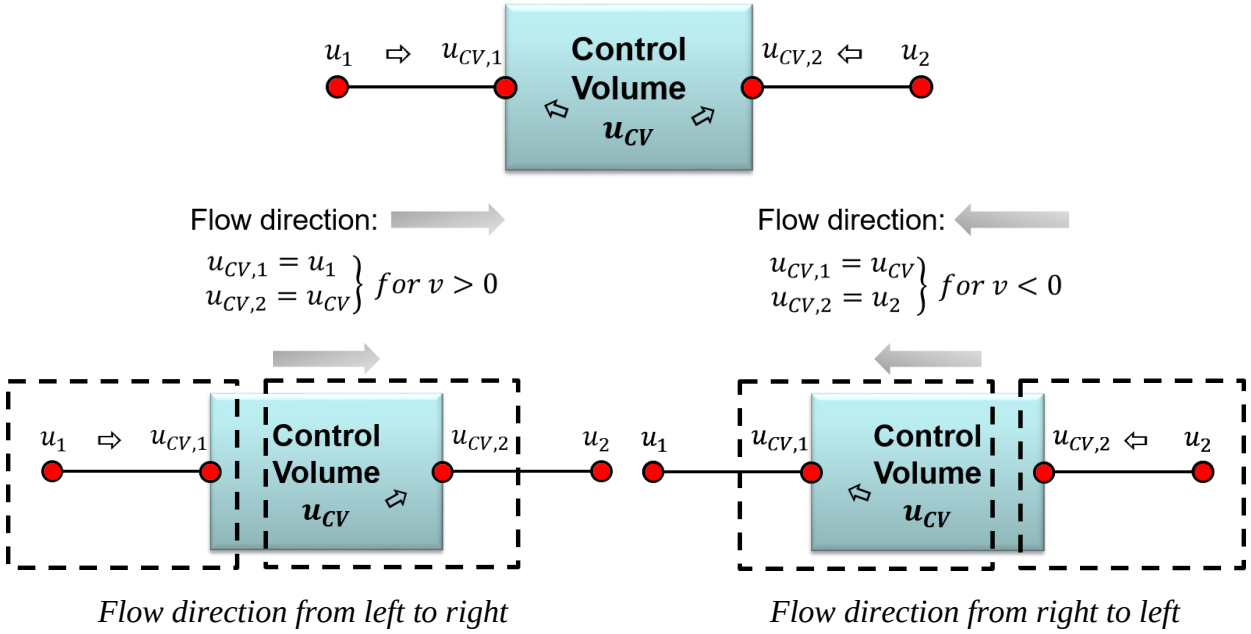

Figure 22. Parameter switching scheme for the control volumes considering varying flow directions

3.4 Other Models

3.4.1 System Control

Different control strategies can be applied to different transmission architectures. The sequential control is mainly utilized for the hydrostatic transmission. In the sequential control, first, the displacement of Unit 1 is adjusted while the displacement of Unit 2 is maintained with the full displacement. If the displacement of Unit 1 reaches 100% or -100%, the displacement of Unit 2 is adjusted according to the extent of the velocity error signal from the PID controller. Figure 23 shows an example case of the sequential control for the hydrostatic transmission.

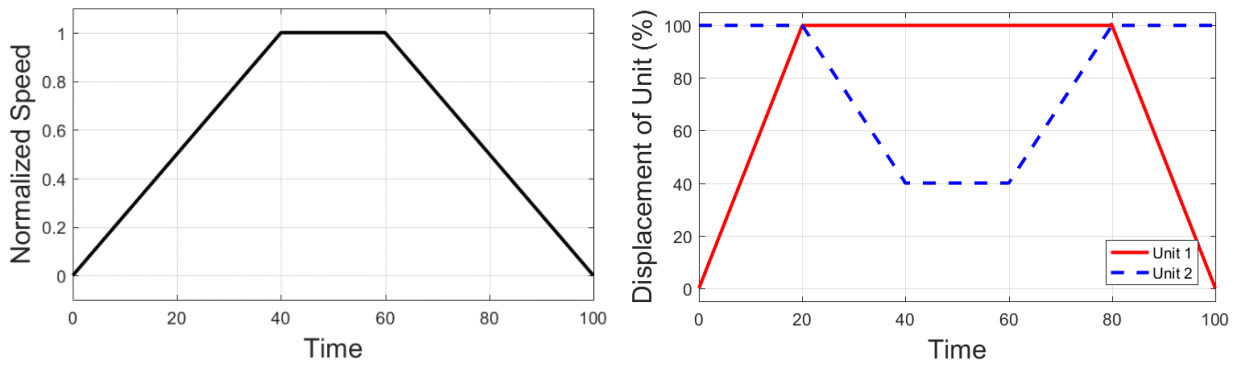

Figure 23. Sequential control for the hydrostatic transmission.

Another control method is the secondary control, which is mainly applied to HHTs. In the secondary control, first, the displacement of the secondary unit is determined based on the torque on a driveline shaft. Then, the displacement of the main unit is adjusted in order to maintain the system pressure according to the torque. The series HHT is controlled by the secondary control to manage the pressure of the accumulator while driving and braking. In this study, a novel HHT,

which utilizes both hydrostatic and hybrid modes, is controlled by both sequential and secondary control methods.

3.4.2 Engine Model

The engine model is utilized for describing the engine dynamics. In the model, the speed variation rate can be calculated from the following equation:

$$\dot{n}_e = \frac{1}{J_e}\left[\frac{u_{CE}}{100}\left(M_{WOT} + M_f\right) - M_f - M_L\right] \quad (45)$$

where n_e is the speed of the engine, J_e is the engine rotational inertia, u_{CE} is the normalized throttle input, M_{WOT} is the wide open throttle (WOT) torque, M_f is the torque loss due to the friction, and M_L is the load torque. The torque loss due to the friction is given by:

$$M_f = \frac{V_{eng}}{4 \cdot \pi}(0.05 \cdot {n_e}^2 + 0.15 \cdot n_e + 0.97) \cdot 10^5 \quad (46)$$

where V_{eng} is the displacement volume of the engine.

3.4.3 Vehicle Dynamics

The torque on the wheel and velocity of the vehicle can be obtained from the vehicle dynamics model. Figure 24 shows the free body diagram for the vehicle. The acceleration of the vehicle can be calculated by the force balance equation as follows:

$$F_{tot} = F_t + F_g + F_r + F_D = ma \quad (47)$$

where F_{tot} is the net force applied to the vehicle, F_t is the traction force, F_g is the gravitational force, F_r is the rolling resistance, F_D is the aerodynamic drag, a is the acceleration of the vehicle,

and m is the mass of the vehicle. The traction force, gravitation force, rolling resistance, and aerodynamic drag can be obtained from the following equations:

$$F_t = \frac{M_w}{r_{dyn}} \tag{48}$$

$$F_g = -mg\sin\theta \tag{49}$$

$$F_r = -C_r \cdot mg\cos\theta \tag{50}$$

$$F_D = -\frac{1}{2}\rho A_f C_d v^2 \tag{51}$$

where M_w is torque loaded on the wheel, r_{dyn} is the wheel dynamic radius, g is the gravitational acceleration, θ is the angle of the slope, C_r is the rolling resistance coefficient, ρ is the density of the air, A_f is the frontal area of the vehicle, C_d is the drag coefficient, and v is the speed of the vehicle. Once the acceleration of the vehicle is obtained from the vehicle dynamics model, the velocity of the vehicle is calculated by the integral of the acceleration.

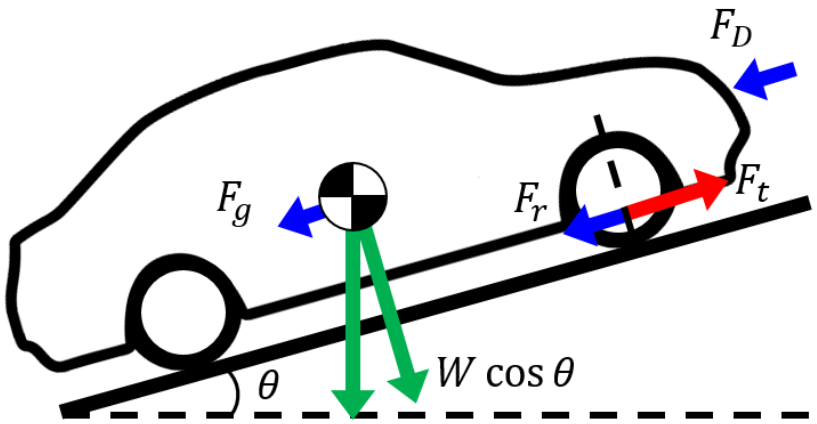

Figure 24. Free body diagram for the vehicle.

CHAPTER 4. MODELING OF SERIES HYDRAULIC HYBRID TRANSMISSION WITH MEASUREMENT IN THE HARDWARE-IN-THE-LOOP TEST RIG

As described in the previous chapters, HHV system architectures can generally be classified as either series, parallel, or power-split depending upon the way power flows through the system. For the validation of the developed thermal model, a closed circuit series HHV was chosen as it is a common hydraulic hybrid configuration. Additionally, it is sufficiently complex as to allow the findings to be extrapolated to the more advanced hydraulic hybrid architectures such as a power split hydraulic hybrid architecture. Figure 25 shows a general hydraulic circuit for a closed circuit series HHV.

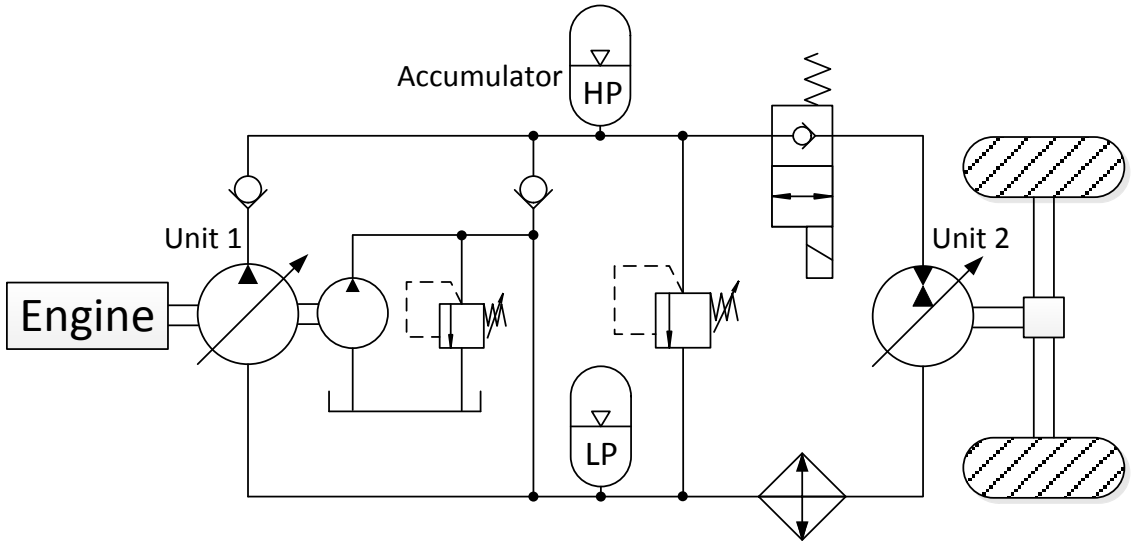

Figure 25. General series hydraulic hybrid system architecture.

Series hybrids consist of a minimum of two positive displacement machines (hydraulic units) connected in series between the engine (Unit 1) and driveline (Unit 2). These hydraulic units, which function as both pumps and motors, convert power between the mechanical and fluid

domains. The volume of fluid they transfer per shaft revolution can be varied by adjusting the displacement between zero and some maximum value. Thus, a continuously variable transmission is formed when at least two of these variable displacement units are placed in series. A hybrid transmission is formed by placing an energy storage device in series between the energy converters. In hydraulic hybrids, energy is stored mechanically in a hydropneumatic accumulator where highly pressurized nitrogen gas is further compressed by additional oil entering the device. Storing mechanical energy in this manner, rather than chemically as occurs in the batteries of HEVs, is one of the principle reasons that HHVs can rapidly store all of the kinetic energy recovered during regenerative braking.

4.1 Main Operating Modes

Series HHVs may operate in several different modes while driving and braking. The process begins with Unit 1 converting mechanical power from the engine into the fluid domain. This power may then be immediately converted by Unit 2 to mechanical power applied to the driveline for driving, stored in the accumulator for future use, or some combination of the two. Alternatively, the entire power required by Unit 2 for driving may be supplied by the accumulator. During regenerative braking, Unit 2 moves over-center resulting in the direction of the fluid flow reversing. Now instead of consuming fluid from the hydraulic system and functioning as a motor, Unit 2 begins pumping fluid into the hydraulic system. In this way, Unit 2 converts mechanical power from the driveline into fluid power enabling the vehicle's kinetic energy to be recovered for future use. Table 3 summarizes the principle modes of operation for a series HHV. Most of these modes are seen to some extent in both the experimental measurements on the test rig, and the simulation detailed in this study.

Table 3. Principle modes of operation for a series HHV.

Mode	Engine	Unit 1	Accumulator	Unit 2	Driveline
1	Idle	Zero Displacement	Idle	Zero Displacement	Idle
2	Motoring	Pumping	Charging	Motoring	Driving
3	Motoring	Pumping	Idle	Motoring	Driving
4	Motoring	Pumping	Discharging	Motoring	Driving
5	Idle	Zero Displacement	Discharging	Motoring	Driving
6	Idle	Zero Displacement	Charging	Pumping	Braking

Figure 26 shows the schematic of the two main operating modes of the series HHV, a driving mode and a braking mode among the principle modes. During the driving mode, Unit 1 works as a pump and Unit 2 works as a motor. The displacements of Unit 1 and Unit 2 maintain positive values while forward driving. During the braking mode, Unit 1 is adjusted to zero displacement and Unit 2 works as a pump to regenerate the energy. The displacement of Unit 2 is over-centered for pumping the flow in the system.

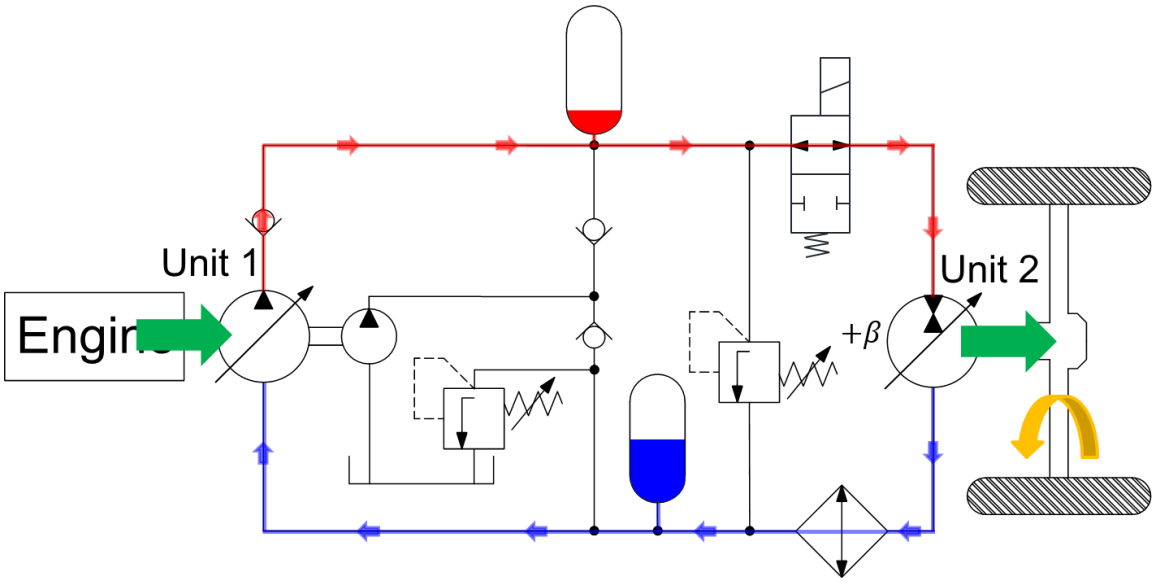

(a)

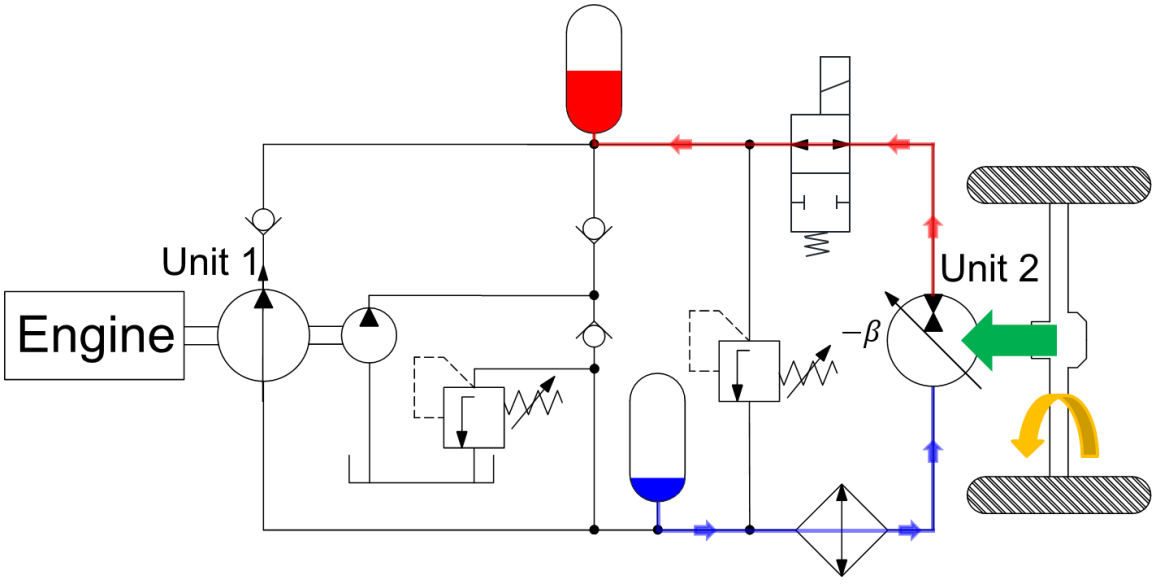

(b)

Figure 26. Schematic of the main operating modes of the series HHV, (a) driving mode and (b) braking mode.

4.2 Hardware-in-the-Loop Evaluation

Both the hydraulic system and thermal models were constructed and validated using experimental data obtained from a hardware-in-the-loop transmission dynamometer. Figure 27 shows the hardware-in-the-loop test rig for a series HHT and Figure 28 shows the hardware-in-the-loop hydraulic circuit of the series HHT. In the test rig, two electric motors replicate the engine and road load dynamics. These electric motors are controlled by a simulation model replicating a vehicle driving the FTP-72 cycle, also known as UDDS cycle, which is a standardized drive cycle for on-road vehicles to compare vehicle performance and efficiency. More information about the FTP-72 cycle can be found from reference (EPA Urban Dynamometer Driving Schedule (UDDS) n.d.). This model captures all relevant transmission loads such as engine torque, inertial loading, aerodynamic drag, and rolling resistance. This test rig closely reproduces the dynamic conditions present in a vehicle such that the transmission behaves just as if it were in a real vehicle. Test data were collected at 100 Hz and then averaged into a 1 Hz data set before being split into individual cycles.

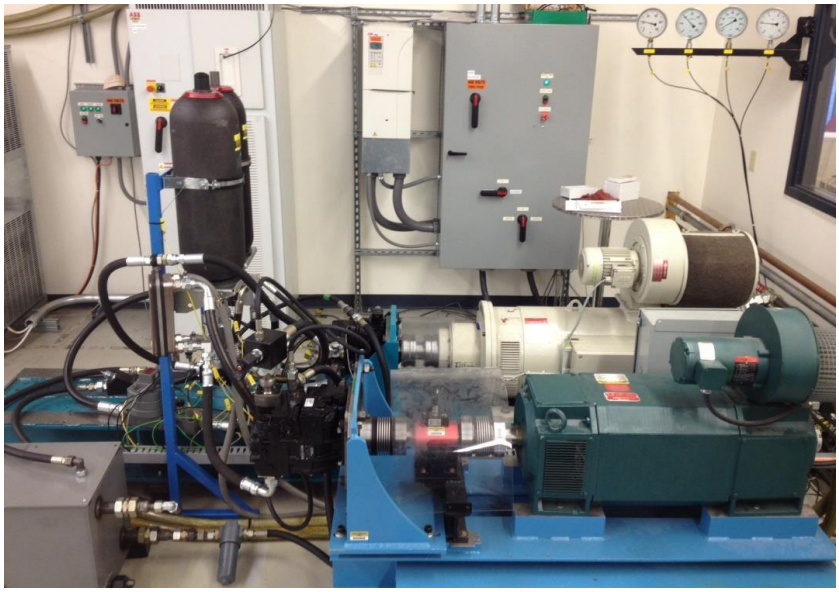

Figure 27. Hardware-in-the-loop test rig for a series HHT.

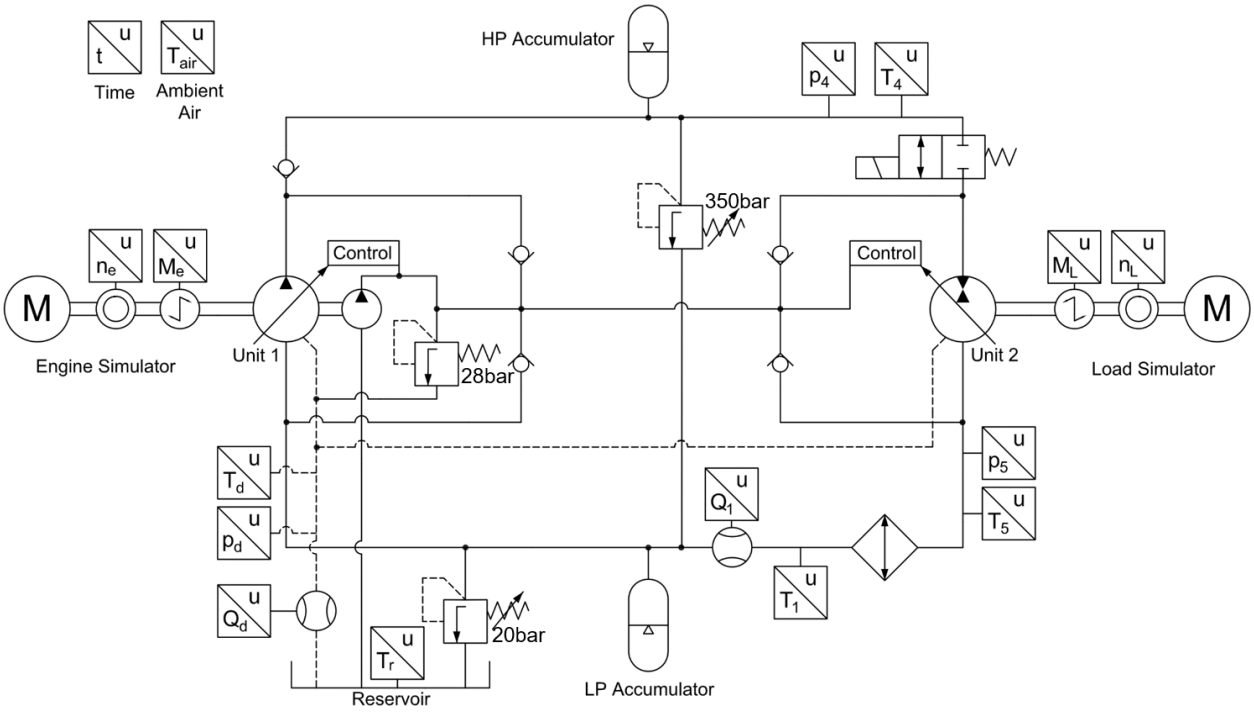

Figure 28. Hardware-in-the-loop hydraulic circuit of the series HHT.

Table 4 shows the transmission components and experimental parameters. For the hydraulic components, two swashplate type variable displacement axial piston machines were used. Unit 1 has a displacement of 42 cc/rev, and Unit 2 has a displacement of 75 cc/rev. The low and high pressure accumulators are bladder type accumulators (20 L each).

Table 4. Transmission components and experimental parameters.

Unit 1	42 cc (Sauer S90)
Unit 2	75 cc (Sauer S90)
Charge Pump	11 cc
HP Accumulator	20 L
LP Accumulator	20 L
HP Accumulator Precharge Pressure	150 bar
LP Accumulator Precharge Pressure	20 bar
Maximum System Pressure	350 bar
Low Pressure Setting	20 bar

The HIL test rig was controlled to follow the FTP-72 driving cycle. Unit 1's displacement was controlled using a simple power management strategy in order to maintain a minimum accumulator pressure of roughly 200 bar. Unit 2's displacement was controlled to provide the tractive torque required to track the FTP-72 driving cycle based on the measured accumulator pressure. Finally, the engine speed was controlled using a rough minimum engine speed strategy such that Unit 1 would operate efficiently at high displacements whenever possible. Figure 29 shows the driving cycle based on FTP-72 used throughout this work.

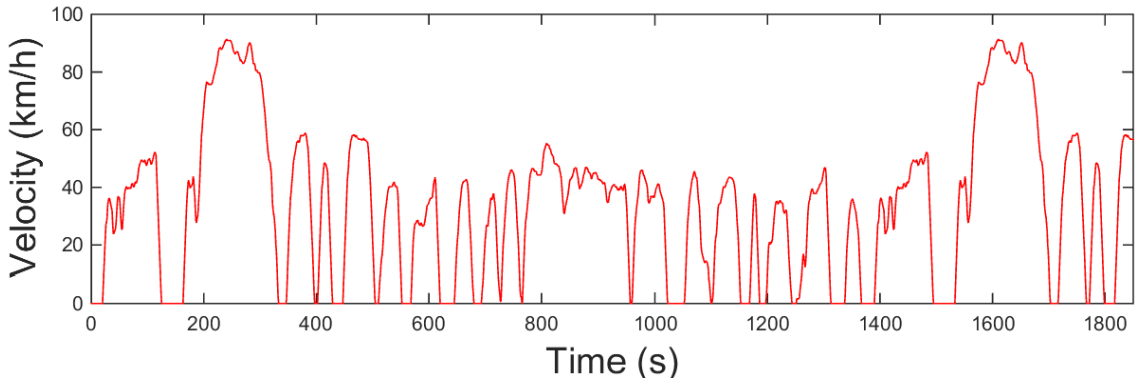

Figure 29. Driving cycle based on FTP-72.

Measurements for the related drive cycles were three times repeated in order to evaluate the reproducibility of the experiment. Figure 30 shows the measured data of the hydraulic system and Figure 31 shows the measured data of the system temperatures. We see that the data for the hydraulic system show a good agreement with each other not only for the overall trend but also absolute values. For the system temperatures, it shows some discrepancy less than 2ºC typically. The temperature in the measurement point has a large discrepancy sometimes around 10ºC due to the rapid transients of the measurement point. The overall trends of the data agree well with each other and it shows an enough reproducibility for the study.

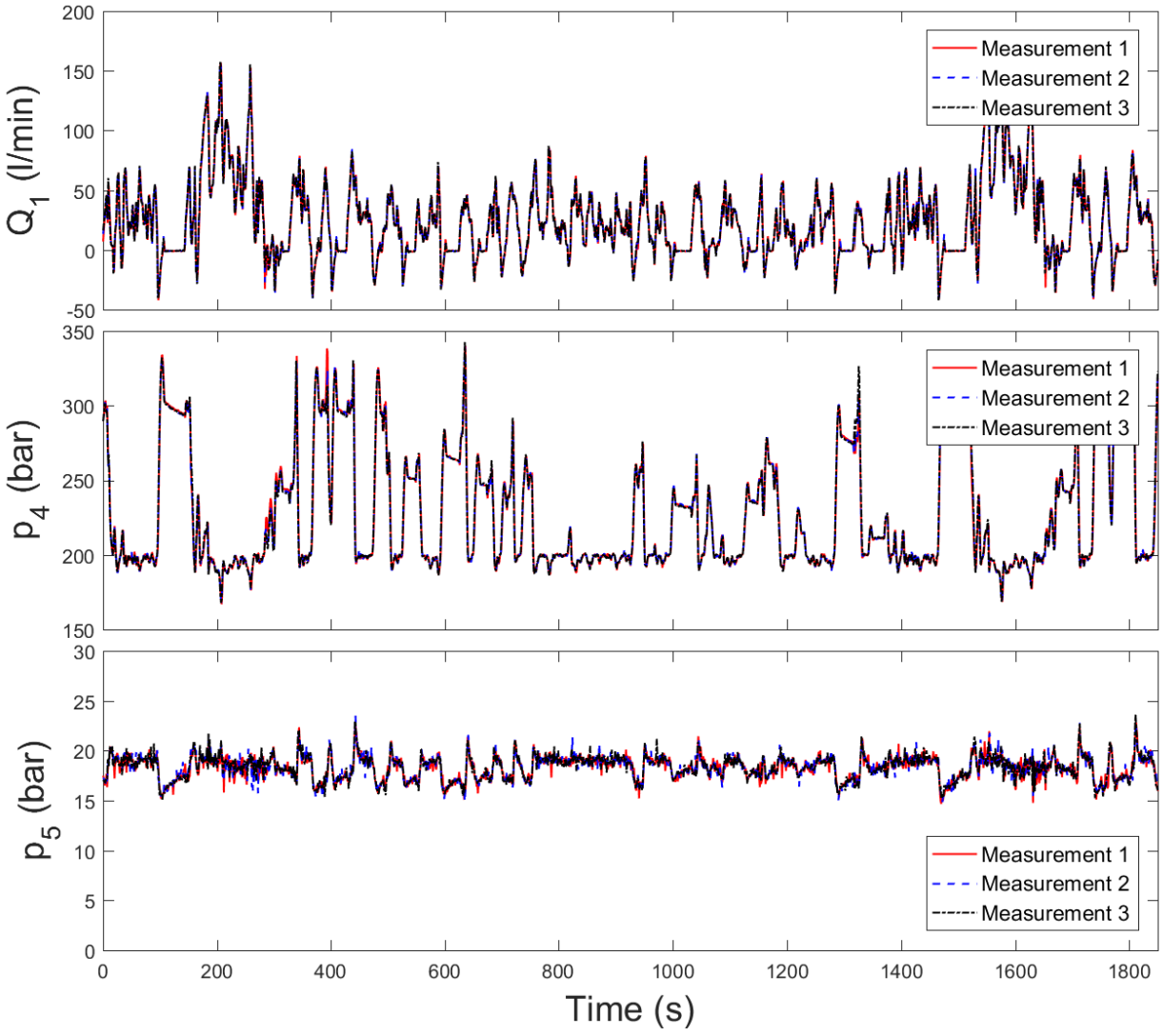

Figure 30. Measured data of the hydraulic system.

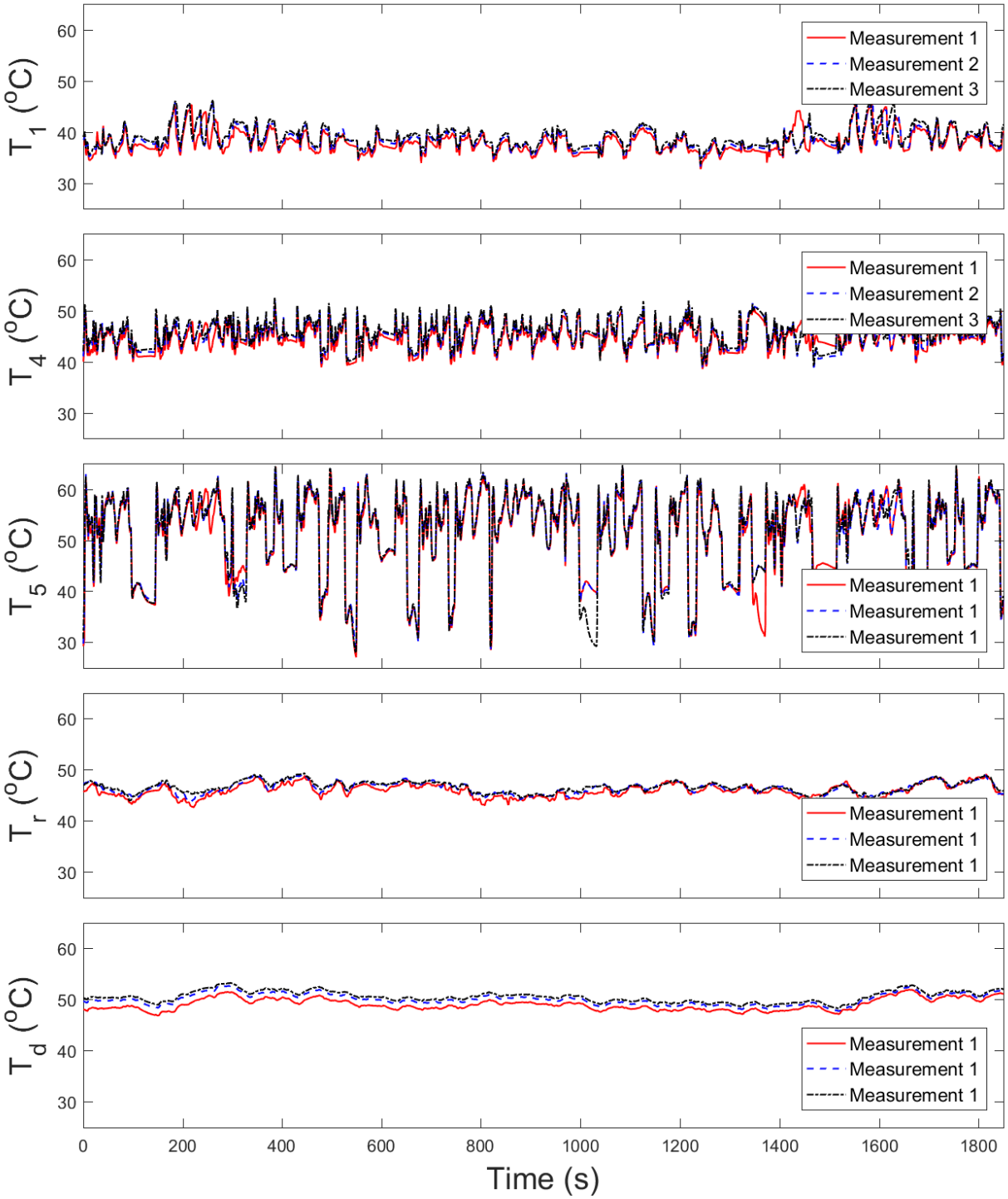

Figure 31. Measured data of the system temperatures.

4.3 Results and Discussion

The hydraulic system was simulated using a backward facing modeling approach. The intent of this model is not to predict how HHVs would perform using this transmission on the FTP-72 cycle, but rather to replicate how the transmission on the HIL test rig functioned during the measurements. Specifically, both Unit 1 and Unit 2 were operated at the same speeds measured on the HIL test rig, Unit 1's displacement was controlled such that the simulated pressure in the high pressure line matched the measured pressure, and Unit 2's displacement was controlled to provide the same flow rate measured with a flowmeter located on the outlet of Unit 2.

Once complete, the hydraulic system model is run over the FTP-72 driving cycle, while pressures and flow rates passing through each component were recorded. Next, the system is divided into a series of thermodynamic control volumes which were then described by lumped parameter thermal models. From here the results from the hydraulic system model are fed into the thermal model and used to predict individual control volume temperatures.

Figure 32 shows the control volumes for the thermal model. The main cycle of the hydraulic system is a quasi-closed system if minor flows are excluded, such as leakage flows from Unit 1 and Unit 2. There are five hydraulic component subsystems in the main closed cycle: Unit 1, Unit 2, the low and high pressure accumulators, and the cooler. Each control volume's temperature is stored every time step and these temperatures are updated at the same rate based on the governing equation derived from the first law of thermodynamics. Finally, results from the thermal model were compared with measured data and then used for further thermal analysis.

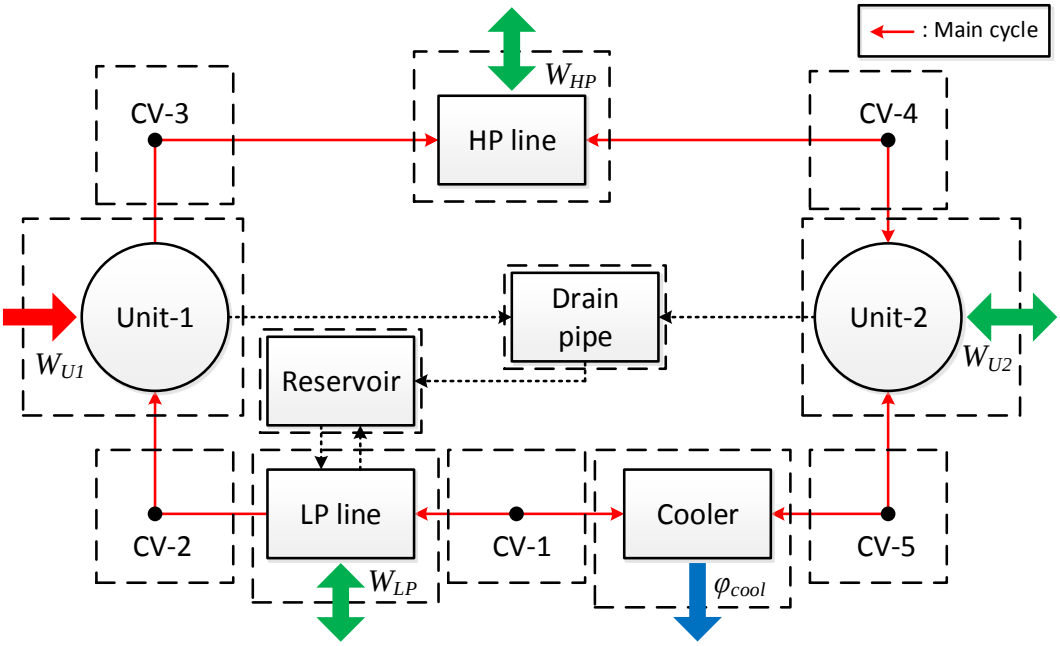

Figure 32. Control volumes for the thermal model.

Simulation results including pressures, flow rates, and temperatures, extracted from the hydraulic and thermal models, were compared and validated against measured data generated on the HIL test rig. Figure 33 shows the results for the hydraulic system model for the pressures in the high and low pressure lines, as well as the volumetric flow rate of Unit 2's low pressure port. The simulated data shows a close agreement with the measured data. This comparison shows that the simulation results are sufficiently accurate to provide confidence in the hydraulic system states predicted by the simulation model.

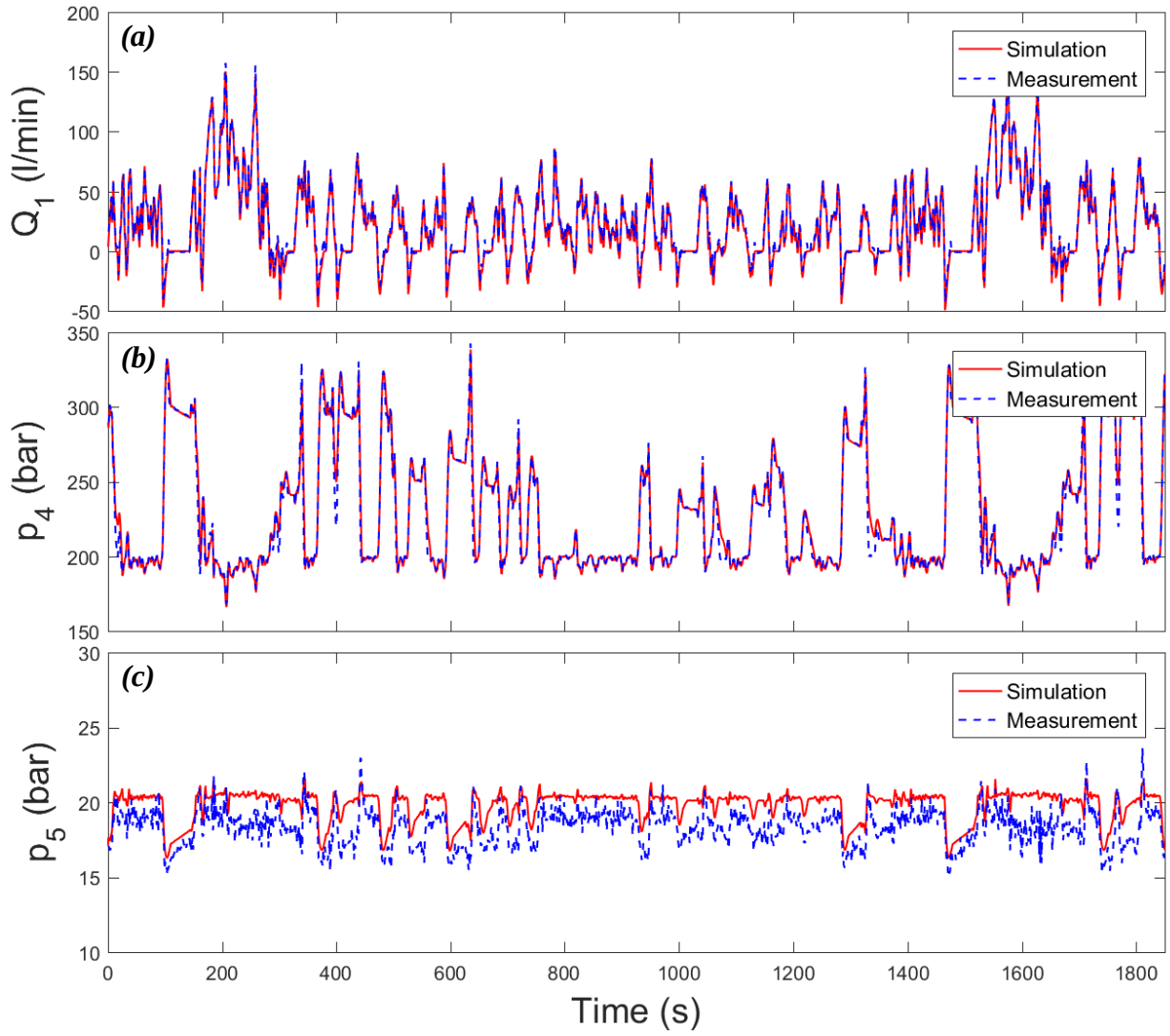

Figure 33. Results for the hydraulic system model, (a) volumetric flow rate in the low pressure line (Q_1), (b) pressure in the high pressure line (p_4), and (c) pressure in the low pressure line (p_5).

For the thermal model, the program has been utilized for two different conditions. First, two measured temperature inputs were used instead of the cooler model. Second, a closed cycle was applied due to the lower accuracy of the cooler model compared to the models for other parts of the system. Figure 34 shows the schematic of the control volumes for the thermal model with two temperature inputs instead of the cooler model and Figure 35 shows the schematic of the control volumes for the thermal model with a closed loop.

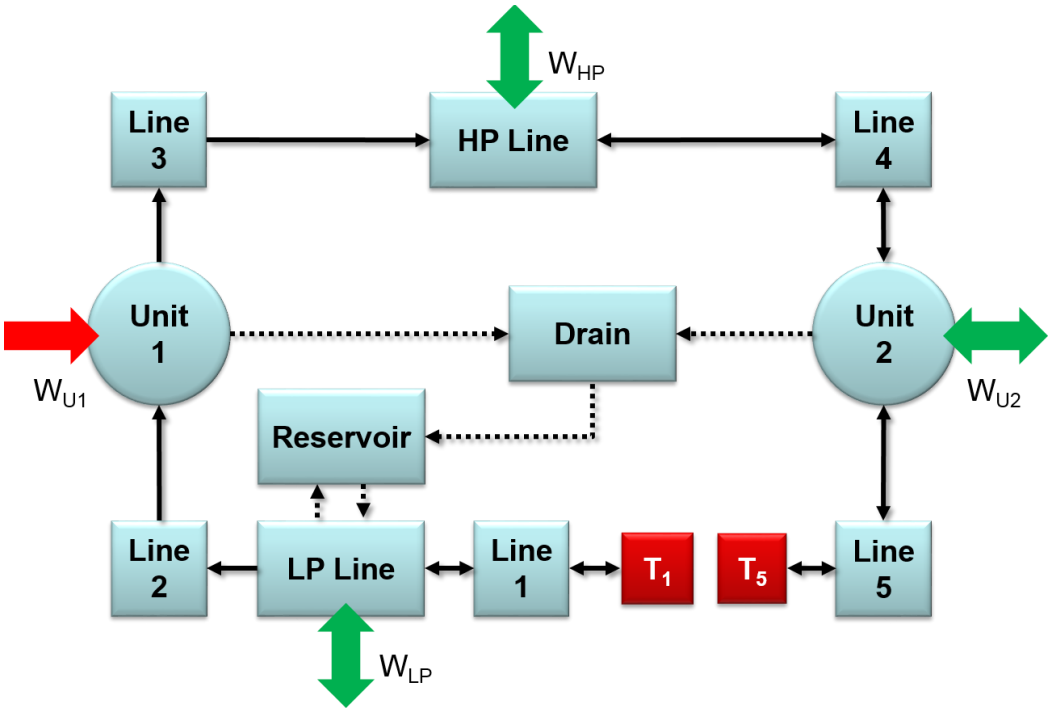

Figure 34. Schematic of the control volumes for the thermal model with two temperature inputs.

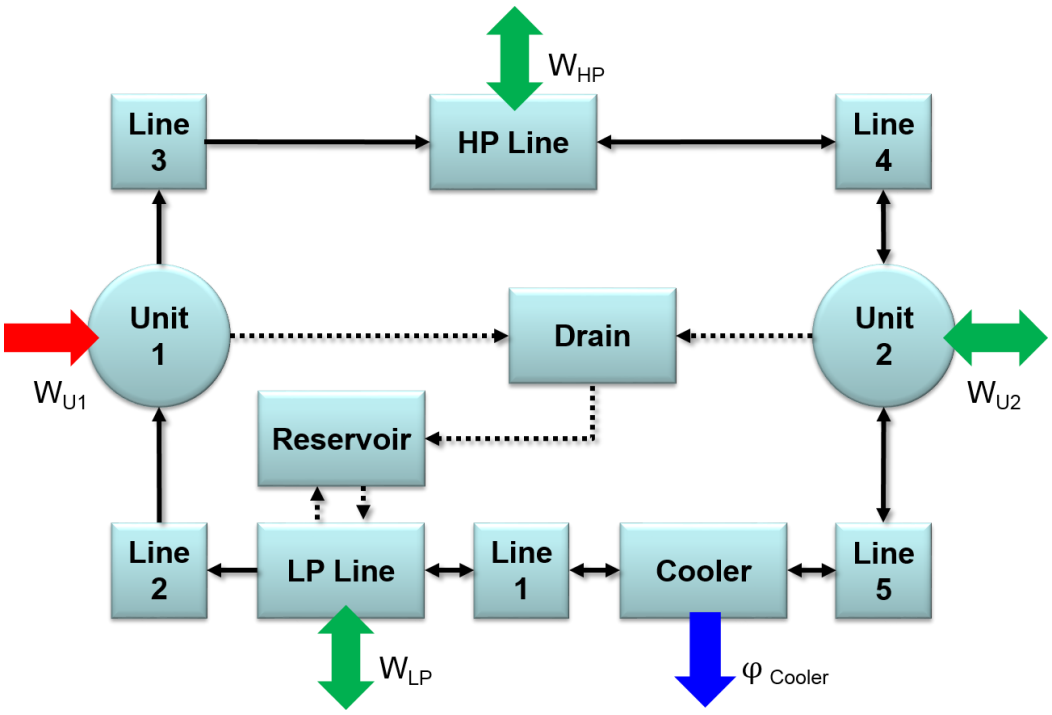

Figure 35. Schematic of the control volumes for the thermal model with a closed loop.

Figures 36 and 37 show the results for the thermal model, with two temperature inputs instead of the cooler model and with a closed cycle, respectively. We see that the temperatures of the control volumes in the main cycle show more fluctuation than the temperatures of the reservoir and drain pipe. The temperature in CV-5 shows larger fluctuation due to the larger temperature difference between the two adjacent control volumes. The temperature in CV-5 becomes low during the regenerative mode due to the flow from the cooler, and it becomes high during the driving mode due to the flow from the CV-4. The results with two measured cooler temperature inputs show a good agreement with the measured data. This indicates that the models for each component, except for the cooler, are sufficiently accurate. While the simulation results with a closed cycle show some difference from the measured data in the narrow range, they agree well with each other in terms of the temperature range of each control volume and the variation trend

over the cycle. Especially, the measured data for CV-5 show a large temperature variation over 30ºC, but the simulation results capture the trend of the experimental data well.

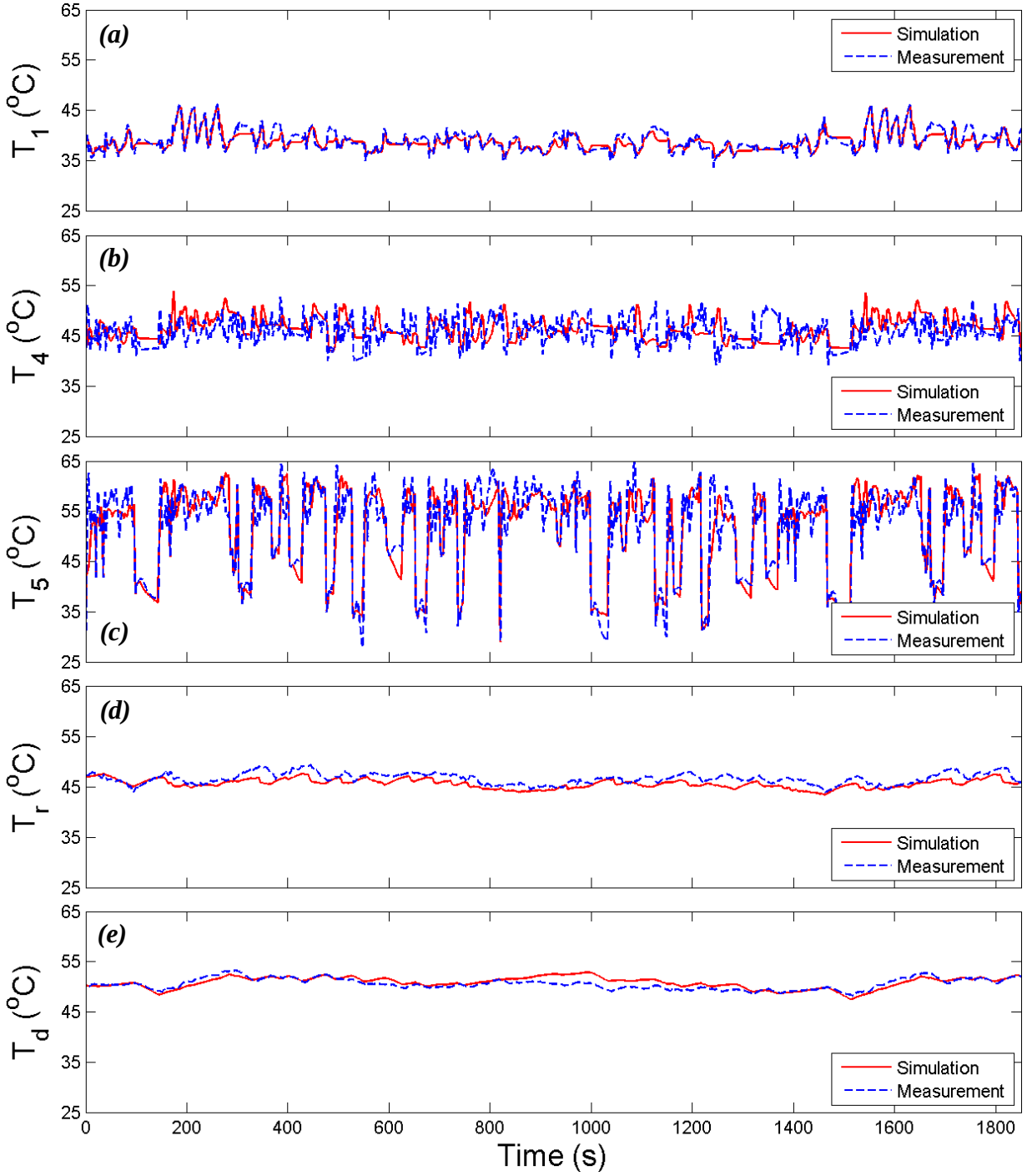

Figure 36. Results for the thermal model with two temperature inputs instead of the cooler model, (a) temperature in CV-1 after the cooler (T_1), (b) temperature in CV-4 before Unit-2 (T_4), (c) temperature in CV-5 after Unit-2 (T_5), (d) temperature in the reservoir (T_r), and (e) temperature in the drain pipe (T_d).

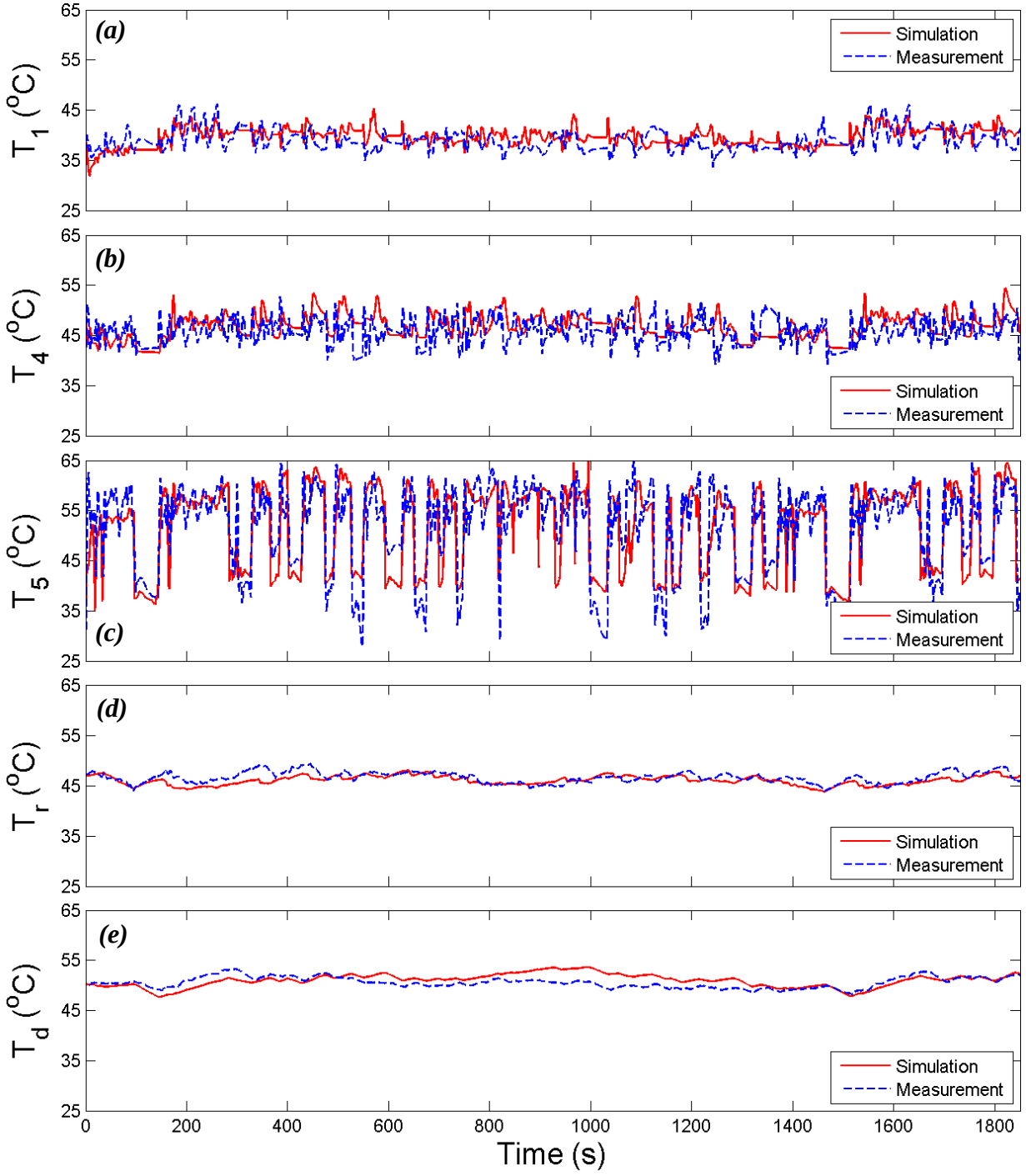

Figure 37. Results for the thermal model with a closed cycle, (a) temperature in CV-1 after the cooler (T_1), (b) temperature in CV-4 before Unit-2 (T_4), (c) temperature in CV-5 after Unit-2 (T_5), (d) temperature in the reservoir (T_r), and (e) temperature in the drain pipe (T_d).

Even though the thermal model shows some error, which is somewhat larger than the error of the hydraulic system model, there are some possible reasons for this discrepancy in the thermal model. First, during the HIL measurements, since each temperature measured from the experiment represents the temperature of the whole control volume, there is some difference according to the measurement position within the control volume. For the temperature measurements, type K thermocouples with the accuracy of ±1ºC were used. Also, since the thermal model uses data from the hydraulic system model as inputs, the error of thermal model is accumulated with the error of the hydraulic system model. For the thermal properties in the model, the values are linearly calculated from the lookup table of the material, and this creates some error of the material properties.

Table 5 shows the discrepancy in temperatures between simulated and measured values. The mean value of the temperature difference of the system is around 2ºC with the standard deviation less than 2ºC. Since temperature variations up to 40ºC are seen within the system, this level of accuracy is sufficient to predict system trends and some degree absolute temperatures.

Table 5. Temperature errors of the results for the thermal model.

Location	CV-1	CV-4	CV-5	Reservoir	Drain	Average
Mean [ºC]	1.82	2.53	4.26	0.81	1.16	2.12
Standard Deviation [ºC]	1.25	2.01	3.18	0.68	0.78	1.58

4.4 Chapter Summary

In this chapter, the transmission of a series HHV has been analyzed using a simulation model based on lumped parameter thermodynamic analysis. A novel method has been suggested

for the thermal model in order to capture the highly transient thermal variation of the unsteady system. The model has been compared and validated with measured data obtained from a HIL test rig tracking the FTP-72 driving cycle. These simulation results show a good correlation with the measured data and demonstrate that the presented approach provides meaningful insights into the thermal system behavior of hydraulic hybrids. The summary of this chapter can be described as follows:

- The thermal model developed for HHV has been applied to a closed circuit HHT.
- The system and thermal modeling results have been validated with the measured data from a HIL test rig with FTP-72 driving cycle.
- It shows a good correlation between the simulation results and experimental data in terms of the overall trend and variation range of the parameters.

CHAPTER 5. MODELING OF A NOVEL HYDRAULIC HYBRID VEHICLE AND VEHICLE MEASUREMENTS

In this chapter, the system and thermal modeling of Maha HHV, which has recently been developed in Maha Fluid Power Research Center, is presented. The thermal model of Maha HHV has been developed and validated with the measured data while driving. The main goal of thermal model in this study is the analysis of the thermal management system while developing Maha HHV. In the future, the system and thermal modeling can be utilized for estimating the thermal stability and vehicle performance for extreme driving cases, which have difficulties to be measured on the road.

There have been various investigations for novel hydraulic hybrid architectures for improvement in terms of performance and efficiency. To this purpose, recently, a novel HHT architecture has been proposed by the Maha Fluid Power Research Center and implemented in the platform of Range Rover 1999 model (Bleazard et al. 2015; Haria and Ivantysynova 2016; Sprengel et al. 2015). This hybrid transmission has mainly two different driving modes, i.e. the hydrostatic driving mode and the hybrid driving mode. The vehicle drives in the hydrostatic mode when the system demands low torque. The special circuit solution allows switching the pressure lines and charging the accumulator while braking. The driving mode is switched to the hybrid mode in order to utilize the stored energy in the accumulator. In the hybrid mode, the vehicle is boosted by the energy stored in the accumulator. The accumulator energy is restored by the regenerative energy during braking. Different control strategies are applied to the different operating modes. Figure 38 shows the prototype of Maha HHV, which is implemented with the novel HHT architecture.

Figure 38. Prototype of Maha HHV.

Figure 39 shows the simplified hydraulic circuit of Maha HHV. Unit 1 is connected to the engine through the gearbox. Unit 2 and Unit 3 are connected to the front and rear wheels, respectively, which makes the vehicle possible on the four-wheel drive. The connection between the high pressure accumulator and Line A is adjusted by the shut-off valve according to the different operating modes. A flushing valve is installed for directing flow to the system cooler.

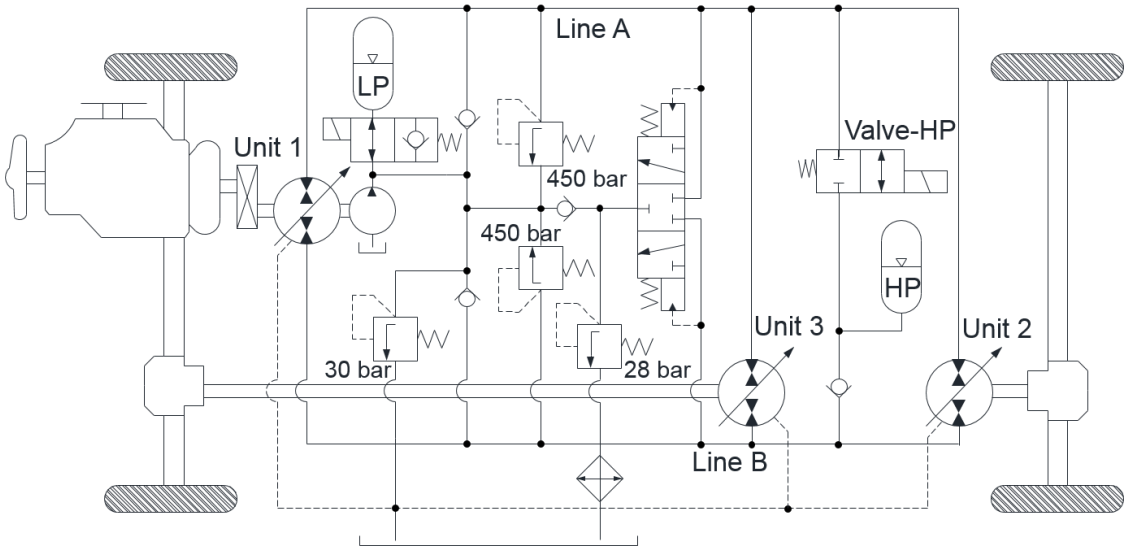

Figure 39. Simplified hydraulic circuit of Maha HHV (HP: high pressure, LP: low pressure).

5.1 Main Operating Modes

Table 6 shows the main operating modes of Maha HHV. When the vehicle is not in motion, all hydraulic units are adjusted to zero displacement. There are two main driving modes, the hydrostatic mode and hybrid mode. During the hydrostatic mode, the shut-off valve for the high pressure accumulator is closed and the transmission operates as a hydrostatic transmission. During the hybrid mode, the shut-off valve is open and the high pressure accumulator is connected to Line A. Thus, the energy stored in the high pressure accumulator is utilized for the driving and the transmission works as a series HHT. During the braking mode, the shut-off valve is closed and the high pressure accumulator is charged by the flow from Line B, with zero displacement of unit 1. Unit 2 and Unit 3 work as pumps and charge the high pressure accumulator for recovering energy from the wheels. Figure 40 shows the schematic of the main operating modes of Maha HHV described in Table 6.

Table 6. Main operating modes of Maha HHV.

Mode	Unit 1	Valve-HP	HPA	Unit 2 / Unit 3	Driveline
1	Zero Displacement	Closed	Idle	Zero Displacement	Idle
2	Pumping	Closed	Idle	Motoring	Driving
3	Pumping	Open	Discharging	Motoring	Driving
4	Zero Displacement	Closed	Charging	Pumping	Braking

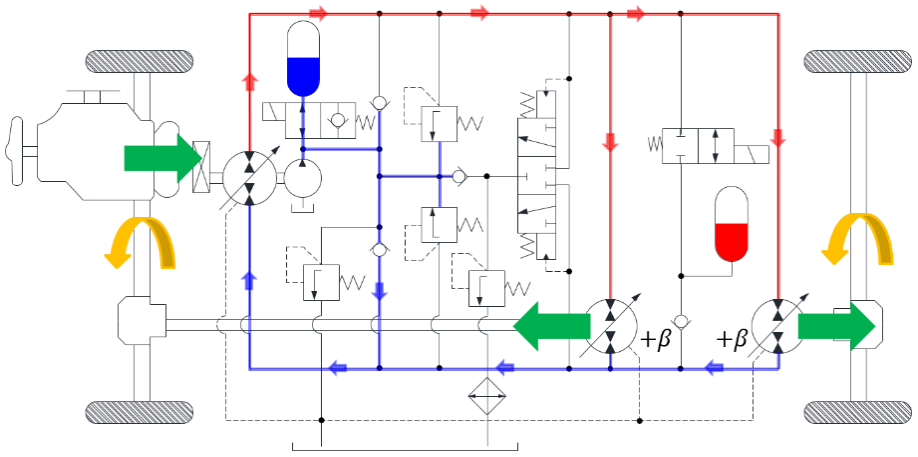

(a)

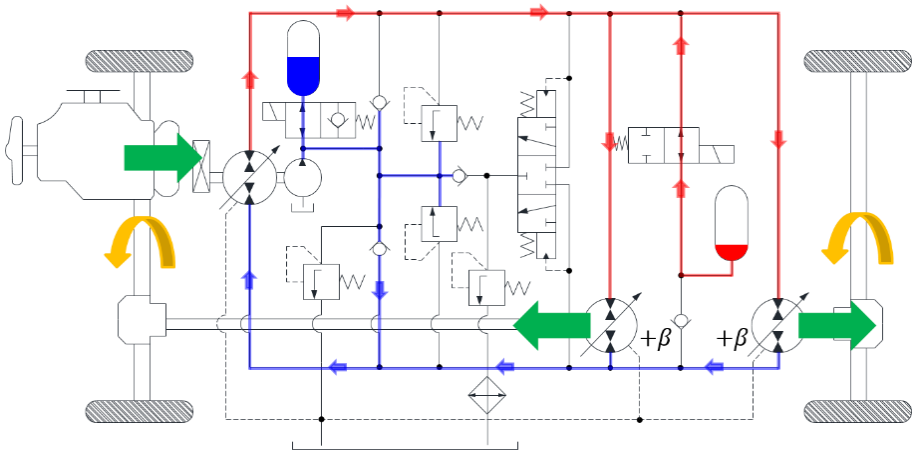

(b)

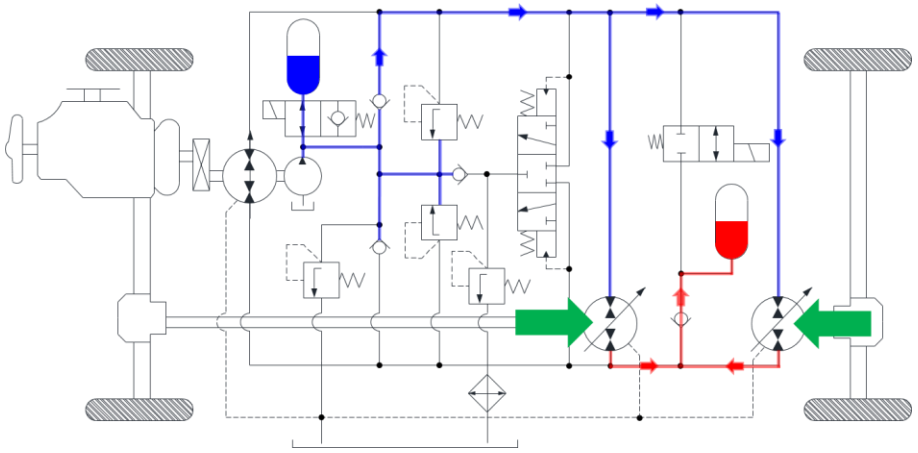

(c)

Figure 40. Schematic of the main operating modes of Maha HHV, (a) hydrostatic mode, (b) hybrid mode, and (c) braking mode.

Sequential control is used for the hydrostatic driving mode and secondary control is used for the hybrid mode. Figure 41 shows an example drive cycle for the different control modes of Maha HHV. During the section with sequential control, the displacement of Unit 2 maintains 100% until the displacement of Unit 1 becomes 100%.

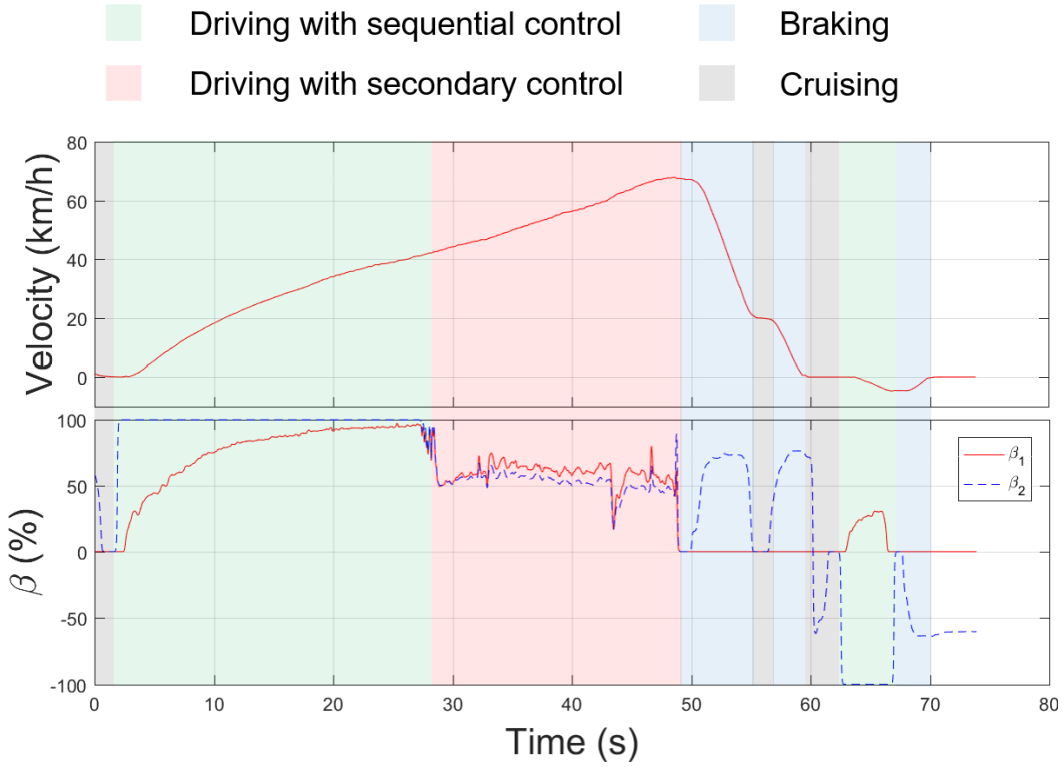

Figure 41. Example drive cycle for the control of Maha HHV.

5.2 Measurement Method

Figure 42 shows the image of the component assembly of Maha HHV. A valve block has been installed in the car, which includes check valves, flushing valve, enabling valve and pressure sensors.

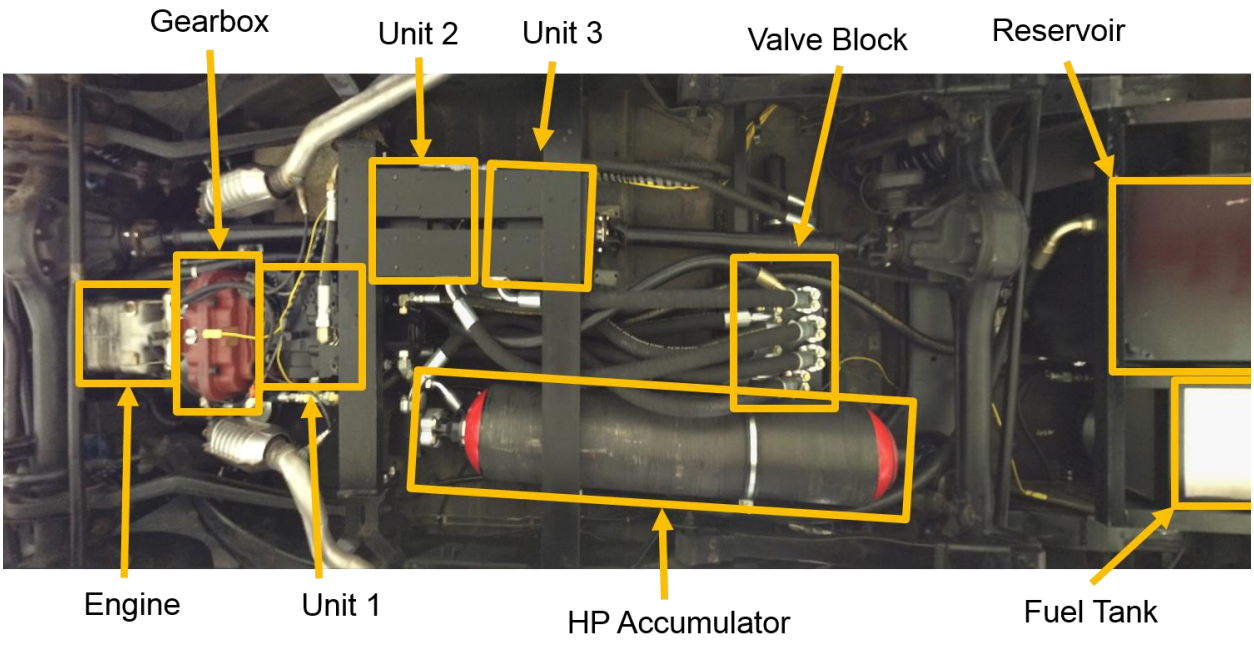

Figure 42. Component assembly of Maha HHV.

Table 7 shows the sizes of the main transmission components. The sizing selection process of Maha HHV is detailed in the reference (Bleazard 2015). Figure 43 shows the detailed hydraulic circuit of Maha HHV. Figure 44 shows the CAD model of the valve block and installation in Maha HHV (Bleazard 2015).

Table 7. Sizes of the main transmission components.

Unit 1	100 cc
Unit 2	75 cc
Unit 3	75 cc
Charge Pump	27 cc
HP Accumulator	32 L
LP Accumulator	42 L

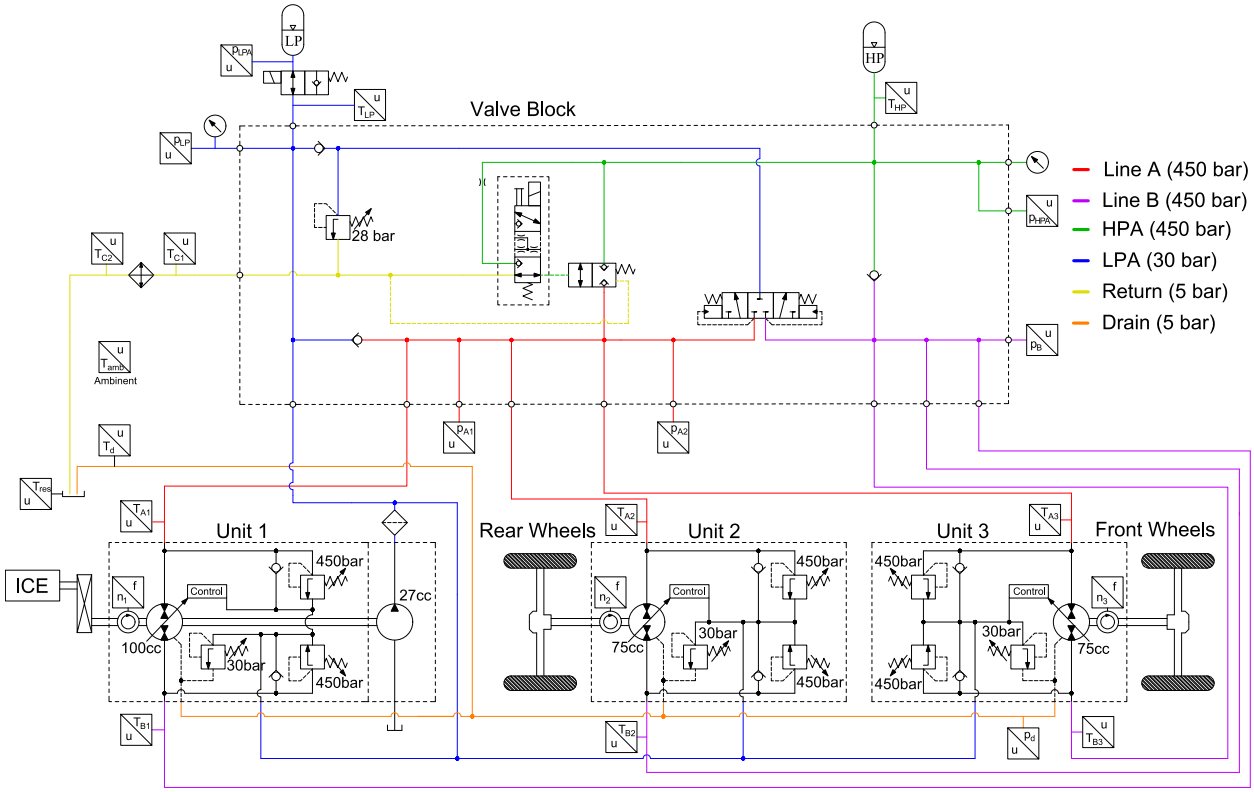

Figure 43. Detailed hydraulic circuit of Maha HHV.

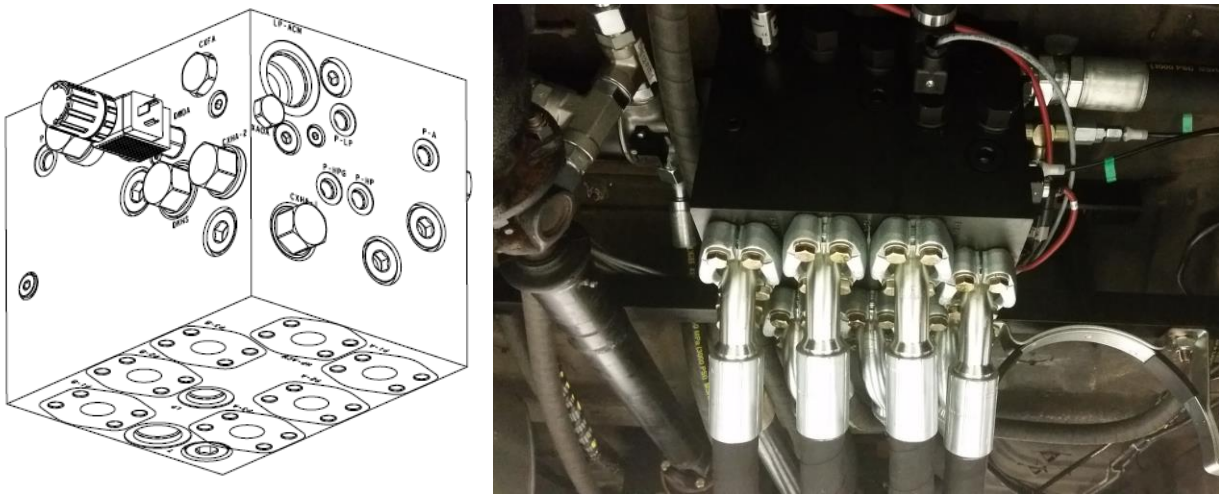

Figure 44. CAD model of the valve block and installation in Maha HHV.

5.3 Thermal Management System of Maha Hydraulic Hybrid Vehicle

There are mainly two ways to cool down the systems. The passive cooling is a method cooling down the system by using the natural airflow of the system. For example, for on-road vehicles, there are plenty of air flows from the front side while driving and the air flow can be utilized for cooling down the system. The advantage of the passive cooling is no use of energy for cooling the system, while it has a disadvantage such as a limitation of cooling ability. Another cooling strategy is the active cooling. The system is cooled down by additional fans or coolers in the active cooling. An advantage of the active cooling is that it can serve relatively higher cooling power when it is installed properly. It has some disadvantages like energy consumption of the system for cooling and requirement of additional equipment and spaces.

In Maha HHV, the cooling system is installed based on the passive cooling strategy. On-road vehicles have a plenty of airflow from the front side, the system can be cooled down by the passive cooling with that airflow. Figure 45 shows the radiator for the hydraulic system installed in Maha HHV. A radiator for the hydraulic system has been installed on the front side of the vehicle in order to cool down the system by airflow from the front side and by airflow generated by the engine fan. The major advantage of this method is that no additional energy is required for the cooling system. After the cooling system was installed based on the passive cooling, the several drive cycles were measured for system temperatures and it showed a stable trend.

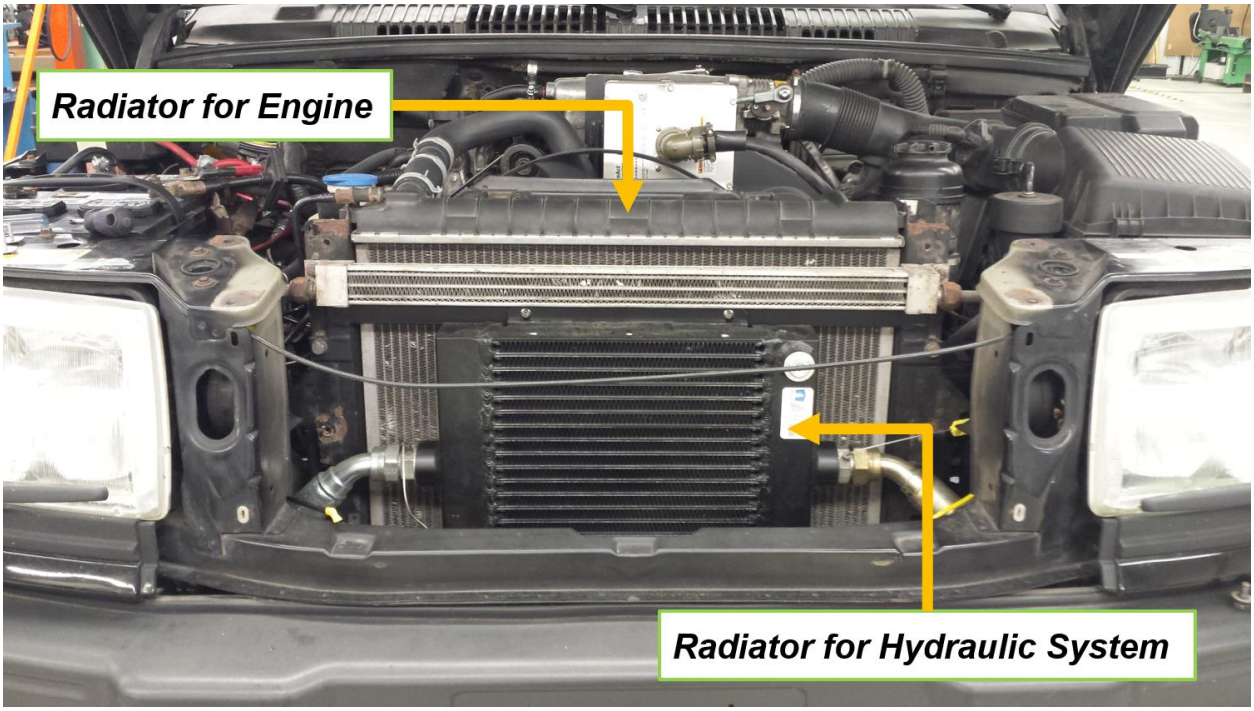

Figure 45. Radiator for the hydraulic system installed in Maha HHV.

5.4 Results and Discussion

After the hydraulic system model runs based on the measured driving cycle of the vehicle, the hydraulic system is divided into several control volumes for the thermal modeling, which are determined based on the main hydraulic components. The results such as pressure and flow rate from the hydraulic system model are utilized for the thermal model as input parameters. Figure 46 shows the control volumes for thermal modeling of Maha HHV. The control volumes include main components of the system such as hydraulic units, high pressure accumulator, hydraulic lines, cooler and reservoir. In addition, hydraulic lines are separated into more control volumes according to the complexity and locations of the lines. In the simulation, each control volume stores its temperature every time step and those are updated based on the governing equation.

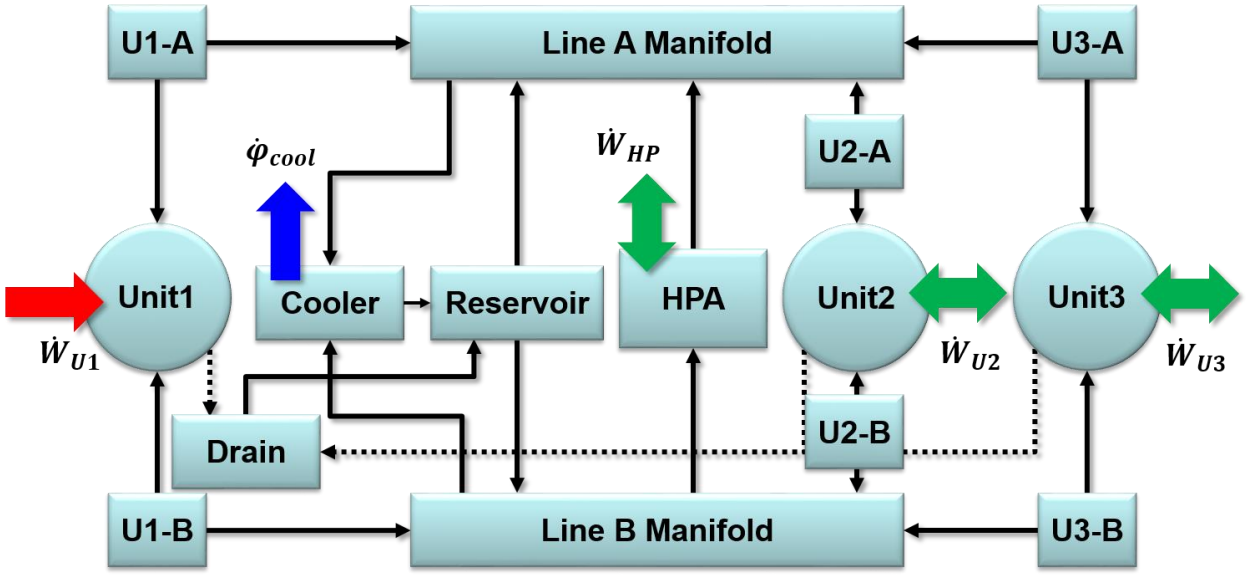

Figure 46. Control volumes for thermal modeling of Maha HHV.

Simulation results from the system and thermal modeling have been compared and validated with the measured data collected from the vehicle. For the hydraulic system model, speed of the vehicle, displacement of the hydraulic units, and pressure of the system were used for comparing the results. Figure 47 shows the comparison of simulation and measurement results for the speed of the vehicle. The simulation results show a good agreement with the measured data in terms of the overall trend. The measured data have some noise spikes due to the error of the speed sensors.

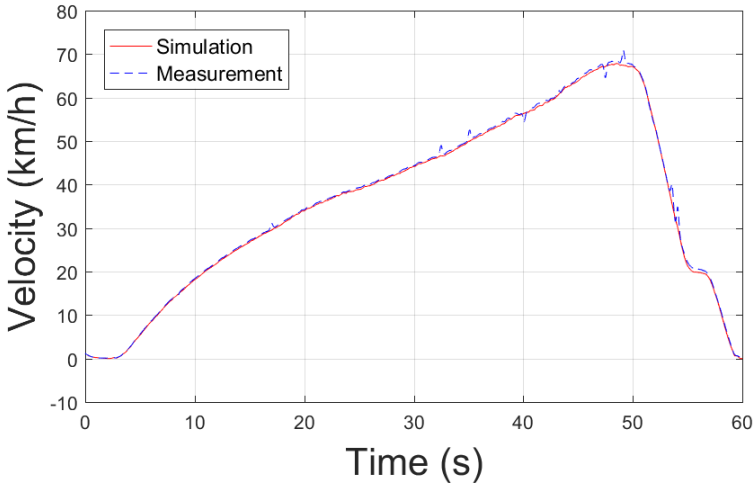

Figure 47. Comparison of simulation and measurement results for the speed of vehicle.

Figure 48 shows the comparison of simulation results and commanded signals for the displacements of hydraulic units. The simulation results follow well with the commanded signal of the hydraulic units. Only two hydraulic units, Unit 1 and Unit 2, are considered in the comparison, because Unit 3 has the same displacement as Unit 2. It shows a good agreement in most sections in terms of the overall variation trend. There is some discrepancy for Unit 2 when the vehicle is under the braking mode between 50 and 60 seconds. The reason of the discrepancy is related to the controller of the units. When the vehicle is in the driving mode, the displacements of hydraulic units are controlled by the feedback signal. On the other hand, during the braking mode, the commanded signal of the displacement is determined by only feedforward based on the brake pedal signal. As a result, the real displacement of the unit has some discrepancy from the commanded signal of the displacement, since the system pressure cannot be matched with the commanded displacement. In the future, in order to prevent the disagreement of the displacements of the units, the control for the braking mode can be modified based on the feedback signals from the pressure and real displacement position as well as the feedforward signal from the brake pedal.

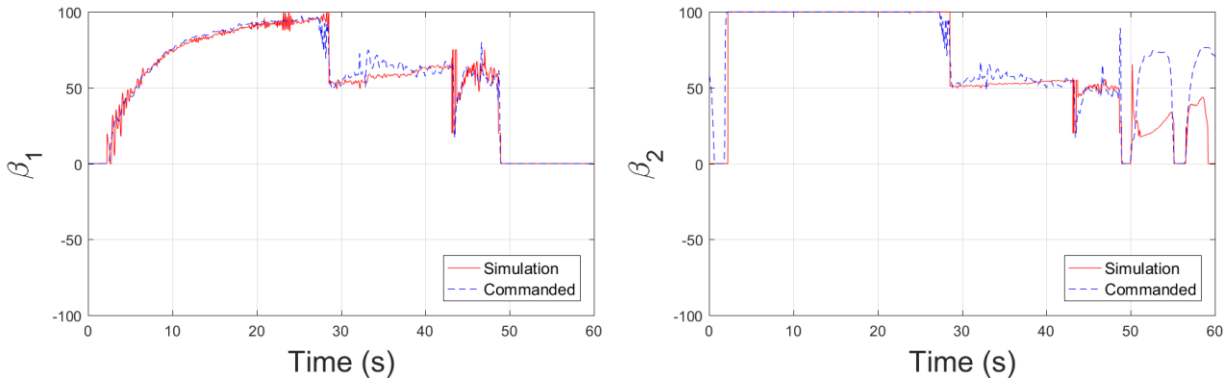

(a) (b)

Figure 48. Comparison of simulation results and commanded signals for the displacements of hydraulic units, (a) Unit 1 and (b) Unit 2.

Figure 49 shows the comparison of simulation and measurement results for the pressure of Line A, Line B, and high pressure accumulator. When the vehicle is in the driving mode, Line A becomes a high pressure line, and when the vehicle is in the braking mode, Line B becomes a high pressure line.

In the figures, we see that the high pressure line is switched at 50 seconds from Line A to Line B. During the hybrid mode, the high pressure accumulator is connected to Line A and the vehicle is controlled by the secondary control. In the figure for high pressure accumulator, we can see that the pressure is dropped between 43 and 50 seconds, since the vehicle is in the hybrid mode. In the simulation results, even though it shows small fluctuations in the result for Line A, overall trends and variation ranges match well with the measured data. Especially, when the operating mode is changed, the pressure follows abrupt variations in the measured data well.

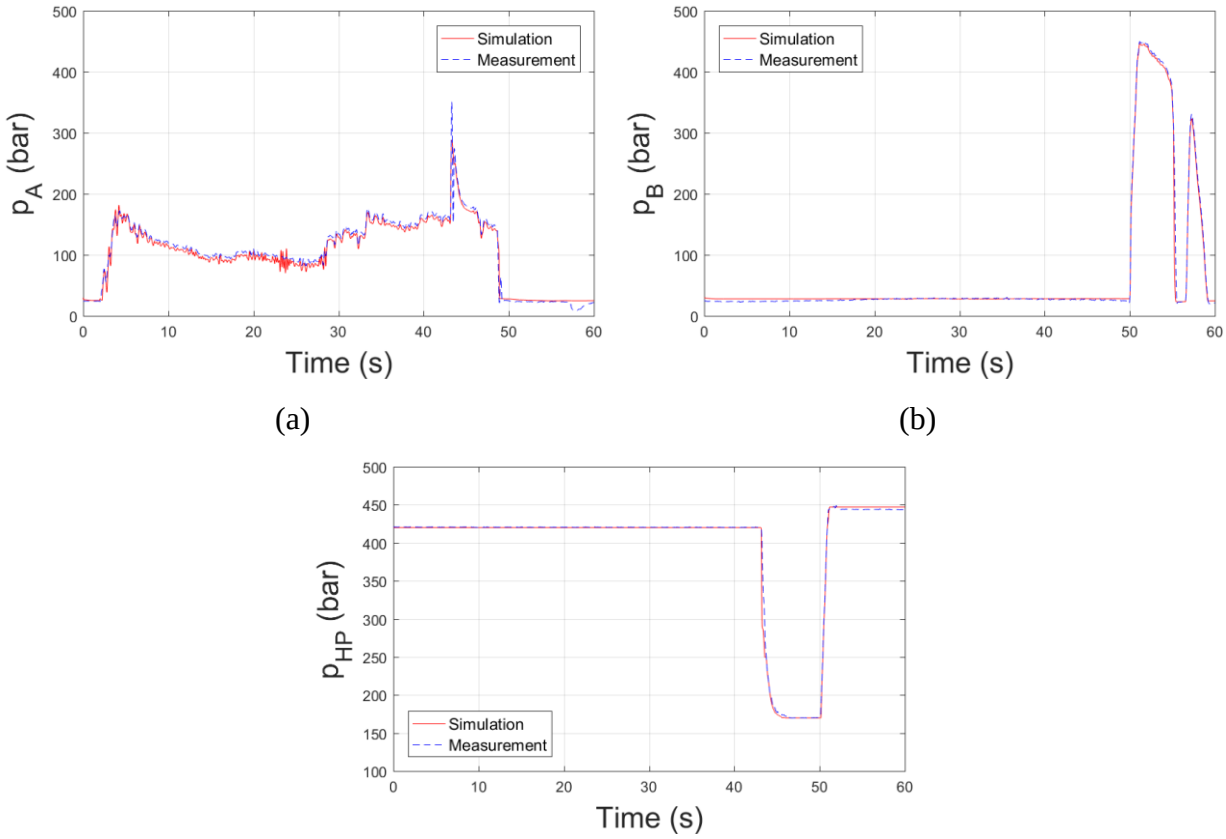

Figure 49. Comparison of simulation and measurement results for the pressure of the system, (a) Line A, (b) Line B, and (c) high pressure accumulator.

For the thermal model, the temperature of the ports of hydraulic units, high pressure accumulator, drainpipe, and reservoir are utilized for the comparison of simulation and measurement results.

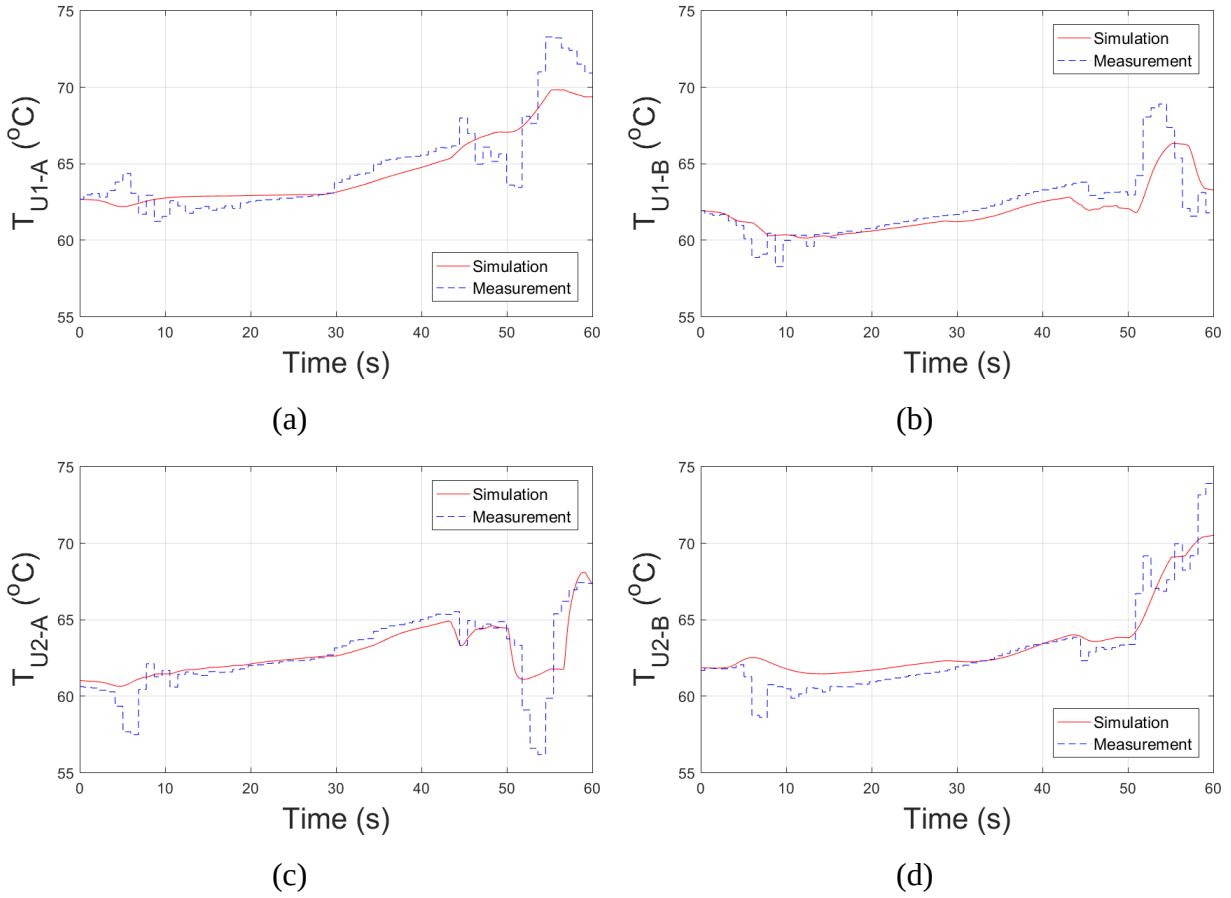

Figure 50. Comparison of simulation and measurement results for the port temperature of hydraulic units, (a) Unit 1 to Line A, (b) Unit 1 to Line B, (c) Unit 2 to Line A, and (d) Unit 2 to Line B.

Figure 50 shows the comparison of simulation and measurement results for the port temperature of Unit 1 and Unit 2 connected to Line A and Line B, respectively. Even though it shows some discrepancy in some areas, the simulation results follow well with the measured data in terms of the variation trend and range.

Figure 51 shows the comparison of simulation and measurement results for the temperature of the high pressure accumulator, drainpipe, and reservoir. As in the results for hydraulic units, those show a good agreement with the measured data in terms of the trend and variation range. For

the high pressure accumulator, there is a large temperature drop when the vehicle mode is switched to the hybrid mode, and the simulation result describes it well.

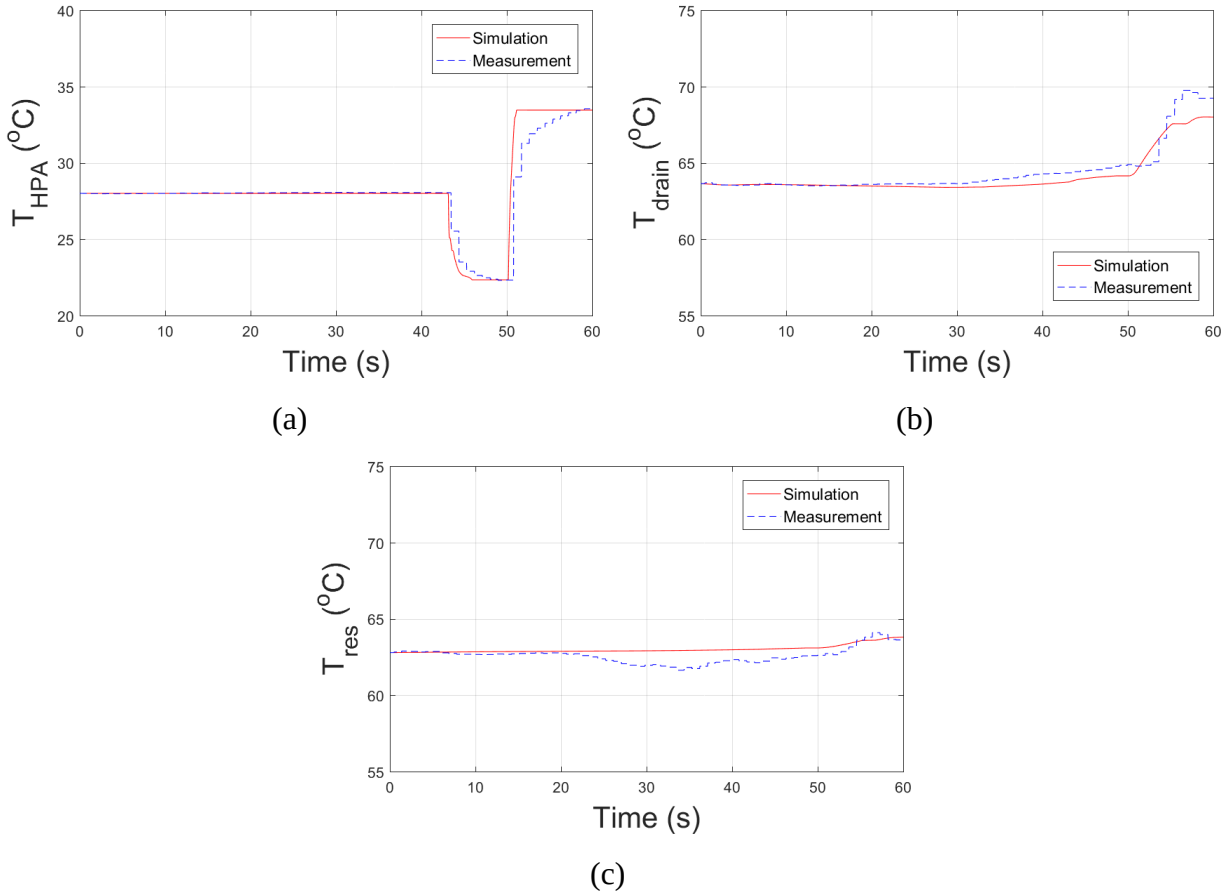

Figure 51. Comparison of simulation and measurement results for the temperature of (a) high pressure accumulator, (b) drainpipe, and (c) reservoir.

In conclusion, the model shows applicable results for analysis of the system in terms of the overall trend and variation ranges. In order to evaluate the error quantitatively, the mean and standard deviation of the temperature difference was calculated. Table 8 shows the discrepancy in temperatures between simulated and measured values. The average values of the mean and standard deviation show less 1ºC. This error range is acceptable compared to the previous studies,

where the typical error range is from 5 to 10ºC, even though it depends on the system complexity and measured duty cycles.

Table 8. Temperature errors of the results for the thermal model for Maha HHV.

Location	U1-A	U1-B	U2-A	U2-B	HPA	Drain	Tank	Average
Mean [ºC]	1.00	1.06	1.01	1.00	0.30	0.52	0.42	0.76
Standard Deviation [ºC]	0.82	1.05	1.13	0.89	0.83	0.50	0.34	0.79

5.5 Chapter Summary

In this chapter, the system and thermal modeling of a novel mode switching HHT, also called as Maha HHV, is presented. The main purpose of the thermal modeling in this study is the analysis of the thermal management system of Maha HHV. The measured data were collected while driving the vehicle and were utilized for validating the program. The results from the modeling show a good agreement with the measured data in terms of the trend and variation ranges. The simulation program can be utilized for performance and stability prediction for different driving cases, which might be difficult to be measured on the road. The summary and future work of the chapter can be described as follows:

- The system and thermal modeling has been presented for a novel HHV, which has recently been developed in the Maha lab.
- The system and thermal modeling results show a good correlation with the data measured in vehicle on the road.

- The thermal model was utilized for analysis of the thermal management system of Maha HHV.
- The developed program can be used for predicting different driving situations, which are difficult to be measured on the road.

CHAPTER 6. THERMAL MANAGEMENT OF OPEN AND CLOSED CIRCUIT HYDRAULIC HYBRID TRANSMISSIONS

In the previous chapters, the methodology for the combined system and thermal modeling has been described and the model has been studied with validation by the different types of transmissions with measured data. Since the model shows the ability to model the rapid transient systems of HHTs under the unsteady conditions, it can be used for handling advanced topics under such conditions, which have not been dealt with in the past. The thermal characteristics of open and closed circuit hybrid systems are one of those topics, and in this chapter, the thermal management of open and closed circuit systems of hydraulic series hybrids are studied using the methodology described in the previous chapters.

The open and closed circuit series hybrids have clear advantages and disadvantages (Cross and Ivantysynova 2011). The open circuit hydraulic hybrid requires a small charge pump to supply the hydraulic unit control systems but does not supply a low pressure system. The open circuit system also does not require a low pressure accumulator because of the absence of a low pressure system. However, the closed circuit system requires both a charge pump and a low pressure accumulator. This simplifies the architecture of the open circuit system, thus decreasing the cost, weight, and space. On the other hand, the open circuit system requires a larger reservoir than the closed circuit system because all hydraulic units are directly connected to the reservoir.

In this chapter, open and closed circuit HHTs have been successfully modeled using a lumped parameter approach in MATLAB/Simulink®, which accurately demonstrated power consumption and transmission performance. High fidelity empirically derived loss models of axial piston machines were used in the hydraulic system model. These loss models were developed from

highly controlled tests of bent-axis machines. Scaling laws were used to account for the different pump sizes. In addition to the hydraulic model, the thermal model described in Chapter 3 was applied to both systems, which is based on a thermodynamic approach.

This study shows the advantages and disadvantages of open and closed circuit hydraulic transmissions. This includes the differences in system cooling requirements, transmission power consumption, reservoir size and the required number of hydraulic components. To ensure a fair and accurate comparison of the two architecture designs, high efficiency bent-axis axial piston machines are used as the pumps and motors, and the unit sizes are the same in the open circuit as in the closed circuit system. The two different architectures were tested using the same loading conditions and are applied to the same drive cycle, thus making a fair comparison between open and closed circuit hydraulic transmissions. The hydraulic system and thermal models also allow for an accurate sizing of charge pumps and cooler sizes, which are essential in minimizing parasitic power losses to the prime mover.

6.1 Open and Closed Circuit Hydraulic Hybrid Transmissions

An open and a closed circuit series HHTs with identical hydraulic units and high pressure accumulator are chosen for comparison. In both systems, Unit 1 is a 100 cc bent-axis unit driven by the engine shaft. Unit 2 and Unit 3 are both 75 cc bent-axis units that are connected to the rear and front axles, respectively. A 32 L high pressure accumulator is chosen for both systems. This size is chosen to capture much of the braking energy of the vehicle. Other hydraulic components were designed based on the system architecture requirements. Table 9 shows the sizes of the main components for both systems.

Table 9. Sizes of the main components for both systems.

Unit 1	100 cc
Unit 2	75 cc
Unit 3	75 cc
HP Accumulator	32 L
LP Accumulator	42 L

Figure 52 shows the hydraulic circuit of an open circuit series HHT. In the open circuit system, the unit control pressure is maintained at 20 bar by a 5 cc charge pump. For thermal management, a recirculation pump is incorporated in the reservoir to provide flow through the cooler. The size of the reservoir is 60 L, which has been selected based on simulation results.

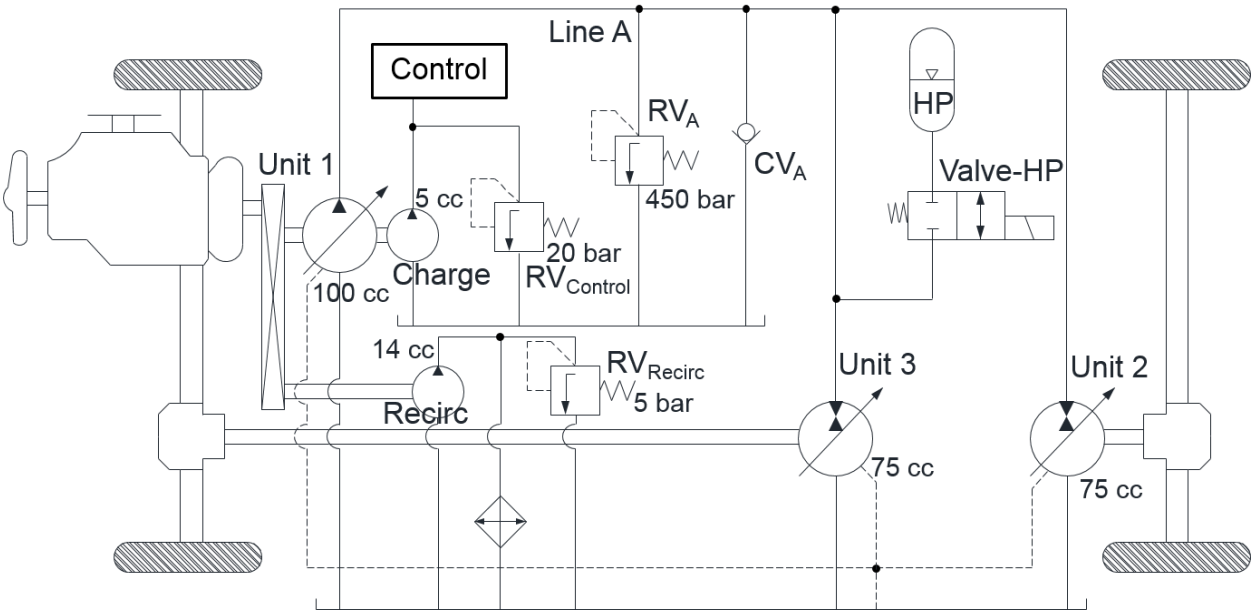

Figure 52. Hydraulic circuit of an open circuit series HHT.

Figure 53 shows the hydraulic circuit of a closed circuit series HHT. A 27 cc charge pump is selected for maintaining a stable pressure in the low pressure line. A larger charge pump is needed in a closed circuit system to resupply the system with the lost flow from the hydraulic units.

A 42 L accumulator is needed in the low pressure line to exchange flow with the HP accumulator during braking and acceleration events. The flow through the pressure relief valve from Line B is sent through the cooler to reduce oil temperature. A reservoir volume of 40 L is chosen for the closed circuit system.

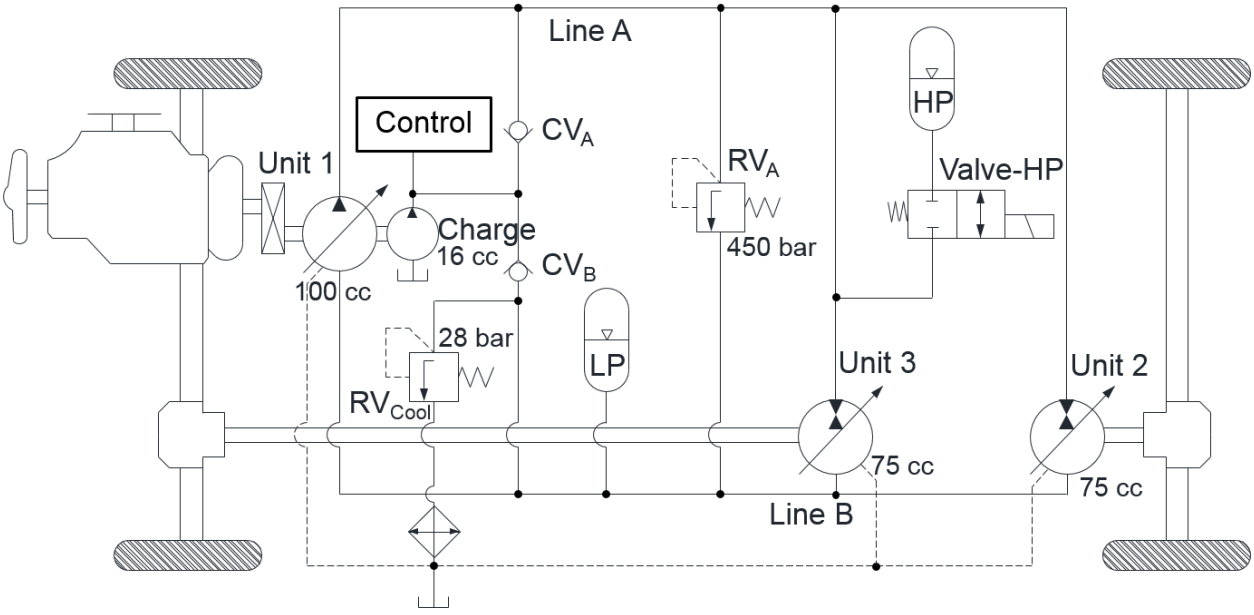

Figure 53. Hydraulic circuit of a closed circuit series HHT.

6.2 Main Operating Modes

There are different operating modes for the series HHTs. Both open and closed circuits used in this study are operated by the same modes and Table 10 shows the main operating modes of the series HHTs used in this study. Most operating modes of the given systems are same as those of Maha HHV. One difference from the operating modes of Maha HHV is that the Valve-HP needs to be open during the braking mode, since the pressure lines are not switchable in the systems used in this study.

Table 10. Main operating modes of the series HHTs used in this study.

Mode	Unit 1	Valve-HP	HPA	Unit 2 & 3	Driveline
1	Zero Displacement	Closed	Idle	Zero Displacement	Idle
2	Pumping	Closed	Idle	Motoring	Driving
3	Pumping	Open	Discharging	Motoring	Driving
4	Zero Displacement	Open	Charging	Pumping	Braking

Figures 54 and 55 show the schematics of the main operating modes of open and closed circuit series HHT, respectively. During the hydrostatic driving mode, the Valve-HP is closed and the transmission works same as a hydrostatic transmission. The high pressure accumulator is connected to the main line during the hybrid mode and the system utilizes the energy stored in the accumulator. During the braking mode, Unit 1 becomes zero displacement and the accumulator is charged by the regenerative energy from the wheel.

Sequential and secondary controls are used for controlling the operating modes. The sequential controller is used when the vehicle is accelerating without the aid of the HP accumulator. During these operating conditions, the vehicle is in a hydrostatic driving mode. The secondary controller is used when the vehicle is braking or accelerating with the use of the HP accumulator. The controllers used in this study are identical in both the open and closed circuit hydraulic system models.

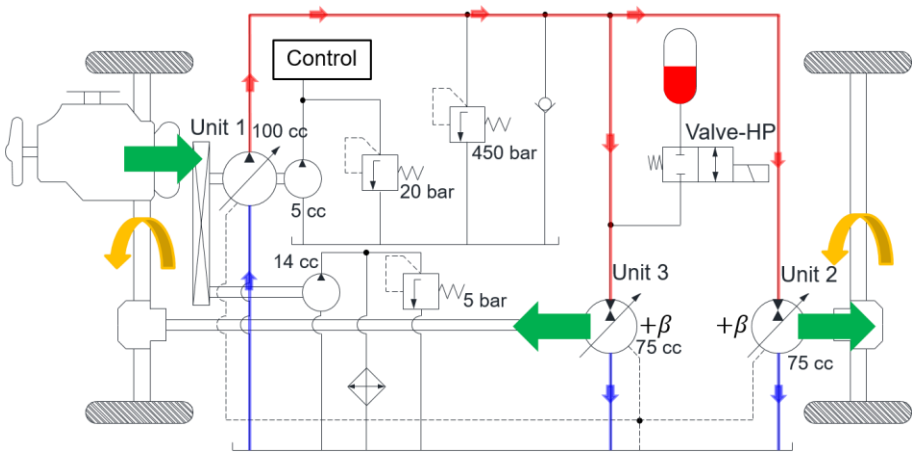

(a) Hydrostatic Mode

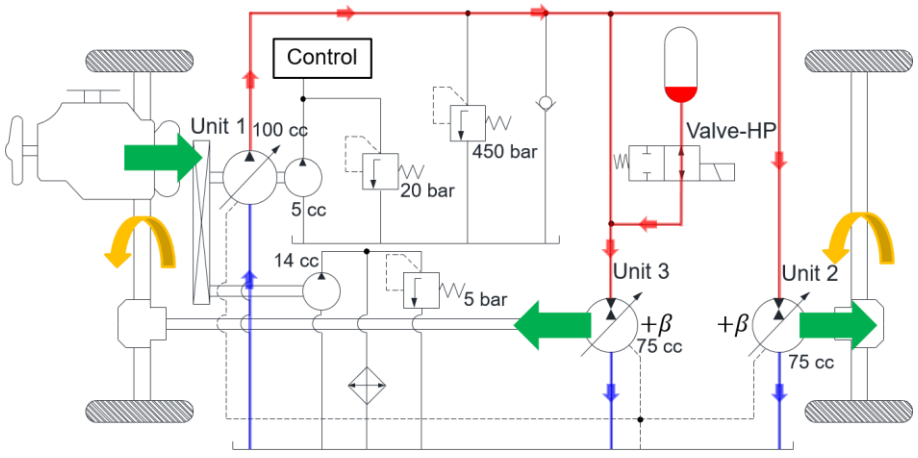

(b) Hybrid Mode

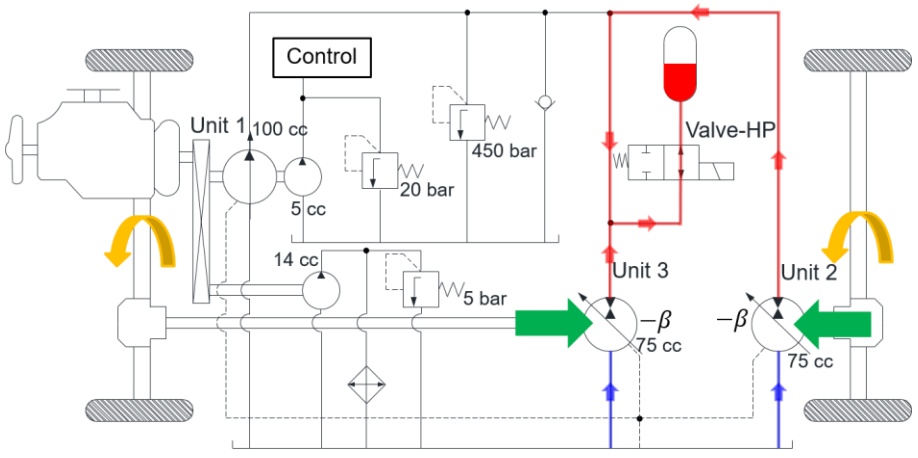

(c) Braking Mode

Figure 54. Schematic of the main operating modes of open circuit series HHT.

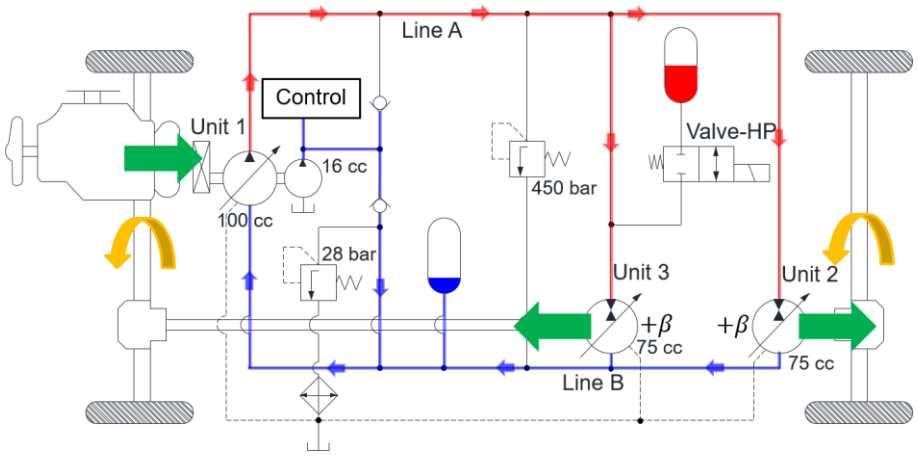

(a) Hydrostatic Mode

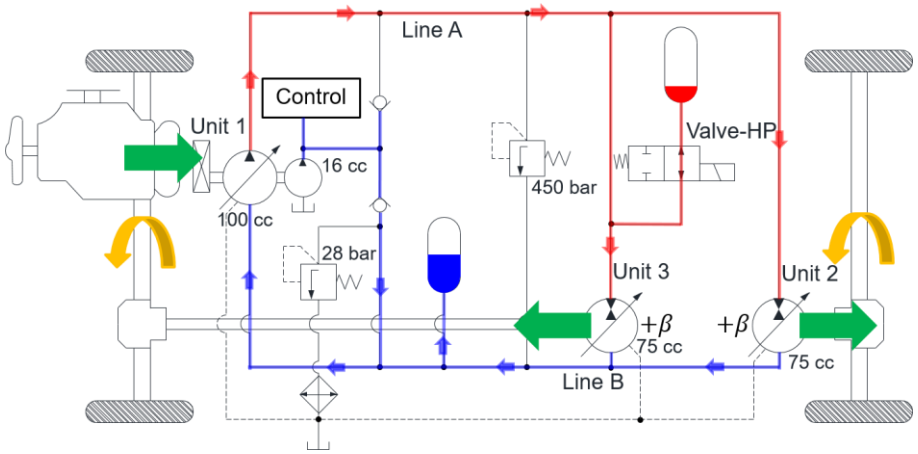

(b) Hybrid Mode

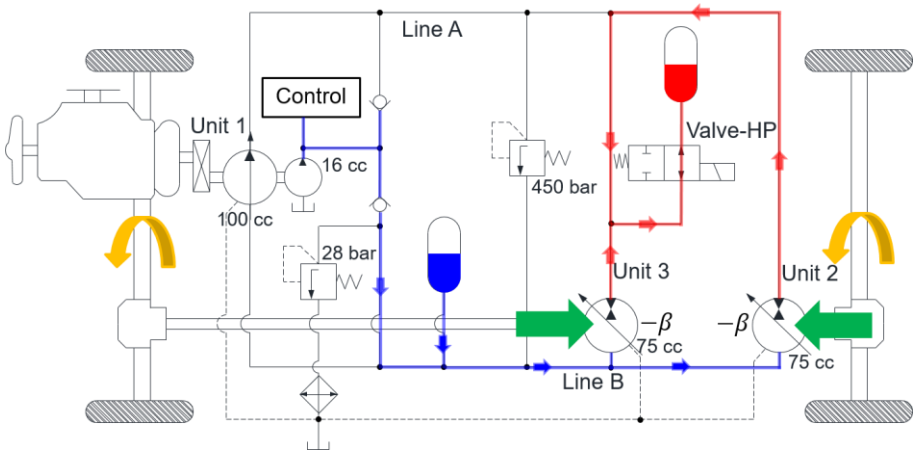

(c) Braking Mode

Figure 55. Schematic of the main operating modes of closed circuit series HHT.

6.3 Thermal Modeling of Open and Closed Circuit Systems

The cooler is used for the management of the temperature within the system. The cooling performance of the cooler is based on empirical data given by manufacturers. The cooling performance curve is assumed as a log function of the flow rate through the cooler. Figure 56 shows the cooling performance curves of the coolers used in this study. The cooler is activated when the input temperature of the cooler is less than 50ºC to prevent excessive cooling, which consumes unnecessary amounts of power.

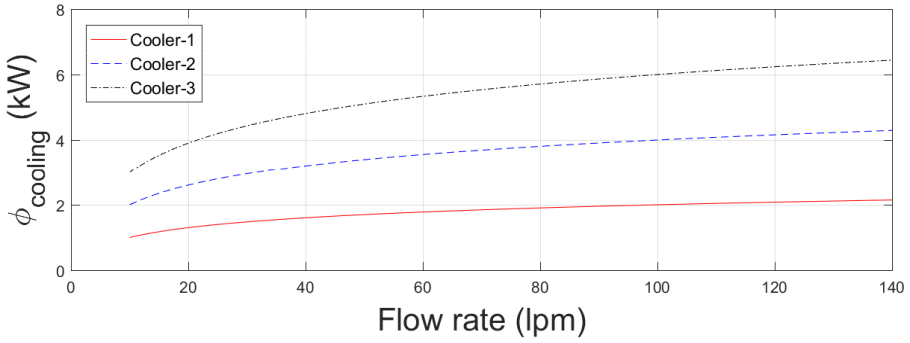

Figure 56. Cooling performance curves of the coolers used in this study (ΔT=10ºC).

The thermal model is divided into several control volumes based on the main hydraulic components in the system. Figures 57 and 58 show the control volumes for the thermal modeling of the open and closed circuit HHTs, respectively. Thermal behaviors of each control volume are calculated based on the governing equation discussed in Chapter 3.

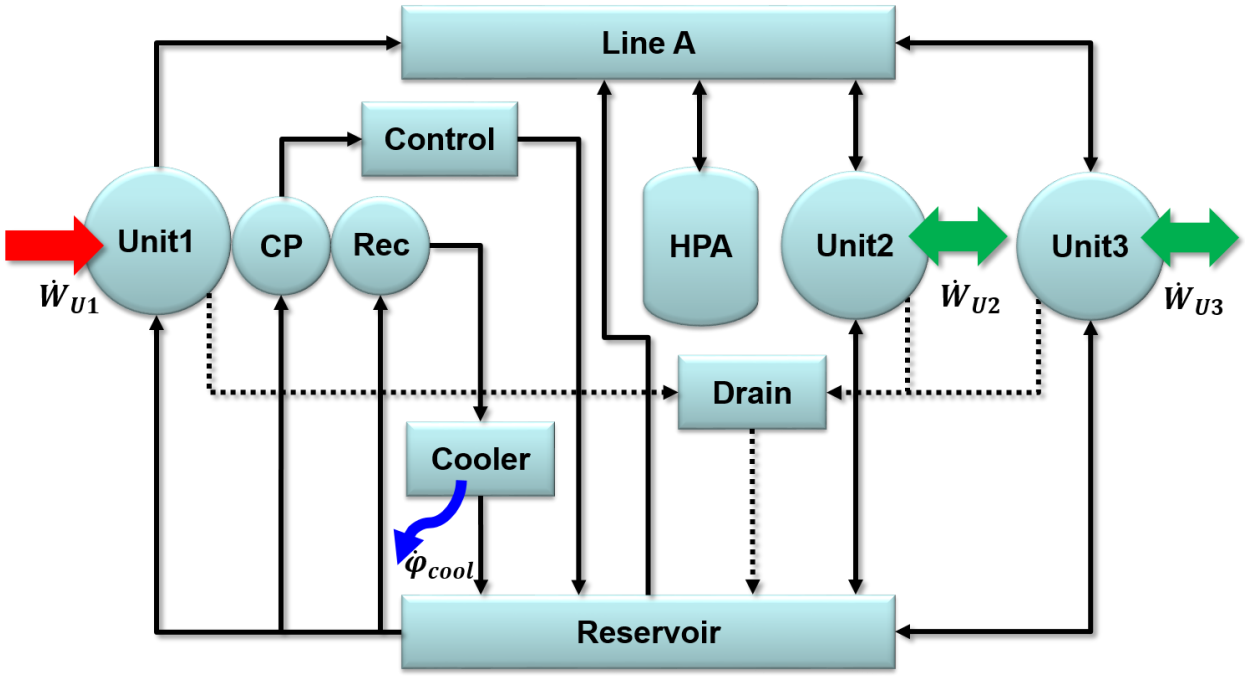

Figure 57. Control volumes for thermal modeling of the open circuit HHT.

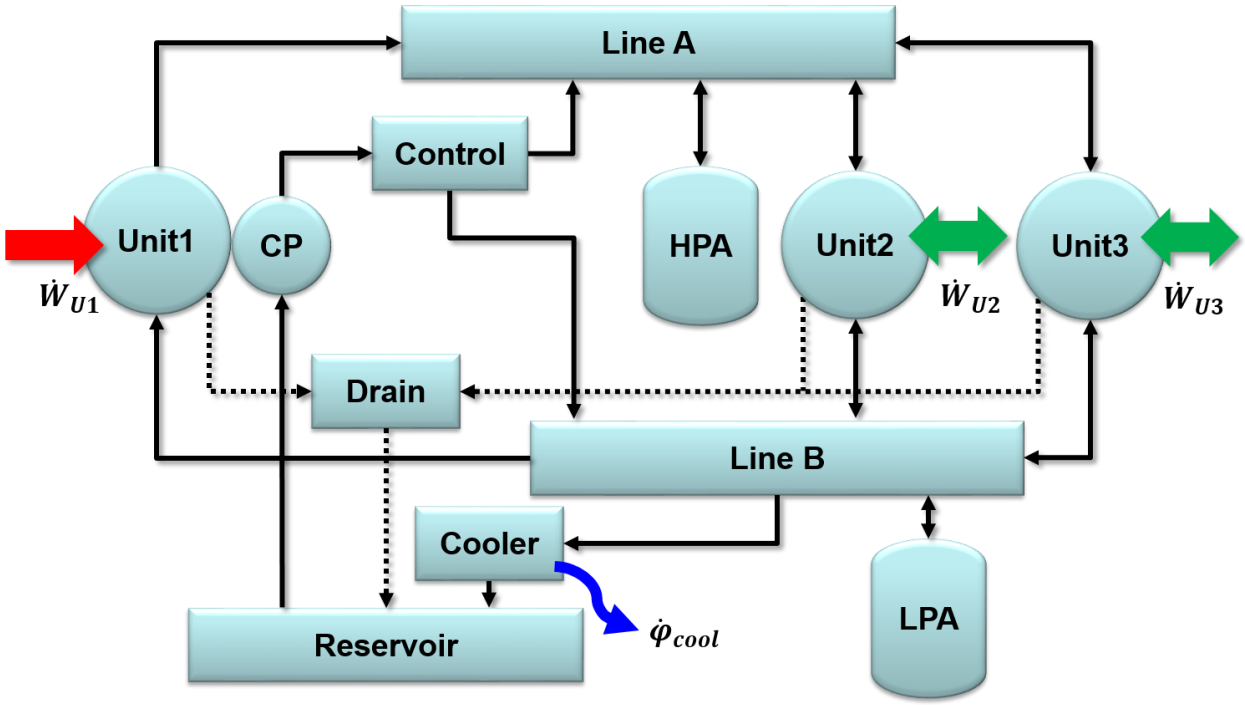

Figure 58. Control volumes for thermal modeling of the closed circuit HHT.

6.4 Results and Discussion

For the hydraulic system, the simulated and commanded vehicle speeds match very well for both the open and closed circuit system architectures. The commanded vehicle speeds are taken from the FPT-72. Figure 59 shows the hydraulic system modeling results for the open and closed circuit hybrids. The pressure differentials across the hydraulic units for both the open and closed circuit systems are nearly identical to one another. This is because both system models contain the exact same vehicle dynamics and the simulated speeds are similar. However, the open circuit system operates at slightly lower pressures due to the lack of a low pressure system.

It is important to note that when the vehicle is braking, the braking energy is being stored in the HP accumulator. That can be seen as the HP accumulator pressure increases during braking events. Equally important is using the power available in the HP accumulator when the vehicle is accelerating. That can be seen as the HP accumulator pressure drops as the vehicle accelerates. Since the control strategies of the open and closed circuit systems are identical, then the displacements of the units are also identical.

The consumed power of the closed circuit system is only slightly higher than that of the open circuit system. This can be attributed to the larger charge pump required for the closed circuit system. Another interesting result to consider is the accumulator state of charge. Notice that the HP accumulator in the closed circuit system does not capture as much fluid as that in the open circuit system. This is caused by the lower differential pressure of the closed circuit system when using the same value for the maximum system pressure. Therefore, the open circuit system in this comparison study can recover slightly more energy than a closed circuit system.

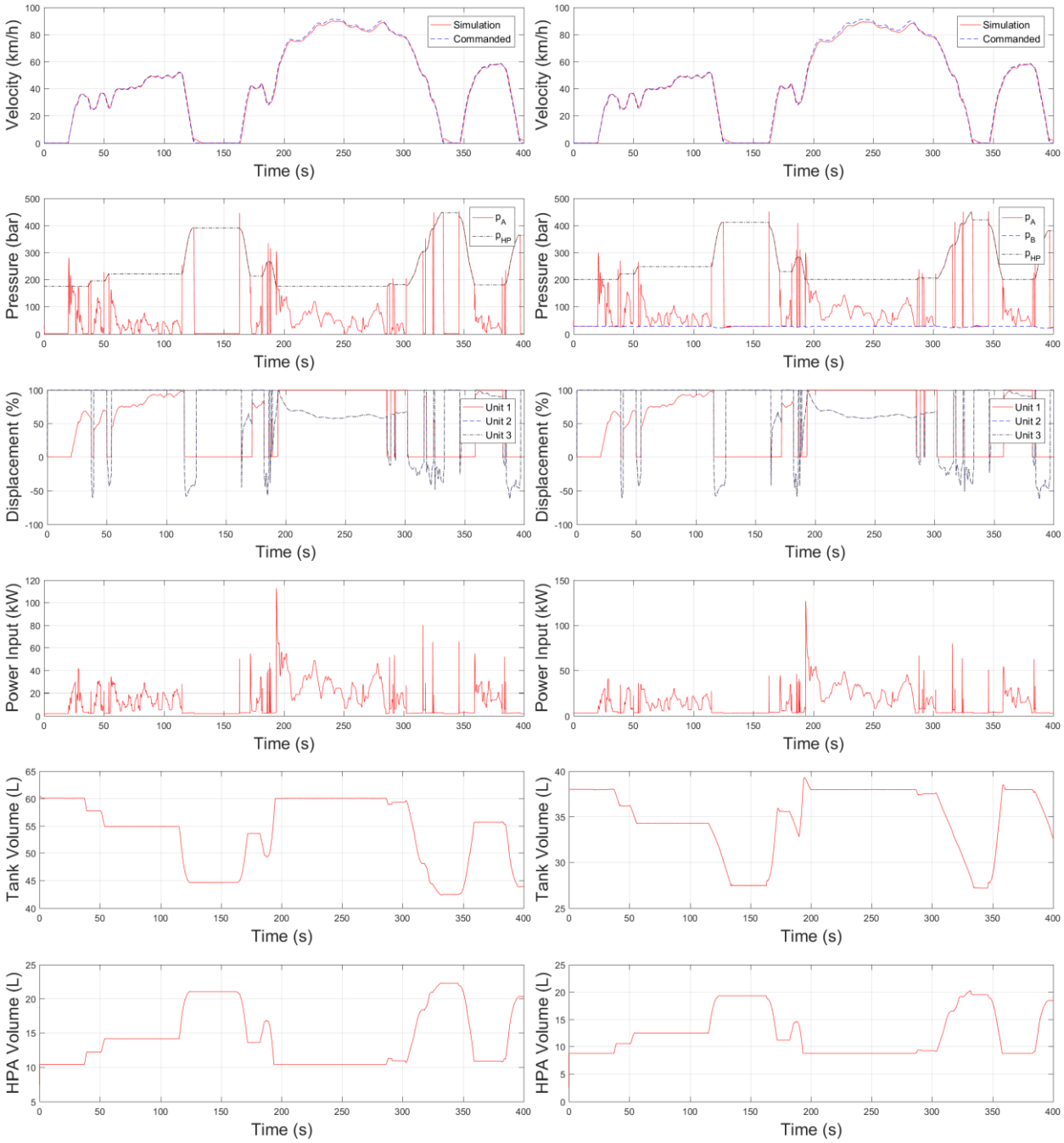

(a) Open circuit system (b) Closed circuit system

Figure 59. Hydraulic system modeling results for the open and closed circuit hybrids.

In order to study the thermal behavior of the systems under investigation, the FTP-72 cycle is repeated five times. Figure 60 shows the drive cycle with simulated velocities for the open and closed circuit systems. The hydraulic system results from this driving cycle are used as input parameters for the thermal model. Since the purpose of this study is the comparison of the thermal management of two different systems, we chose a representative driving cycle instead of extreme driving cycles.

The cooling system should be chosen based on the different extreme driving conditions including high torque situation such as a going uphill situation and also high speed situation. In our study, we focus the comparison of two different hydraulic systems and we just compared the required cooler for the given same driving cycles. Since the driving cycle we used is not an extreme case, the cooling system need to be larger for other extreme driving conditions.

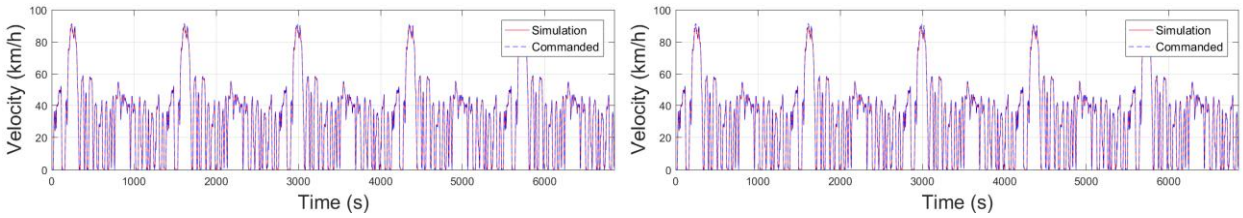

(a) Open circuit system (b) Closed circuit system

Figure 60. Driving cycle and simulation results for the open and closed circuit systems.

In the thermal systems, the hydraulic units are the main sources of heating up the systems. A cooler is installed for cooling down the systems and the system is naturally cooled down with natural heat transfer of each hydraulic component.

Figure 61 shows the system temperature without cooling for the open and closed circuit systems. Since the systems do not use a cooler, the temperature for both systems rises to over 100ºC. The open circuit system shows a slightly lower temperature distribution than that of the

closed circuit system. In the open circuit system, large amounts of flow circulate through the reservoir and this results in relatively large amounts of heat transfer through natural convection.

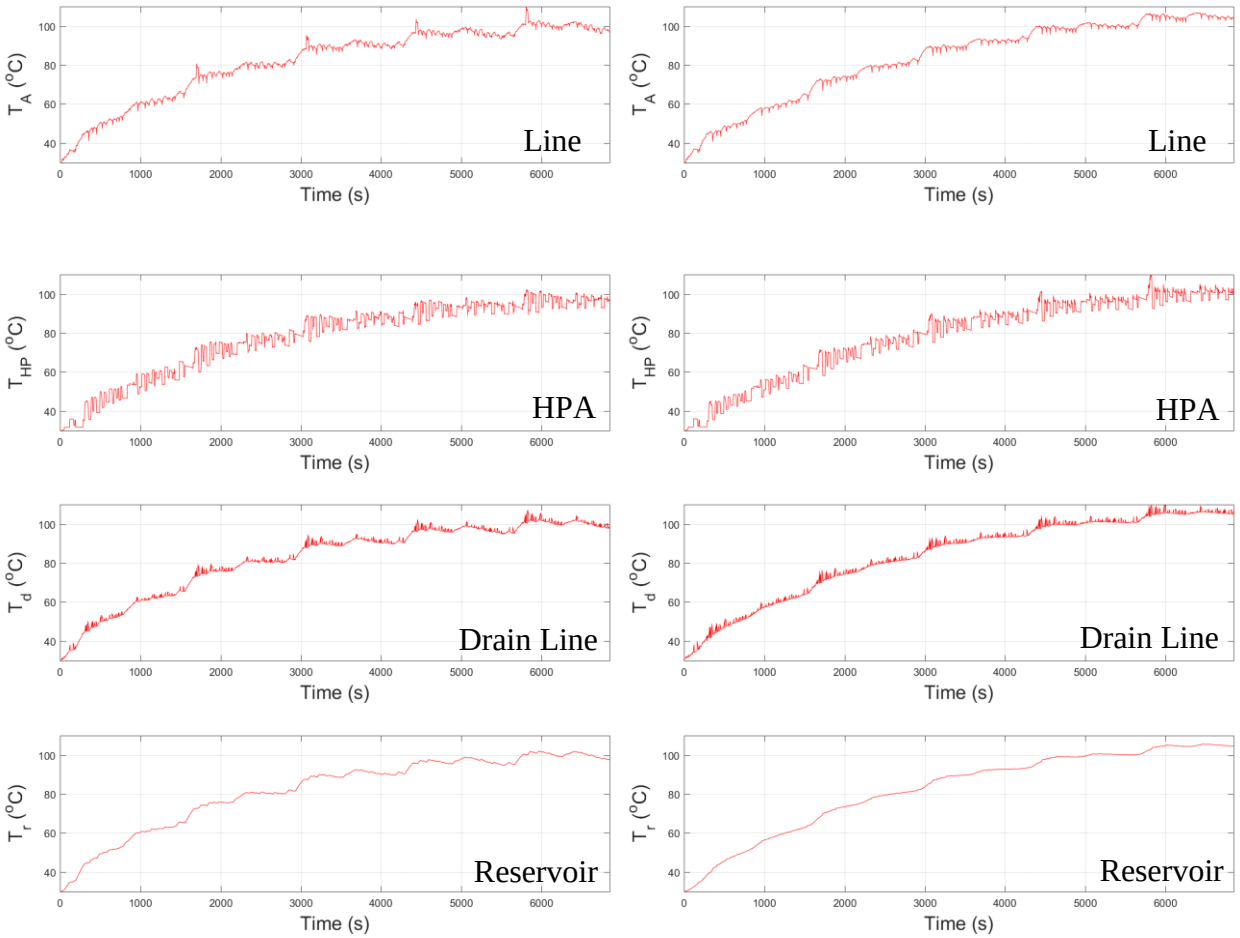

(a) Open circuit system (b) Closed circuit system

Figure 61. System temperature without cooling.

The temperature in the closed circuit system increases at a slower rate than the open circuit system because the capacitance of the closed circuit system is significantly larger than that of the open circuit system. The capacitance is larger because of the presence of a low pressure system and a low pressure accumulator.

Figure 62 shows the system temperatures with the cooling conditions shown in Figure 56. For both circuits, the system temperatures are sufficiently reduced with Cooler-2. The systems are slightly too warm with Cooler-1, and the systems are over-cooled using Cooler-3. Without cooling, the open circuit system has a slightly lower temperature distribution compared to the closed circuit system. The open circuit consumes less power and would require a smaller cooler size than the closed circuit system. The coolers used in this study was chosen based on a representative driving cycle for the comparison of different systems, not for the cooling system optimization; thus the cooling system needs to be sized based on extreme conditions for choosing an optimal cooler for the systems.

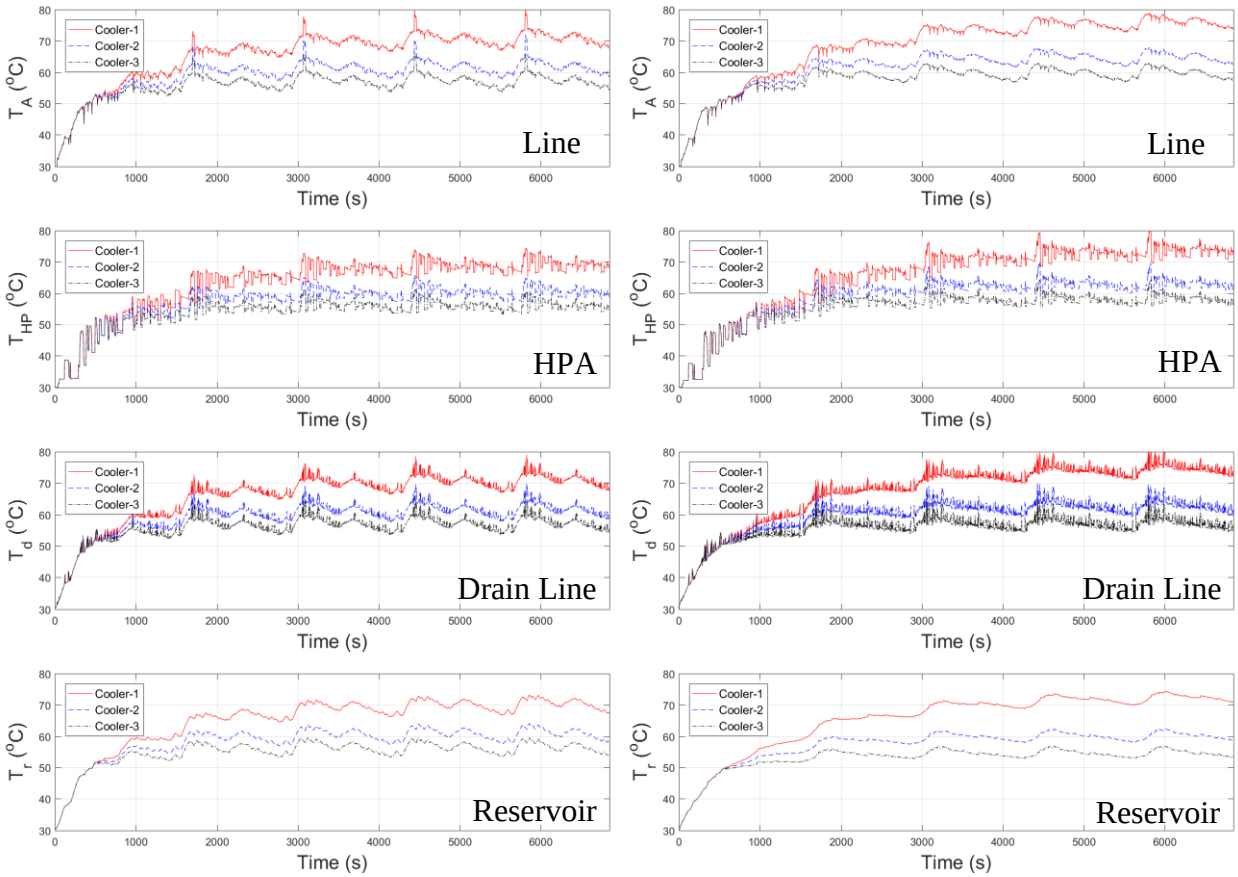

(a) Open circuit system (b) Closed circuit system

Figure 62. System temperature with different cooling conditions.

6.5 Chapter Summary

In this chapter, the thermal management of the open and closed circuit HHTs has been compared based on the simulation results. The hydraulic and thermal system behavior of the open and closed circuit systems were successfully modeled using a lumped parameter approach. The temperature of both open and closed circuit systems have been compared using different cooling conditions based on the FTP-72 driving cycle. During the design process, the open circuit systems have a possibility to need less costs, weight and space without the low pressure system, even though they require a larger reservoir compared to the closed circuit systems. The simulation results show that the open circuit systems have the potential to require smaller heat exchangers as compared to closed circuit systems. In addition, the open circuit system consumes less power from the prime mover and incorporates a smaller charge pump. The summary of the chapter can be described as follows:

- This study is firstly compared the thermal characteristics of the open and closed circuit systems by simulation.
- The thermal management of the open and closed circuit series HHTs has been analyzed with the same sizes of hydraulic components to ensure a fair and accurate comparison.
- The open circuit system shows a potential to require not only smaller heat exchangers but also smaller charge pumps. The open circuit system consumes less power from the prime mover compared to the closed circuit system.

CHAPTER 7. CONCLUSIONS

In this dissertation, a comprehensive system and thermal modeling approach has been proposed for HHTs. A system and thermal modeling methodology based on a novel numerical scheme, which considering the flow directions for the input parameters in the control volumes, and accurate theoretical description has been proposed in order to capture the rapid thermal transient under unsteady state conditions. The model has been verified through application to a series HHT and validated with the measured data from the HIL test rig with a standard driving cycle, FTP-72. In addition, the proposed thermal modeling methodology has been used to analyze the thermal management system of a novel HHV architecture, which is implemented in a vehicle in the Maha lab. The modeling results have been compared with the measured data while driving in the vehicle. In both studies, the simulation results show a good agreement with the experimental data in terms of the overall trends and variation ranges. The thermal study in this dissertation has not only a contribution in the research area in terms of hydraulic hybrid systems under unsteady state conditions, but it also shows better accuracy compared to the previous thermal studies. As an advanced topic of this research, the thermal characteristics of an open and a closed circuit series hydraulic systems have been evaluated by simulation, which has not been studied in the past. Those systems were analyzed and compared within the same main hydraulic components for a fair and accurate comparison. The open circuit system shows a possibility to require not only smaller heat exchangers but also smaller charge pumps compared to the closed circuit system.

In this study, the following original contributions have been accomplished for the HHTs:

- First study on the combined system and thermal modeling for HHTs

- Development of a thermal system modeling methodology based on a novel numerical scheme and physics based models for capturing the rapid thermal transient in the hydraulic system under unsteady state conditions
- Analysis of thermal characteristics of a series HHT with validation by the measured data in the HIL test rig
- Analysis and optimization of the thermal management system of a novel HHT, which is implemented in a SUV
- First modeling study on the thermal management of open and closed circuit hydraulic hybrid systems

In the future, the comprehensive system and thermal modeling method can be used for different advanced topics. It can be used for system and thermal performance prediction, thermal management system optimization, and thermal failure prevention based on the proper design of thermal management systems. Also, it can be applied to studying and analyzing the systems according to the different factors such as the weather conditions and different working temperatures. Different configurations of HHTs, like various power-split hydraulic hybrid architectures, can be studied for predicting the system and thermal performance by simulation to save time and costs.

REFERENCES

Andersson, J., P. Krus, K. Nilsson, and K. Storck. 1999. “Modeling and Simulation of Heat Generation in Electro-Hydrostatic Actuation Systems.” In *Proceedings of the 4th JHPS International Symposium on Fluid Power*, Tokyo, Japan, 81–94.

Bae, C. O., D. P. Vuong, and Y. S. Park. 2012. “Pump Efficiency Instrumentation Based on Thermodynamic Method and Traditional Technique.” In *2012 International Conference on Control, Automation and Information Sciences*, Saigon, Vietnam, 359–63.

Baseley, S., C. Ehret, E. Greif, and M. G. Kliffken. 2007. “Hydraulic Hybrid Systems for Commercial Vehicles.” *SAE Technical Papers* (724): 2007-01–4150.

Beachley, N. H., C. Anscomb, and C. R. Burrows. 1983. “Minimization of Energy Storage Requirements for Internal Combustion Engine Hybrid Vehicles.” *Journal of Dynamic Systems, Measurement, and Control* 105: 113–19.

Bender, F. A., T. Bosse, and O. Sawodny. 2014. “An Investigation on the Fuel Savings Potential of Hybrid Hydraulic Refuse Collection Vehicles.” *Waste Management* 34(9): 1577–83.

Bender, F. A., M. Kaszynski, and O. Sawodny. 2013. “Drive Cycle Prediction and Energy Management Optimization for Hybrid Hydraulic Vehicles.” *IEEE Transactions on Vehicular Technology* 62(8): 3581–92.

Bleazard, T. 2015. “Hydraulic Hybrid Four Wheel Drive Sport Utility Vehicle - Utlilizing the Blended Hybrid Architecture.” Master Thesis, Purdue University.

Bleazard, T., H. Haria, M. Sprengel, and M. Ivantysynova. 2015. “Optimal Control and Performance Based Design of the Blended Hydraulic Hybrid.” In *Proceedings of the ASME/ Bath Symposium on Fluid Power and Motion Control*, Chicago, IL, USA.

Boetcher, S. K. S. 2014. *Natural Convection from Circular Cylinders*. Cham: Springer International Publishing.

Bowns, D., N. Vaughan, and R. Dorey. 1981. “Design Study of a Regenerative Hydrostatic Split Power Transmission for a City Bus.” In *IMechE Hydrostatic Transmissions for Vehicle Application*, Coventry, England, 29–38.

Buchwald, P., H. Christensen, H. Larsen, and P. S. Pedersen. 1979. “Improvement of City Bus Fuel Economy Using a Hydraulic Hybrid Propulsion System—a Theoretical and Experimental Study.” *SAE Technical Papers*: 790305.

Busquets, E., and M. Ivantysynova. 2013. “Temperature Prediction of Displacement Controlled Multi-Actuator Machines.” *International Journal of Fluid Power* 14(1): 25–36.

Chen, J.-S. 2015. “Energy Efficiency Comparison between Hydraulic Hybrid and Hybrid Electric Vehicles.” *Energies* 8(6): 4697–4723.

Chen, Y., X. Liu, X. Wang, and Y. Song. 2017. “Control Strategies and Optimization Analyses of Front-Mounted Parallel System.” *Cluster Computing*: 1–13.

Chenggong, L., and J. Zongxia. 2008. “Calculation Method for Thermal-Hydraulic System Simulation.” *Journal of Heat Transfer* 130: 84503.

Cheong, K. L., Z. Du, P. Y. Li, and T. R. Chase. 2014. “Hierarchical Control Strategy for a Hybrid Hydro-Mechanical Transmission (HMT) Power-Train.” In *American Control Conference*, Portland, OR, USA, 4599–4604.

Cheong, K. L., P. Y. Li, and T. R. Chase. 2011. “Optimal Design of Power-Split Transmissions for Hydraulic Hybrid Passenger Vehicles.” In *Proceedings of American Control Conference*, San Francisco, CA, USA, 3295–3300.

Chicurel, R. 1999. “A Compromise Solution for Energy Recovery in Vehicle Braking.” *Energy* 24(12): 1029–34.

Churchill, S. W., and H. H. S. Chu. 1975. “Correlating Equations for Laminar and Turbulent Free Convection from a Vertical Plate.” *International Journal of Heat and Mass Transfer* 18(11): 1323–29.

Clegg, S. J. 1996. “A Review of Regenerative Braking Systems.” Working Paper 471. University of Leeds.

Cross, M., and M. Ivantysynova. 2011. “Practical Considerations for Pump / Motor Selection in Hydraulic Hybrid Vehicles.” In *Proceedings of the 52nd National Conference on Fluid Power 20112*, Las Vegas, NV, USA.

Davies, A. S. 1987. “Fuel Economy and Emissions Potential of a City Bus, Regenerative Power Train.” *SAE Technical Papers*: 872267.

———. 1989. “The Reduction of City Bus Exhaust Emissions by Means of a Regenerative Powertrain.” *SAE Technical Papers*: 890267.

Davis, S. C., S. E. Williams, and R.t G. Boundy. 2017. *Transportation Energy Data Book*. 36th ed. United States. Department of Energy.

Deppen, T. O., A. G. Alleyne, J. J. Meyer, and K. A. Stelson. 2015. “Comparative Study of Energy Management Strategies for Hydraulic Hybrids.” *Journal of Dynamic Systems, Measurement, and Control* 137(4): 41002.

Deppen, T. O., A. G. Alleyne, K. A. Stelson, and J. J. Meyer. 2012. “Optimal Energy Use in a Light Weight Hydraulic Hybrid Passenger Vehicle.” *Journal of Dynamic Systems, Measurement, and Control* 134(July 2012): 41009.

Dewey, C., F. Elder, and D. Otis. 1974. “Accumulator-Charged Hydrostatic Drive for Cars Saves Energy.” *Hydraulics and Pneumatics*: 180–83.

Dorey, R., and N. Vaughan. 1984. “Computer Aided Design of Split Power Hydrostatic Transmission Systems.” *IMechE, Part B: Journal of Engineering Manufacture* 198B(2): 61–69.

Du, Z., K. L. Cheong, P. Y. Li, and T. R. Chase. 2013. “Fuel Economy Comparisons of Series , Parallel and HMT Hydraulic Hybrid Architectures.” In *Proceedings of American Control Conference*, Washington, DC, USA, 5974–79.

Dunn, H., and P. Wojcienchowski. 1972. “High-Pressure Hydraulic Hybrid with Regenerative Braking.” In *7th Intersociety Energy Conversion Engineering Conference*, San Diego, CA, USA, 989–95.

———. 1974. “Energy Storage and Conversion Efficiency in a Hydraulic/Gas–Turbine Hybrid.” In *ASME 1974 International Gas Turbine Conference and Products Show*, Zurich, Switzerland: ASME.

———. 1975. “Energy Regeneration and Conversion Efficiency in a Hydraulic-Hybrid Propulsion System.” *High Speed Ground Transportation Journal* 9: 383–92.

Elder, F. T., and D. R. Otis. 1973. “Simulation of a Hydraulic Hybrid Powertrain.” *ASME* (73-ICT-50): 1–6.

“EPA Urban Dynamometer Driving Schedule (UDDS).” https://www.epa.gov/emission-standards-reference-guide/epa-urban-dynamometer-driving-schedule-udds (January 18, 2017).

Filipi, Z. et al. 2004. “Combined Optimisation of Design and Power Management of the Hydraulic Hybrid Propulsion System for the 6 X 6 Medium Truck.” *International Journal of Heavy Vehicle Systems* 11: 372–402.

Filipi, Z., and Y. J. Kim. 2010. “Hydraulic Hybrid Propulsion for Heavy Vehicles: Combining the Simulation and Engine-In-the-Loop Techniques to Maximize the Fuel Economy and Emission Benefits.” *Oil & Gas Science and Technology – Revue de l’Institut Français du Pétrole* 65(1): 155–78.

Gray, C. L. 2004. “Hydraulic Hybrid Vehicle.” : US Patent 6719080 B1.

Haria, H., and M. Ivantysynova. 2016. “Novel Mode-Switching Hydraulic Hybrid - A Study of the Architecture and Control.” *SAE Technical Papers*: 2016-01–8111.

Heggie, W. S., and R. Sandri. 1980. “An Energy Saving Hydro-Pneumatic Power Plant for the Automobile.” *Journal of Fluid Control* 12(4): 1–20.

Heskitt, M., T. Smith, and J. Hopkins. 2012. *Design & Development of the LCO-140H Series Hydraulic Hybrid Low Floor Transit Bus*.

Ho, T. H., and K. K. Ahn. 2010. “Modeling and Simulation of Hydrostatic Transmission System with Energy Regeneration Using Hydraulic Accumulator.” *Journal of Mechanical Science and Technology* 24(5): 1163–75.

———. 2012. “Design and Control of a Closed-Loop Hydraulic Energy-Regenerative System.” *Automation in Construction* 22: 444–58.

Hu, J. P., and K. J. Li. 2015. “Thermal-Hydraulic Modeling and Analysis of Hydraulic System by Pseudo-Bond Graph.” *Journal of Central South University* 22(7): 2578–85.

Hugosson, C. 1993. “Cumulo Hydrostatic Drive – A Vehicle Drive with Secondary Control.” In *3rd Scandinavian International Conference on Fluid Power*, Linkoping, Sweden.

Hui, S., J. Ji-hai, and W. Xin. 2009. “Torque Control Strategy for a Parallel Hydraulic Hybrid Vehicle.” *Journal of Terramechanics* 46(6): 259–65.

Hui, S., and J. Junqing. 2010. “Research on the System Configuration and Energy Control Strategy for Parallel Hydraulic Hybrid Loader.” *Automation in Construction* 19(2): 213–20.

Hui, S., Y. Lifu, and J. Junqing. 2010. “Hydraulic/electric Synergy System (HESS) Design for Heavy Hybrid Vehicles.” *Energy* 35(12): 5328–35.

Hui, S., Y. Lifu, J. Junqing, and L. Yanling. 2011. “Control Strategy of Hydraulic/electric Synergy System in Heavy Hybrid Vehicles.” *Energy Conversion and Management* 52(1): 668–74.

“Hybrid Air, an Innovative Full Hybrid Gasoline System.” https://www.groupe-psa.com/en/newsroom/automotive-innovation/hybrid-air/ (August 1, 2016).

Incropera, F. P., and D. P. DeWitt. 2001. *Fundamentals of Heat and Mass Transfer*. Wiley.

Ivantysyn, J., and M. Ivantysynova. 2001. *Hydrostatic Pumps and Motors*. Akademia Books International.

Ivantysynova, M., B. Carl, and K. Williams. 2008. “Power Split Transmission with Energy Recovery.” : US Patent 20080081724 A1.

Johri, R., S. Baseley, and Z. Filipi. 2011. “Simultaneous Optimization of Supervisory Control and Gear Shift Logic for a Parallel Hydraulic Hybrid Refuse Truck Using Stochastic Dynamic Programming.” In *ASME 2011 Dynamic Systems and Control Conference and Bath/ASME Symposium on Fluid Power and Motion Control*, Arlington, VA, USA, 99–106.

Johri, R., and Z. Filipi. 2010. “Low-Cost Pathway to Ultra Efficient City Car: Series Hydraulic Hybrid System with Optimized Supervisory Control.” *SAE International Journal of Engines* 2(2): 505–20.

Kepner, R P. 2002. “Hydraulic Power Assist – A Demonstration of Hydraulic Hybrid Vehicle Regenerative Braking in a Road Vehicle Application.” *SAE Technical Papers*: 200-01–3128.

Kim, N., and A. Rousseau. 2013. “A Comparative Study of Hydraulic Hybrid Systems for Class 6 Trucks.” *SAE Technical Papers*: 2013-01–1472.

———. 2015. “Thermal Impact on the Control and the Efficiency of the 2010 Toyota Prius Hybrid Electric Vehicle.” *Proceedings of the Institution of Mechanical Engineers, Part D: Journal of Automobile Engineering*: 1–11.

Kim, Y. J., and Z. Filipi. 2007. “Series Hydraulic Hybrid Propulsion for a Light Truck – Optimizing the Thermostatic Power Management.” *SAE Technical Papers*: 2007-24–0080.

Kjolle, A. 1978. *Thermodynamic Methods for Determining Losses in Hydraulic Components - a Survey*. Glasgow, UK.

———. 1989. “Efficiency Tests of a Hydraulic Transmission - Comparison of Thermodynamic and Hydraulic Measurement Methods.” In *Proceedings of the Second Bath Inter-National Fluid Power Workshop*, Bath, UK, 229–58.

———. 1993. “The Thermodynamic Method Applied to Hydraulic Transmission.” In *Proceedings of the 2nd JHPS International Symposium on Fluid Power*, Tokyo, Japan: Elsevier, 639–44.

Klop, R., and M. Ivantysynova. 2011. “Investigation of Noise Sources on a Series Hybrid Transmission.” *International Journal of Fluid Power* 12(3): 17–30.

Kumar, R., and M. Ivantysynova. 2009. “An Optimal Power Management Strategy for Hydraulic Hybrid Output Coupled Power-Split Transmission.” In *Proceedings of the ASME Dynamic Systems and Control Conference*, Hollywood, CA, USA, 299–306.

———. 2010. “The Hydraulic Hybrid Alternative for Toyota Prius – A Power Management Strategy for Improved Fuel Economy.” In *7th International Fluid Power Conference*, Aachen, Germany.

Lammert, M. P., J. Burton, P. Sindler, and A. Duran. 2014. “Hydraulic Hybrid and Conventional Parcel Delivery Vehicles’ Measured Laboratory Fuel Economy on Targeted Drive Cycles.” *SAE International Journal of Alternative Powertrains* 4(1): 2014-01–2375.

Li, C., and Z. Jiao. 2006. “Thermal-Hydraulic Modeling and Simulation of Piston Pump.” *Chinese Journal of Aeronautics* 19(4): 354–58.

Li, C.-T., and H. Peng. 2010. “Optimal Configuration Design for Hydraulic Split Hybrid Vehicles.” In *Proceedings of American Control Conference*, Baltimore, MD, USA, 5812–17.

Li, J., X. Zhang, Y. Yin, and J. Zhang. 2011. “Dynamic Temperature Simulation of an Accumulator in Aircraft Hydraulic Systems.” In *Proceedings of 2011 International Conference on Fluid Power and Mechatronics, FPM 2011*, Beijing, China, 653–57.

Li, K., Z. Lv, K. Lu, and P. Yu. 2014. “Thermal-Hydraulic Modeling and Simulation of the Hydraulic System Based on the Electro-Hydrostatic Actuator.” *Procedia Engineering* 80: 272–81.

Li, P. Y. 2010. “Optimization and Control of a Hydro-Mechanical Transmission Based Hybrid Hydraulic Passenger Vehicle.” In *7th International Fluid Power Conference*, Aachen, Germany.

Li, P. Y., J. D. Van de Ven, and C. Sancken. 2007. “Open Accumulator Concept for Compact Fluid Power Energy Storage.” *Proceedings of IMECE* 4: 127–40.

Li, Y., X. Su, H. Xu, and D. Li. 2008. “Thermal-Hydraulic Modeling and Simulation of High Power Hydro-Motor.” In *7th Intl. Conf. on Sys. Simulation and Scientific Computing*, Beijing, China, 841–44.

Liu, G.-Q., Y.-C. Yan, J. Chen, and T.-M. Na. 2009. “Simulation and Experimental Validation Study on the Drive Performance of a New Hydraulic Power Assist System.” In *2009 IEEE Intelligent Vehicles Symposium*, Xian, China, 966–70.

Macor, A., A. Benato, A. Rossetti, and Z. Bettio. 2017. “Study and Simulation of a Hydraulic Hybrid Powertrain.” *Energy Procedia* 126: 1131–38.

Manco, S., and N. Nervegna. 1989. “Experimental Investigation on the Efficiency of an External Gear Pump by the Thermodynamic Method.” In *Proceedings of the Second Bath International Fluid Power Workshop*, Bath, UK, 259–73.

Martini, S. 1984. “The M.A.N. Hydrobus: A Drive Concept with Hydrostatic Brake Energy Recovery.” In *International Symposium on Advanced and Hybrid Vehicles*, Glasgow, UK, 27–34.

Matheson, P., and J. Stecki. 2003. “Development and Simulation of a Hydraulic-Hybrid Powertrain for Use in Commercial Heavy Vehicles.” *SAE Technical Papers*: 2003-01–3370.

Midgley, W. J. B., and D. Cebon. 2012. “Comparison of Regenerative Braking Technologies for Heavy Goods Vehicles in Urban Environments.” *Proceedings of the Institution of Mechanical Engineers, Part D: Journal of Automobile Engineering* 226(7): 957–70.

Moran, M. J., H. N. Shapiro, D. D. Boettner, and M. B. Bailey. 2010. *Fundamentals of Engineering Thermodynamics*. Wiley.

Nakazawa, N., Y. Kono, E. Takao, and N. Takeda. 1987. “Development of a Braking Energy Regeneration System for City Bus.” *SAE Technical Papers*: 872265.

Norgard, J. S. 1973. “Thermodynamic Determination of Power Loss in Hydraulic Components.” *Journal of Fluids Engineering* 95(1): 2–7.

Nykanen, T. 2003. “Methods for On-Line Condition Monitoring of a Fixed Displacement Hydraulic Motor.” In *The Eight Scandinavian International Conference on Fluid Power, SICFP’03*, Tampere, Finland.

Oppermann, M. 2007. *A New Approach for Failure Prediction in Mobile Hydraulic Systems*. VDI-Verlag.

Panchal, S., I. Dincer, and M. Agelin-Chaab. 2016. “Thermodynamic Analysis of Hydraulic Braking Energy Recovery Systems for a Vehicle.” *Journal of Energy Resources Technology* 138(1): 11601.

Pease, G., and J. M. Henderson. 1988. “Simulation of a Hydraulic Hybrid Vehicle Using Bond Graphs.” *Journal of Mechanisms, Transmissions, and Automation in Design* 110: 365–69.

Pesaran, A. A. 2002. “Battery Thermal Models for Hybrid Vehicle Simulations.” *Journal of Power Sources* 110(2): 377–82.

Pomierski, W. 1999. “Condition Monitoring of Hydrostatic Transmission by Using the Volumetric Loss Method.” In *Proceedings of the Sixth Scandinavian International Conference on Fluid Power*, Tampere, Finland, 303–12.

———. 2001. “Condition Monitoring Thermodynamic Method for Testing Hydrostatic Transmissions in Non-Steady State of Working Conditions.” In *The Seventh Scandinavian International Conference on Fluid Power*, Linköping, Sweden, 229–41.

Pourmovahed, A., N. H. Beachley, and F. J. Fronczak. 1992a. “Modeling of a Hydraulic Energy Regeneration System: Part I—Analytical Treatment.” *Journal of Dynamic Systems, Measurement, and Control* 114(1): 160.

———. 1992b. “Modeling of a Hydraulic Energy Regeneration System: Part II—Experimental Program.” *Journal of Dynamic Systems, Measurement, and Control* 114(1): 160.

Pourmovahed, A., and D. R. Otis. 1984. “Effects of Thermal Damping on the Dynamic Response of a Hydraulic Motor-Accumulator System.” *Journal of Dynamic Systems, Measurement, and Control* 106(1): 21.

———. 1990. “An Experimental Thermal Time-Constant Correlation for Hydraulic Accumulators.” *Journal of Dynamic Systems, Measurement, and Control* 112(1): 116.

Puddu, P., and M. Paderi. 2013. “Hydro-Pneumatic Accumulators for Vehicles Kinetic Energy Storage: Influence of Gas Compressibility and Thermal Losses on Storage Capability.” *Energy* 57: 326–35.

Ramachandran, R., S. S. Hiremath, and M. Singaperumal. 2010. “Power Bond Graph Modeling of Series Hydraulic Hybrid System.” In *International Conference on Fluid Mechanics and Fluid Power*, Chennai, India.

———. 2012. “Theoretical Investigations on the Effect of System Parameters in Series Hydraulic Hybrid System with Hydrostatic Regenerative Braking.” *Journal of Mechanical Science and Technology* 26(5): 1321–31.

———. 2014. “Design Strategy for Improving the Energy Efficiency in Series Hydraulic/electric Synergy System.” *Energy* 67: 422–34.

Ramdan, M. I., and K. A. Stelson. 2016. “Optimal Design of a Power-Split Hybrid Hydraulic Bus.” *Proceedings of the Institution of Mechanical Engineers, Part D: Journal of Automobile Engineering* 230(12): 1699–1718.

Rossetti, A., and A. Macor. 2013. “Multi-Objective Optimization of Hydro-Mechanical Power Split Transmissions.” *Mechanism and Machine Theory* 62: 112–28.

Schneider, K., and W. Krautler. 2009. “Hydraulic Drive System.” : US Patent 0100830 A1.

Scott, D., and J. Yamaguchi. 1984. “Regenerative Braking for Buses Gives Big Fuel Saving.” *Automotive Engineering* 92(10): 95–99.

Shang, L., and M. Ivantysynova. 2015. “Port and Case Flow Temperature Prediction for Axial Piston Machines.” *International Journal of Fluid Power* 16(1): 35–51.

Shiber, S. 1979. “Automotive Energy Management System.” In *National Conference on Fluid Power*, Chicago, IL, USA, 141–47.

———. 1980. “Multi-Mode Transmission.” : US Patent 4196587.

Sidders, J. A., D. G. Tilley, and P. J. Chapple. 1996. “Thermal-Hydraulic Performance Prediction in Fluid Power Systems.” *Journal of Systems and Control Engineering* 210: 231–42.

Sim, T. P., and P. Y. Li. 2009. “Analysis and Control Design of a Hydro-Mechanical Hydraulic Hybrid Passenger Vehicle.” In *ASME 2009 Dynamic Systems and Control Conference*, Hollywood, CA, USA, 667–74.

Soriano, F., J. M. Moreno-Eguilaz, J. Alvarez, and J. Riera. 2016. “Topological Analysis of Powertrains for Refuse-Collecting Vehicles Based on Real Routes – Part I: Hybrid Hydraulic Powertrain.” *International Journal of Automotive Technology* 17(5): 873–82.

Sparrow, E. M., and A. J. Stretton. 1985. “Natural Convection from Variously Oriented Cubes and from Other Bodies of Unity Aspect Ratio.” *International Journal of Heat and Mass Transfer* 28(4): 741–52.

Sprengel, M. 2015. “Influence of Architecture Design on the Performance and Fuel Efficiency of Hydraulic Hybrid Transmissions.” PhD Thesis, Purdue University.

Sprengel, M., T. Bleazard, H. Haria, and M. Ivantysynova. 2015. “Implementation of a Novel Hydraulic Hybrid Powertrain in a Sports Utility Vehicle.” *IFAC-PapersOnLine* 48(15): 187–94.

Sprengel, M., and M. Ivantysynova. 2013. “Investigation and Energetic Analysis of a Novel Hydraulic Hybrid Architecture for On-Road Vehicles.” In *The 13th Scandinavian International Conference on Fluid Power*, Linköping, Sweden, 87–98.

———. 2014a. “Investigation and Energetic Analysis of a Novel Blended Hydraulic Hybrid Power Split Transmission.” In *Proceedings of the 9th International Fluid Power Conference (IFK)*, Aachen, Germany.

———. 2014b. “Recent Developments in a Novel Blended Hydraulic Hybrid Transmission.” In *Proceedings of the 2014 SAE Commercial Vehicle Engineering Congress*, Rosemont, IL, USA.

———. 2017. “Neural Network Based Power Management of Hydraulic Hybrid Vehicles.” *InternatIonal Journal of fluId Power* 18(2): 79–91.

Stephan, P. et al., eds. 2014. *VDI Heat Atlas*. Springer-Verlag.

Strohmaier, K. G., P. M. Cronk, and J. D. Van de Ven. 2015. “Design Optimization of a Hydraulic Flywheel Accumulator for a Hydraulic Hybrid Vehicle.” *International Journal of Fluid Power* 16(3): 149–61.

Svensson, H., J. Andersson, and K.-E. Rydberg. 1999. “Modelling of Losses and Temperature Calculations in Fluid Power Systems.” In *The Sixth Scandinavian Conference on Fluid Power*, Tampere, Finland, 569–81.

Tollefson, S., N. Beachley, and F. Fronczak. 1985. “Studies of an Accumulator Energy-Storage Automobile Design with a Single with a Single Pump/motor Unit.” *SAE Technical Papers*: 851677.

Toulson, R. 2008. “Evaluation of a Hybrid Hydraulic Launch Assist System for Use in Small Road Vehicles.” In *IEEE International Symposium on Industrial Electronics*, Cambridge, UK, 967–72.

Van de Ven, J. D. 2013. “Constant Pressure Hydraulic Energy Storage through a Variable Area Piston Hydraulic Accumulator.” *Applied Energy* 105: 262–70.

Van de Ven, J. D., M. W. Olson, and P. Y. Li. 2008. “Development of a Hydro-Mechanical Hydraulic Hybrid Drive Train with Independent Wheel Torque Control for an Urban Passenger Vehicle.” In *Proceedings of the International Fluid Power Exposition*, Las Vegas, NV, USA.

Vu, T.-V., C.-K. Chen, and C.-W. Hung. 2014. “A Model Predictive Control Approach for Fuel Economy Improvement of a Series Hydraulic Hybrid Vehicle.” *Energies* 7: 7017–40.

Wendel, G. R. et al. 2007. “Hydraulic Hybrid Vehicle System Panel.” In *Michigan Clean Fleet Conference*, Detroit, MI, USA.

Wicks, F., J. Maleszweski, C. Wright, and J. Zarybnicky. 2002. “Analysis of Compressed Air Regenerative Braking and a Thermally Enhanced Option.” In *37th Intersociety Energy Conversion Engineering Conference*, Washington, DC, USA, 406– 411.

Witt, K. 1974. “Die Berechnung Physikalischer Und Thermodynamischer Kennwerte von Druckflüssigkeiten, Sowie Die Bestimmung Des Gesamtwirkungsgrades an Pumpen Unter Berücksichtigung Der Thermodynamik Für Die Druckflüssigkeit.” PhD Thesis, TH Eindhoven.

Witt, K., and W. M. J. Schlosser. 1977. “Thermodynamic Measurements on Hydraulic Components.” In *ICMES Conference,* France, Paris.

Wu, Bin et al. 2002. “Optimization of Power Management Strategies for a Hydraulic Hybrid Medium Truck.” In *Proceeding of the 2002 Advanced Vehicle Control Conference*, Hiroshima, Japan.

———. 2004. “Optimal Power Management for a Hydraulic Hybrid Delivery Truck.” *Vehicle System Dynamics* 42(734): 23–40.

Wu, P., F. J. Fronczak, and N. H. Beachley. 1985. “Fuel Economy and Operating Characteristics of a Hydropneumatic Energy Storage Automobile.” *SAE Technical Papers*: 851678.

Wu, W. et al. 2014. “Investigation of Energy Efficient Hydraulic Hybrid Propulsion System for Automobiles.” *Energy* 73: 497–505.

Wu, W., J. Hu, S. Yuan, and C. Di. 2016. “A Hydraulic Hybrid Propulsion Method for Automobiles with Self- Adaptive System.” *Energy* 114: 683–92.

Xu, L. et al. 2017. “Investigation on the Optimal Energy Recovery System for the Military Hybrid Vehicle Based upon the Comprehensive Evaluation Method.” In *ICMD 2017: Advances in Mechanical Design*, Springer, Singapore, 923–35.

Yan, Y., G. Liu, and J. Chen. 2010. “Integrated Modeling and Optimization of a Parallel Hydraulic Hybrid Bus.” *International Journal of Automotive Technology* 11(1): 97–104.

Yang, Y., C. Luo, and P. Li. 2017. “Design and Performance Analysis on a New Electro-Hydraulic Hybrid Transmission System.” *International Journal of Electric and Hybrid Vehicles* 9(2): 134.

Yi, T., F. Ma, C. Jin, and Y. Huang. 2018. “A Novel Coupled Hydro-Pneumatic Energy Storage System for Hybrid Mining Trucks.” *Energy* 143: 704–18.

Zhang, H., F. Wang, and K. A. Stelson. 2017. “Modeling and Design of a Hydraulic Hybrid Powertrain for Passenger Vehicle.” In *ASME/BATH 2017 Symposium on Fluid Power and Motion Control*, ASME, V001T01A075.

Zhang, Z., J. Chen, and B. Wu. 2012. “The Control Strategy of Optimal Brake Energy Recovery for a Parallel Hydraulic Hybrid Vehicle.” *Proceedings of the Institution of Mechanical Engineers, Part D: Journal of Automobile Engineering* 226(11): 1445–53.

Zhao, Y., and O. Tatari. 2017. “Carbon and Energy Footprints of Refuse Collection Trucks: A Hybrid Life Cycle Evaluation.” *Sustainable Production and Consumption* 12: 180–92.

Zhou, J., C. Wei, and J. Hu. 2015. “A Novel Approach for Predicting Thermal Effects of Gas Cavitation in Hydraulic Circuits.” *Energy* 83: 576–82.

VITA

Hyukjoon Kwon

School of Mechanical Engineering, Purdue University

Education

B.S., School of Mechanical and Aerospace Engineering, February 2007, Seoul National University, Seoul, South Korea

M.S., School of Mechanical and Aerospace Engineering, February 2012, Seoul National University, Seoul, South Korea

Major Professor: Jack J. Yoh

Ph.D., School of Mechanical Engineering, May 2018, Purdue University, West Lafayette, Indiana, USA

Thesis: System and Thermal Modeling of Hydraulic Hybrids: Thermal Characteristics Analysis

Major Professor: Monika Ivantysynova

PUBLICATIONS

Journal

Kwon, H., Sprengel, M. and Ivantysynova, M. 2016. "Thermal Modeling of a Hydraulic Hybrid Vehicle Transmission based on Thermodynamic Analysis." *Energy* 116: 650–60.

Lee, K.-C., Baek, W.-K., **Kwon, H.**, Shin, W.-S. and Yoh, J. J. 2013. "Analysis of Melt-through Process of 1.07 μm Continuous Wave High Power Laser Irradiation on Metal." *Journal of Mechanical Science and Technology* 27: 1745–52.

Kwon, H. and Yoh, J. J. 2012. "Polarized Reflectance of Aluminum and Nickel to 532, 355 and 266 nm Nd:YAG Laser Beams for Varying Surface Finish." *Optics & Laser Technology* 44: 1823–8.

Kwon, H., Baek, W. K., Kim, M. S., Shin, W. S. and Yoh, J. J. 2012. "Temperature-Dependent Absorptance of Painted Aluminum, Stainless Steel 304, and Titanium for 1.07 μm and 10.6 μm Laser Beams." *Optics and Lasers in Engineering* 50: 114–21.

Conference

Kwon, H., Keller, N. and Ivantysynova, M. 2018. "Thermal Management of Open and Closed Circuit Hydraulic Hybrids – a Comparison Study." In The 11th IFK International Conference on Fluid Power, Aachen, Germany.

Kwon, H. and Ivantysynova, M. 2017. "System and Thermal Modeling for a Novel On-road Hydraulic Hybrid Vehicle by Comparison with Measurements in the Vehicle." In The ASME/BATH 2017 Symposium on Fluid Power & Motion Control, Sarasota, FL, USA.

Kwon, H., Baek, W. K., Kim, M. S. and Yoh, J. J. 2011. "Absorptances of Metals for Fiber Laser and CO2 Laser at Elevated Temperatures." In The Korean Society of Laser Processing Conference, Danyang, South Korea.

Kwon, H., Baek, W. K., Shin, W. S. and Yoh, J. J. 2011. "Absorptances of Paint Coated Al, SS304, and Ti for Fiber and CO2 Lasers." In The Korea Institute of Military Science and Technology Conference, Jeju, South Korea.

Lee, K. C., Baek, W. K., Kim, Y. H., Gojani, A. B., **Kwon, H.** and Yoh, J. J. 2011. "Study on 1 μm and 10 μm Continuous Wave Laser Irradiation on the Metals with Various Coatings." In The 49th AIAA Aerospace Sciences Meeting, Orlando, FL, USA.

Lee, K. C., Yoh, J. J., Gojani, A. B., Lee, H. H., Choi, S. J., Kim, Y. H., **Kwon, H.** and Baek, W. K. 2010. "Ballistics Kill of Using High Power Laser." In The Stanford-SNU Workshop, Stanford, CA, USA.